Investigating Wind-Waves Impact and Sea Level Rise on the Long-term Morphological Development of Estuarine Shoals

Jiechen Zheng

Investigating Wind-Waves Impact and Sea Level Rise on the Long-term Morphological Development of Estuarine Shoals

by

Jiechen Zheng

to obtain the degree of Master of Sience
at the Delft University of Technology,
to be defended publicly on Thursday December 19, 2019 at 10:00 AM

Thesis committee:

Prof. Zheng Bing Wang	TU Delft
Dr. Mick van der Wegen	Deltares
Dr. Bram van Prooijen	TU Delft
Hesham Elmilady MSc.	Deltares
Lodewijk de Vet MSc.	Deltares

Contents

Summary

Estuarine shoals are valuable areas with functions of nature, safety and navigation. It is of utmost importance to understand their underlying physical processes and long-term evolution to achieve protection. The first aim of this report is to determine the impact of wind-waves on long-term morphological development of estuarine shoals. The rapid sea level rise requires a valid model prediction of esturine shoal evolution in the future. Whether waves should be included for forecast needs to be evaluated. This rises the second aim to investigate wind-waves impact on estuarine shoals evolution under the sea level rise.

A 2-D, process-based numerical model (Delft3D) is applied. This study sets up a large scale realistic model covering the whole Western Scheldt geometry and focuses on shoal Van Ossenisse by constructing high resolution grids and imposing wind-waves. Simulations are compared on a timescale of 50 years, with and without wave effects. Results revels that waves tend to slightly migrate shoals along their propagation direction. Waves erode sediment in the intertidal area, resulting in a lowering elevation of the shoal and high suspended sediment concentrations in water column. On the one hand, high SSC combined with wave asymmetry and wind-driven flow enhance sediment transport rate along wave propagation direction over top of the shoal, causing more sediment appearing in the lee side of the shoal. On the other hand, wave-induced suspended sediment follows tidal currents and transport to shoal edges where low bed shear stress exists. These cause shoal widening at lower intertidal area and upper subtidal area. Channel velocity hence increases with response to channel area reduction. This leads to erosion in the channel and channel deepening. In a longer timescale, waves impact do not lead to fundamental difference on estuarine autonomous behaviors. It reveals that waves impact may be sensitive to some parameters (eg. sediment grain size, tidal range, type of boundary conditions), especially in the inner channel. It is recommended to do more investigations.

Sea level rise scenarios are carried out by imposing gradually sea level rise at the seaward boundary. Its timescale is 100 years. Both in wave and no wave case, sea level rise leads to elevation of shoal height and area lose in shoal edges, resulting in steeper slope in the intertidal area. Larger channel area and volume are presented with sea level rise. Waves maintain their function under the sea level rise. It lowers and widens the shoal, resulting in the increase of intertidal area and

volume. Sea level rise does not change the tendency of waves impact.

Acknowledgement

I am approaching the time to hand out my report. Before doing it, I would like to finalize my report by presenting my acknowledgement and gratitude during this whole master period.

I am very glad that I made the choice to pursue my Master Degree in Tu Delft. It is a place where teachers have huge passion to share their knowledge and respect new ideas from young people. Students have chances being exposed to extensive and in-depth theoretical knowledge and innovative management. I am happy to see my growth during the whole master period.

With the interests of numerical modelling and knowing the physical processes in coastal area, I chose this topic as my thesis. It turns out that not only this topic is of interests but also my committee are very supportive. Hesham, my daily supervisor, is detail-oriented. He helps me from the global view of the research to every detailed, single question. Everytime when I ask for a question, he is willing to solve it with me immediately. Thank you, Hesham, for your dedication. Mick, as my main supervisor, provides me with comprehensive guide over the whole work. I learned from you with how to do wise management of a work and how to make things getting to the point. Thank you for your encouragements all the time and your arrangement for my further research. Thank you, Bram, Wang and Lodewijk, for your beautiful suggestions and contribution. Finally, I acknowledge Deltares for the financial support for this work.

Beside, I would like to thank people who are around me and make up my daily life. The most importantly, I would like to thank my parents. Thank you for your support during this whole master period. You treat me like a close friend and give me as much as freedom to plan my life path. Thank you, my long-distance friends, Yi Liu and Lei Lu. Your kind words and accompany help me overcome the most struggling days and your wisdom helps me better perceive my inner part and build up my comprehensive personalities. Thank you, Boyao. We have common interests and curiosities towards this mysterious world. You share me a totally new way to view this world. Thanks bro, for making life happy and enjoyable. Thank you, all my friends, Jianbiao, Zixin, Ge Gao, Jiangshan, Rida, Tyo, Camille, Nianlei, Chu Chen, Wataru and others whom I unintentionally forget. I am grateful to meet you all in my life. At last, I would like to thank me, for always being happy and positive.

List of Figures

List of Tables

Chapter 1

Introduction

1.1 Motivation

Estuary is defined as a partially enclosed coastal body of brackish water with one or more rivers or streams flowing into it, and with a free connection to the open sea. With the variations of temperature, salinity, turbidity and flow discharge, estuaries are very important to marine life. Its dynamism results in seasonal variation of marine fish communities and provides critical habitats to a variety of species that rely on estuaries for life-cycle completion (Osborn, 2017). In addition, it also supports many other important ecosystem functions: biogeochemical cycling and movement of nutrients, mitigation of floods and biological production (Meire et al., 2005). From a socio-economic point of view, estuaries provide indispensable goods and services. About 60% of the world population live along the bank of the estuaries considered as nurseries of the sea (EPA, 1997). Estuaries provide people commercial fish catch and recreational fish catch. As important recreational areas, people visit estuaries to boat, swim, watch birds and other wildlife. Many estuaries are important centers of transportation and international commerce. Ports are constructed along estuaries to transform goods every day.

Intertidal flats in the estuaries are areas that are covered at high tide and exposed at low tide. Usually, they include habitats such as sandy beaches, rocky shores and mud flats. Due to water level variations, the environmental conditions are harsh. Species have to adapt to the harsh conditions but also take advantage of them. Sunlight penetrates the shallow water, allowing organisms that rely on sunlight to grow well on the shore bottom. These organisms include plants, seaweeds and corals. This in turn shelters and feeds other life (Tan et al., 2007). A particular large varieties of flora and fauna are found in the intertidal areas because of tidal shifts (Tan et al., 2007). Large marine life, such as seals, sea lions and fish find food at high tide, while a large varieties of shorebirds, look for their food on the intertidal zones at low tide. This

makes an area of high value for the ecosystem.

In favour of the functions nature, safety and navigation, knowing the morphological change both in the short term and long term is very important when carrying out coastal management. However, an estuary is usually a very complex and dynamical system due to its complicated hydro-morphological conditions and human interventions (dredging, sand mining and dike embankment). Numerous research has being carried out to understand the interactions between its hydrodynamics and morphodynamics (e.g. Kuijper et al., 2004; Wang et al., 2002; Van den Berg et al., 1996; Van der Werf et al., 2015). Originally, empirical models are widely used based on observation data. In the past few decades, process-based numerical models have become more and more popular and as a virtual laboratory to investigate estuarine morphological evolution mechanisms. Wang et al. (1995) show the potential of numerical model to reproduce a characteristic pattern in tidal inlet. Van der Wegen and Roelvink (2012) start from a flat bed and reproduced two distinct time-scales: channel-shoal pattern formation within decades and longitudinal profile development for centuries. Although obtaining representable predictions in realistic conditions requires more investigations (Wang et al., 2002), some research showes the potential of process-based modeling for obtaining insight into the long-term morphological evolution (e.g. Dam et al., 2016; Elmilady et al., 2019; Van der Wegen et al., 2016).

With the approaches of observations and various models, people have been getting deeper insight of estuarine hydro-morphodynamics. Tidal forcing is well-known to be the dominant forcing on estuarine morphological change and its channel-shoal pattern formation. However, waves can be of a high relevance, especially for intertidal area development (Friedrichs, 2011). From a large scale perspective (estuarine scale), recent studies usually neglect local wind-waves impact to save computational time and reduce model complexity (e.g. Van der Wegen and Roelvink, 2012; Dam et al., 2016; Wang, Z. B and Elias, EPL and Briere, 2007). Small scale studies on intertidal flats reveal the importance of wind-waves on shoal profile (e.g. Friedrichs, 2011; Roberts et al., 2000; Elmilady et al., 2019; Van der Wegen et al., 2011; Maan et al., 2018). However, these studies use schematized boundary conditions with limited shoal-channel interactions. Schuttelaars and de Swart (1999) point to the importance of advective contributions or non-linear effects for the exchange of sediment between estuarine regions. Therefore, it might cause problem when research focuses on isolated estuarine subsystems. In addition, when we look into the the intertidal flat development, many research focuses on mudflats or mixture sediment compositions (e.g. Van der Wegen et al., 2016; Elmilady et al., 2019; Maan et al., 2018). Limited research focuses on only sand transport, including both bedload and suspended sediment transport.

Based on existing knowledge gaps, this study focuses on the morphodynamic evolution of sandy shoals. In particular, we focus on the evolution of a single shoal in the Western Scheldt estuary.

Global warming will result in a rise of sea level till the end of 21^{th} century (from Intergovernmental Panel on Climate Change). In the past centuries, 20 cm sea level rise was observed (Kemp et al., 2011). However, sea water level rapidly rises from nineteenth century and shows the potential

to accelerate in the future. Global SLR forecast reveals a range between 0.2 to 2m till the end of 21^{th} century (Parris et al., 2012). Impact of sea level rise is worldwide, especially on low lying coasts such as estuaries. This would lead to its notable morphological change and may even cause degeneration of the intertidal system with extreme sea level rise rate (e.g. Dissanayake et al., 2012; Van der Wegen, 2013). Based on that, adaption of coastal management strategies is required. Since climate change is continuously happening, it is urgent to understand the behaviors of estuaries with response to sea level rise and further do forecast for the future. Therefore, one consideration is put forward. Under the impact of sea level rise, what is the relevance of local wind-waves to estuarine adaption. It is associated with whether we should include wind-waves or not in Sea Level Rise prediction model.

Overall, in this research, we investigate (1) impact of wind-waves on long-term morphological development of estuarine shoals; (2) under sea level rise, the impact of wind-waves on long-term morphological development of estuarine shoals. Understanding the underlying physical process ensures a more efficient coastal management.

1.2 Literature Review

Non-cohesive sediment transport

Generally, for non-cohesive sediment like sand, there are two different transport modes: Bed load transport and suspended load transport. Bed load transport is defined when sediment transport in contact with the bed. The movement is steered by shear stress. Suspended load transport is defined as the sediment is suspended in the water column and transported by water parcels. The particles are supported by turbulence diffusive forces. Wash load is also suspended in the water column, but it never settle into bed, and therefore has limited influence on the bed level change, so it is not considered into sediment transport here. The total sediment transport is the summation of bed load transport and suspended load transport.

When talking about suspended sediment transport, the horizontal velocity signal is very important. If we neglect the density variations, the horizontal transport of sediment is related to lag effects, tidal flow asymmetries, Stokes' drift compensation, river flow and wind/wave effects, etc. In other words, the residual sediment transport is contributed by the asymmetry of the horizontal tide and tide-averaged residual currents (river flow, compensation for Stokes's drift, secondary flow, wind/wave effects,etc.). For bed load transport which respond instantaneous to shear stress variation, it is steered by maximum horizontal velocity.

Channel-shoal pattern

Carter (2013) distincts three types of tidal basins: tidal lagoons, tidal bays and estuaries. Estuaries experience fresh water from upstream, but the hydrodynamics is more controlled by tides rather than by the river discharge. The author classifies the sedimentation sources: (i)inflowing streams, (ii)the coast, and (iii) from the margins of estuarine basin itself. Van Veen (1950) describes a very high-quality observations on the ebb and flood channel systems of Dutch tidal basins. They believe all channels can be divided into flood channels and ebb channels, although different tidal basin varies among each other. Robinson (1960) and Ahnert (1960) describe various ebb-flood channel patterns and meander type and forms an excellent introduction to dynamic channel systems in estuaries, tidal inlets and tidal basins with work from Van Veen (1950). Figure 1.1 shows a schematic diagram of estuary meanders. Both the river meanders before the present of postglacial eustuary and tide path distortion in ebb and flood period contribute to the meanders.

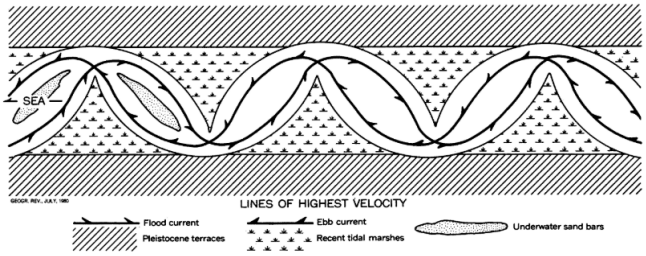

Figure 1.1: A schametic diagram of estuary meanders (Ahnert, 1960)

Originally, empirical and semi-empirical models are used worldwide by analyzing relationships between different state variables. O'Brien (1969) and Jarrett (1976) study the empirical relationship between the minimum inlet cross-section area and the tidal prism on sandy coast, and forms an equilibrium equation between them.

In recent years, mathematical-physical models have become a popular approach to study estuarine morphology. Scientists start focusing on isolated processes to gain fundamental understanding about the physical mechanics.

To get insight into the initial pattern formation and explain a higher morphological activity in natural tidal basins, Schuttelaars and de Swart (1999) model a two-dimensional rectangular embayment with only bottom erodible. They study various combinations of the model parameters to understand the stability of the linearly sloping equilibrium bottom profile. The model shows the interactions between tidal flow and the bottom which explained a inherent positive feedback mechanism in the initial channel-shoal formation. Strength of the bottom friction, the width of the embayment and the grain size determine the instability and the growth rate of patterns.

The results show that a nonlinear theory is necessary to predict possible new equilibrium profile. Schramkowski et al. (2002) set up a two-dimensional idealized rectangular embayment model, considering both embayment width and tidal excursion length as relevant length scale of bottom patterns. It demonstrats that estuarine bars with typical scale length on the order of the tidal excursion can result in positive feedback mechanism in the initial channel-shoal formation. The instability that occurs in the initial bottom patterns development can be triggered by the combined effect of bottom friction and advective processes. Van Leeuwen and De Swart (2004) give a similar results of the relevant importance of advective and diffusive transport. In Schramkowski et al. (2002)'s result, whether the longitudinal length scales or the order of tidal excursion is unstable or not is independent of the ratio of the width to the tidal excursion length. Based on the similar assumptions, Hibma et al. (2003) set up a 2-D numerical model to resemble the channel and shoal patterns in Western Scheldt. The results are validated with field observations by Ahnert (1960) and turned to be well-compared.The initial formed undulations are corresponding with the results from Schramkowski et al. (2002). Both of them show that the growing bars is in the order of the tidal excursion length.

Although Hibma et al. (2003) find that the global pattern tends to be stable after approximately a century, research studying the final formation of the patterns are still limited. Investigating both initial (one tidal cycle) simulation and long-term (300 years) simulations, Hibma et al. (2004) find that channel-shoal pattern evolution is independent of the initial perturbation, although the amplitude of different wavelengths exhibit an exponential growth during the first decades. In these simulations, it seems that the dominant wavelengths depend on the width of the basin and the local maximum velocity. Van Der Wegen and Roelvink (2008) emphasize on the pattern formation and longitudinal equilibrium profiles, respectively, by setting up 2-D schematized model up to 1600 years and 1-D model up to 8000 years. Their model applies a process-based model by Lesser et al. (2004) but doing some adjustments. They studies channel-shoal pattern generation over time. They describe how the shoal-channel pattern formation. Initially, things happen in the landward side of the estuary, after long-term, sin-shape channel is generated. After then, occasionally, ebb-flood channel is generated and shoal appears in between them. Both 1-D and 2-D results show that equilibrium was not reached. Pattern formation development is dominantly determined by local hydrodynamic conditions over decades, which longitudinal profile determined by the feedback between its profile and tidal forcing. The major morphological length scales are directly related to tidal wave characteristics such as tidal excursion. They also compare data from Western Scheldt (Ahnert, 1960) with empirical relationships in terms of the tidal prism versus the cross-sectional area and the channel volume versus the tidal prism and show well performance.

The research that we discuss until now is carried out with a highly schematized geometry, where the channel and shoal development is highly influenced by initial perturbations. Van der Wegen and Roelvink (2012) start to carry out a realistic geometry of Western Scheldt. Many runs are applied based on different parameter settings. By using BSS method Sutherland et al. (2004),

They compare the model results with field observation data of 1998. Sensitivity analysis show the importance of different factors that influence the initial formation and long-term development. Initial geometry turns to play an important role in the character of emerging patterns. In terms of the longitudinal profile, it is shown that tidal asymmetry and overtides contributed to the deepening domain. The morphological activities decrease in long-term timescale but still continue to take place. Dam et al. (2016) hindcast the morphological behavior of Western Scheldt over 110 year period (1860-1970) based on real bathymetry. They demonstrate the well performance of process-based model in long-term situation. The model results have a good resemblance after 110 years and showed the interactions between tidal forcing and geometry of the estuary overrules other interactions. It also show the trend of energy dissipation and less activities in estuary.

Estuarine shoals evolution

Tidal force is dominant in the channel-shoal system development, while local waves also play an important role (Van der Wegen et al., 2016). The interaction between shoal and channels are investigated by using 2D model (Van Der Wegen and Roelvink, 2008; Hibma et al., 2003; Dissanayake et al., 2009). However, this model setups do not include local wind waves.

Some observations demonstrate that the shape of tidal flats tends to become more convex-up with the increase of tidal range relative to wave height. (Kirby, 2000). In terms of flats width, observations also suggest that tidal-dominant flats become wider with increasing tidal range, as a results of higher sediment concentrations. Observations of wave-dominant flats show that flats become wider with the increase of wave energy. Obviously, apart from tidal currents, waves also play an important role in the tidal flat.

When trying to understand the mechanisms behind these characteristics, people present both analytical solutions and numerical solutions.

Friedrichs (1993) and Friedrichs and Aubrey (1996) show analytical solutions for cross-shore profile in the case of tides alone under assumption that the maximum value for bed shear stress over the tidal cycle is constant in space when a tidal flat is in equilibrium. They derive equilibrium profiles under sinusoidal tidal forcing are convex-up, and are more obvious near the tidal front. In contrast, the profiles under the impact of wind waves favors concave hypsometries.

With the improvement of previous analytical solution (Friedrichs and Aubrey, 1996), Friedrichs (2011) used the approach of dynamic equilibrium concept, which means there are no cases that tidal flats stay statically in equilibrium. The profile can develop between purely tide-dominant convex and purely wave-dominant concavracteristics such as profile shape, bed slope and grain size as a function of sediment supply and wave tidal forcing. They distinguish net transport due to spatial (Lagrangian) asymmetries and Eulerian asymmetries. Net sediment transport by Lagrangian asymmetry is suspended sediment dispersion due to spatial gradients in velocity, stress

or concentration. Friedrichs (2011) assess trends in hydrodynamic energy across tidal flats by distribution of tide- and wave- induced velocities. Depth-averaged tidal velocity is approximated based on only continuity equiation, and wave-induced velocity is based on linear, unbroken, shallow-water waves. The distribution of velocity shows that energy-driven Lagrangian asymmetries across a linealy sloping tidal flat favors landward net transport of suspended sediment in the presence of sinusoidally forced tides and seaward net transport of suspended sediment in the presence of non-dissipative waves. Observations on tidal flats of spatial gradients in suspended sediment concentration showed that the tidally averaged flux of suspended sediment across tidal flats in the Dutch Wadden Sea was landward in absence of waves but offshore when wave height grew (Janssen-Stelder, 2000). Correspondingly, on a suite of tidal mudflats in Severn Estuary, UK, Allen and Duffy (1998) observe accretion during low wave energy months and reduction of mudflat elevation during high wave energy months.

Apart from Lagrangian asymmetry, Friedrichs (2011) point out that in the case of Eulerian asymmetries, net transport occurs over tidal cycle in response to Eulerian (i.e., local, time-dependent) asymmetries. In tidal flats, the most important Eulerian example is usually distortion of periodic tidal velocity, especially for coarse sediment. Observations confirm tendency that, on most tidal flats, tidal processes alone usually lead to landward sediment transport in the absence of wave.

Many analytical models based on dynamic equilibrium theory are not capable to handle a real tidal flats by assuming spatially and temporally varying bed shear stress. Therefore, Hu et al. (2015) build up dynamic equilibrium theory-ESTMORF model to test its capability and also explain the morphological change with response to tidal currents, wind waves, sediment supply and other drives. Their work serves a good explanation of equilibrium theory from Friedrichs in 1996 and 2011.

Roberts et al. (2000) set up 1-D schematic mathematical models to study the relationship between hydrodynamic forcing, sediment transport and the equilibrium profile shape of intertidal mudflats. studies only two cases of hydrodynamic forcing which are cross-shore currents alone and cross-shore currents combined with waves. Results show that the action of waves makes the mudflat steeper and concave-up. The effect of waves in steepening the calculated profiles in comparison to the currents alone case is more pronounced in the upper part of the mudflat. They propose the explanation that the depth at high water is less in the upper flat, which means it has larger proportion to be affected by wind waves over tidal cycle.

Van der Wegen et al. (2016) develope a 1-D morphodynamic profile model with tides and waves entering from the channel toward the shore. Profile development shows that wave action limits mudflat accretion at the edge of mudflat and also the accretion rate in mudflat by resuspending sediment. Larger waves lead to lower mudflat. More evidence reveals that highest SCC (Suspended sediment concentration) happens in the intertidal zone, larger than that in the subtidal area. This tendency is matched with measured SSC at stations in San Francisco Bay (MacVean

and Lacy, 2014; Brand et al., 2010). In the scenario without wave (only tide), huge deposition occurs at the side close to the channel, which is far away from the measurement bed level. Model settings of different diffusivity coefficient show hardly difference with the standard profile.

Fagherazzi et al. (2007) apply a stochastic point model to study the influence of tidal currents and wind waves on tidal flat equilibrium. They find the equilibrium elevation depends on the relationship between shear stress caused by wind waves and depth. The importance of local-generated wind waves is further studied by Maan et al. (2018). Authors use a 2-D horizontal process-based model (Delft3D) to study the feedback mechanism on the long-term evolution of an mudflat in the Western Scheldt. In their model, the research areas are relatively small compared to the whole estuary system and even adjacent channels. Based on the considering that the boundaries need to be independent of the evolution of the mudflats, they made hydrodynamic model in the whole estuary system with fixed geometry and the surrounding morphology, and morphological model in the mudflats. It is shown that small wind waves have important stabilizing effect on it. The relationship between water depth and wave-induced bed shear stress can explain the stability effect. In the subtidal domain, the decreasing water depth causes high wave-induced bed shear stress, and consequently, it causes erosion of the bed sediment. In the intertidal domain, the wave impact increases due to wave shoaling along the cross-shoal direction. These two feedback mechanisms both lead to negative morphologic feedback loops. This results agree with model results simulated by Van der Wegen et al. (2016).

To understand the intertidal morphology under the impact of wind waves, much research has been carried out under the assumption of constant hydrodynamic conditions exerted by waves and tides along channels (e.g. Friedrichs, 2011; Van der Wegen et al., 2016; Maan et al., 2018). However, the change of shoal formation under the influence of waves can also alter the hydrodynamic regime over the entire estuary and again change the shoal formation reversely (Hunt et al., 2015). Therefore, to gain a better knowledge of the shoal development, it is suggested to create hydrodynamic conditions over the whole estuary.

Impact of Sea Level Rise

Based on observed field data (O'Brien, 1969), a wealth of empirical equations have been proposed to describe the impact on tidal basin because of sea level rise. Van Goor et al. (2003) study the geomorphology of tidal basins to investigate weather they can maintain equilibrium under a rising sea level rise. It is found that when a constant sea level rise takes place, the system will import sediment to reach a new equilibrium state. However, there is an upper boundary of the state. If the sea level rise is larger than this boundary, the system will not be able to reach its equilibrium state and finally degenerate.

To get deeper insight into the physical behavior in spatial scales, Dissanayake et al. (2012) set up a 2D process-based model over 110 years with schematized domain. Three scenarios, which

are no relative sea level rise (RSLR), RSLR and high RSLR were carried out. The existing flood dominant system continue to import sediment in the case of RSLR, while the tidal flats will eventually degenerate in the case of high RSLR. The trend is similar with results from Van Goor et al. (2003). However, their critical high RSLR rates are significantly different (0.2 m SLR by 2100 compared to 1990 by Dissanayake et al. (2012) and 10.5 mm/year by Van Goor et al. (2003)).

Differing from the work by Dissanayake et al. (2012), Van der Wegen (2013) use a 2D highly schematized model mimicking an elongated embayment which is Western Scheldt. They impose gradual sea leve rise at different time representing different initial bathymetry. After imposing SLR, the morphodynamic evolution has significant change. The intertidal area was drowned. As an exporting sediment basin, Western Scheldt shifts to import sediment. The decrease in intertidal area and the resulting M4 constituent contribute to the flood propagation. The sensitivity analysis reveals that the decrease of intertidal area is vulnerable to low tidal forcing and high SLR rate.

Van der Wegen et al. (2016) study the mudflat morphodynamics as well as the sea level rise impact on it. They combine observations and 1D process-based model to study a mudflat in South San Francisco Bay. Sea level rise is imposed after the model reach a relatively steady state. To adapt the sea level rise, accretion landward occurs and the mudflat profile grows similar to the profile before imposing sea level rise. However, when the sea level rise is too large, landward directed mudflat growth comes to a halt. it come to water depth at which the wind-waves are not able to stir sediment on the bed. If equilibrium state will be reached was still unclear. Elmilady et al. (2019) show that sea level rise made the mudflat intertidal area in San Pablo Bay, California alter from erosion to deposition.

1.3 Research Approach and Methodology

1.3.1 Main Objective

The aim of this thesis is to determine the wind-waves impact and sea level rise on long-term morphological change of estuarine evolution by application of a process-based numerical model.

1.3.2 Research Questions

To achieve the main objective, we propose two research questions:

(1) What is wind-waves impact on the long-term morphological change of estuarine shoals?

(2) Under the sea level rise, what is wind-waves impact on the long-term morphological change of estuarine shoals?

1.3.3 Methodology

Strategy

In this thesis, a 2-D, process-based numerical model (Delft3D) is applied based on a realistic setting. It carries out a case study on shoal Van Ossenisse and its surroundings located in Western Scheldt. Shoal Van Ossenisse is selected for several reasons: (1) It is far away from seaward side and not affected by ocean waves. (2) It mainly consists of sand.

Our model setup covers the entire Western Scheldt. In this way, we are able to provide shoal Van Ossenisse with an estuarine environment to ensure a realistic bathymetry, hydraulic conditions and sediment transport.

All scenarios are executed in no wave and wave case. No wave case includes local wind without generating waves in the flow. Wave case not only includes local wind but also the generates waves. By doing this, impact of waves is isolated.

Modelling tool

This thesis relies on process-based model Delft3D (version 4) as a virtual laboratory. Morphological update is applied in this model. Sediment transport caused by hydrodynamics leads to the change of bed topography, which in turn changes hydrodynamics. Hydro-morphodynamics interaction is displayed in figure. A flow-wave coupled calculation is implemented in this model with waves imposed in shoal Van Ossenisse and its surroundings.

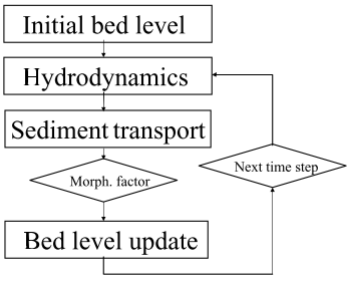

Figure 1.2: Morphology update scheme (Van der Wegen et al., 2008)

Evaluation

To answer research question (1), simulations of 50-year morphological change are executed in wave and no wave cases. Parameters which are listed below are compared over time to observe the wind-waves impact on estuarine shoal morphology.

- Bathymetry maps
- Hypsometry curve
- Intertidal area; intertidal volume; channel area; channel volume

Suspended sediment concentration, bed shear stress, residual sediment transport, flow velocity are assessed to understand the governing process behind the observations.

To answer question (2), sea level rise is imposed at seaward side boundary from initial time. Simulations of 100-year morphological change are executed in wave and no wave cases under different sea level rise. Parameters similar to list above are compared to observe the morphological difference induced by waves under sea level rise.

Chapter 2

Study Area

2.1 General

The Netherlands is situated at the North Sea, in the deltas of the rivers Rhine, Meuse and the Scheldt. Its coast system is divided into three types of coasts: the Delta coast with various estuaries in the Southwest delta area, the Hollland coast and the Wadden coast with a series of Wadden Sea tidal inlets in the North. Western Scheldt is located along the lower part of the Zeeschelde (Sistermans and Nieuwenhuis, 2004).

The Western Scheldt is one of the youngest natural estuaries in Western Europe. It is a funnel-shaped mouth of river Scheldt where the tide can be felt up to Ghent, located around 160km upstream. The part of the estuary between Ghent and Dutch-Belgian border is called Sea Scheldt. From this border to seaward side is a system of channels and shoals with an area of about 370 km^2 and length about 60km. Its cross-section decreases exponentially from the estuary mouth at Vlissingen with around 5km wide to the estuary head near Gent with around 1km wide. The width-averaged depth decreases from about 15 m at Vlissingen to 3 m at Gent. The width of the estuary reduces from 6 km at the mouth to less than 100 near Gent.

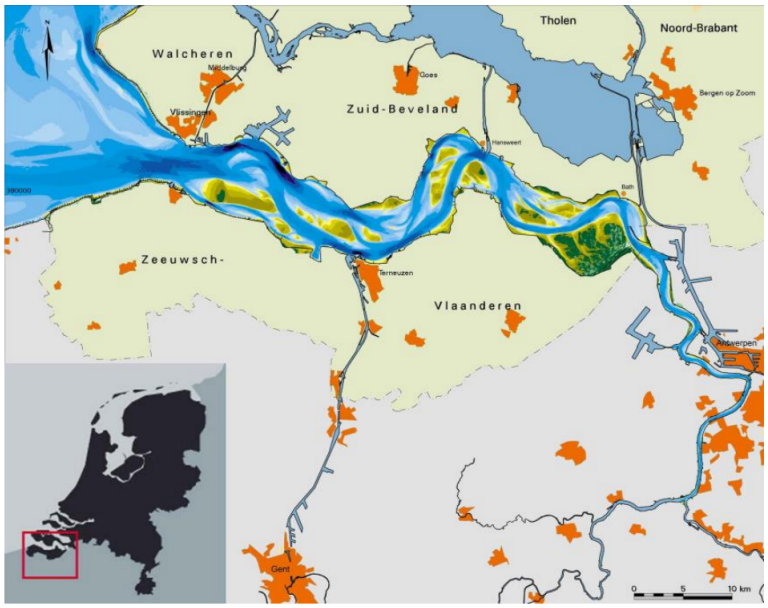

Figure 2.1: Overview of the Western Scheldt estuary (Van der Werf and Briere, 2013)

2.2 Hydrodynamic Characteristics

Work from Kuijper et al. (2004) showed the major hydrodynamic characteristics. The annual-averaged discharge from River Scheldt at the confluence of the Rupel and the Scheldt amounts to 110 m^3/s. The variation from year to year ranges from 50 to 200 m^3/s. The tidal wave is semi-diurnal with a mean tidal range of 3.8 m at Vlissingen, 5.2 at Rupelmonde and 1.9 at Gent. The most important tidal components are semi-diurnal (with a period of 12h25m) and quarterly diurnal tides (with a period of 6h21m) Wang et al. (2002). The ratio between the rise and fall time of the tidal wave is 0.88 at Vlissingen, 0.75 at Rupelmonde and 0.39 at Gent, which shows the asymmetry of the vertical tide. The range of the maximum flow velocities in the main channels is between 1 and 1.5 m/s.

2.3 Historical Morphological Change

It is the seaward marine section (60 km) of the tide-dominated Scheldt estuary, which has a length of 160 km and stretches up to the source of river Scheldt in Gent, Belgium. During Holocene evolution, this area once had been part of the North Sea, but silted up completely by BC 3100. It changed to peat bog area and was dissected by river Scheldt. From around AD 200, this area was gradually deteriorated, and large estuaries and tidal basins were formed (DHV,

2004). According to the phenomenological analysis (Van der Spek, 1994), the first historical data on the Scheldt estuary dating from AD 1000, during that time, the estuary was wide and shallow, though much smaller. In the next five centuries, storms, floods, subsidence and a continuing sea level rise leads to a rapid increasing size of Western Scheldt. Peat mining activities aggravated this change. In this period, the present sinusoidal plan and major channel system were formed. Figure 2.2 showed the evolution of it from 1650 to 1968. Embankments prevented it from erosion, and land formation from salt marsh evolution results in the gradually decreasing size (Toffolon and Crosato, 2007).

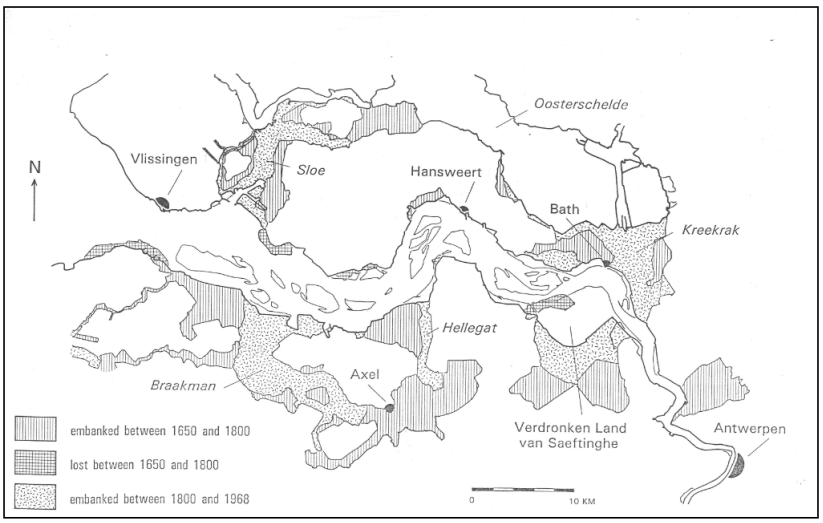

Figure 2.2: Western Scheldt evolution during period from year 1650 to 1968 (Toffolon and Crosato, 2007)

Western Scheldt is a multiple channel system. Ebb channels and flood channels are separated by intertidal shoal (Van Veen, 1950). The ebb channels display meandering characters, while the flood channels are straighter. The maximum velocity of ebb flow occurs near mean sea level (MSL), while the maximum velocity of flood flow occurs one hour before high water (Van den Berg et al., 1996). The requirement of continuity conservation results in deeper ebb channels (Van den Berg et al., 1996).

During the period year 1878 to 1952, the Western Scheldt imported sediment from the sea with an annual-averaged amount of 1.3 $Mm^3/year$. Since 1955, alternating period from sand import to sand export took place which is related to 18.6 year nodal tidal variations caused by astronomical phenomena (Van der Wegen and Roelvink, 2012). The sand balance is determined by nature erosion and sedimentation and human interventions which include dredging, dumping and sand mining.

In the period from 1860-1970, some minor dredging activities took place in the navigation channel in the eastern part of the estuary. Despite of this, the morphology of Western Scheldt changed significantly during that period. The steady tidal forcing at the mouth and the limited sea level rise seems not to be the cause of this morphological change, it is more likely that the changes before 1860 results in the morphological development with the response to its own system (Dam et al., 2016). Two major dredging activities took place in the periods 1970-1974 and 1998. Deepening of the navigational channel has been carried out to allow vessels with greater draught to enter the port of Antwerp (Dam and Labeur, 2008). Large amount of mud have been removed from the Lower Sea Scheldt since 1992 Toffolon and Crosato (2007). Dredging events from that time have significant impacts on the morphological change of Western Scheldt. Between 1800 and 1980, the estuary is narrowed by embankment.

2.4 Morphological Change between 1963-2013

Figure 2.3 displays names of channels and shoals in Western Scheldt for the convenience of description. These names will be used to describe the estuary within the whole report.

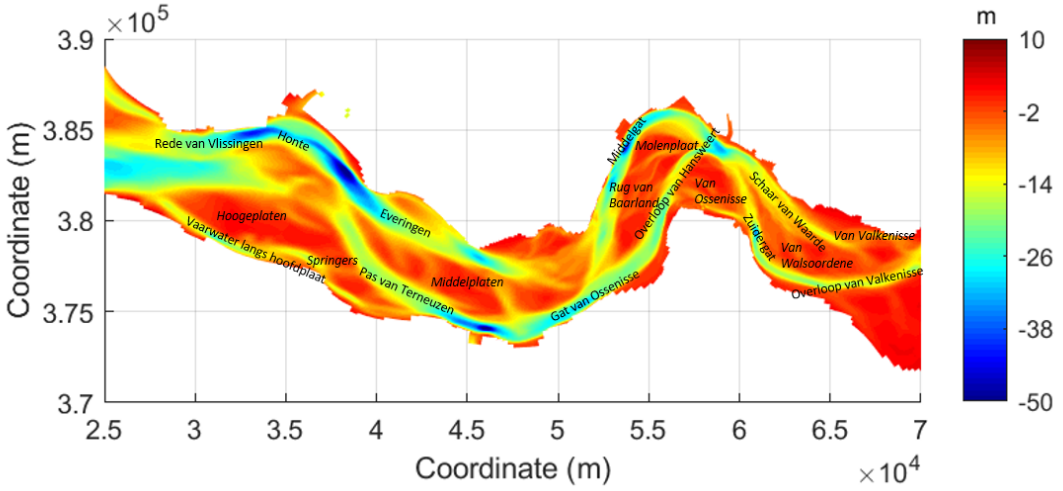

Figure 2.3: The Western Scheldt in 1963 with channel names and shoal names

During the period of our simulation time 1963-2013, the morphological change of Western Scheldt is due to natural development and human impacts. According to previous literature review, from 1963-1970, the morphology is more based on natural development toward the way of energy dissipation (Van der Wegen et al., 2008), while from 1970-2013, human interventions have huge impacts. In the 1970's and 1990's, a first and second deepening of the navigation channel have

been carried out. Near the head of the Western Scheldt, i.e. the area between Hansweert and Doel is significantly influenced by dredging and dumping activities Wang et al. (2002). At the seaward side of estuary, between Vlissingen and Hansweert, the natural processes dominated the channel and shoal evolution until 1997 (Wang et al., 2002).

Figure 2.4 shows the observed and measured bathymetry evolution during 1963-2013. In the following part, the morphological behavior of channels and shoals will be discussed from eastern to western part of the estuary.

The most eastern-located part of the estuary in figure 2.4 consists of ebb channel Zuidergat and Overloop van Valkenisse, and main flood channel Schaar van Waarde and Van Valkenisse (Van den Berg et al., 1996). Channel Zuidergat and Overloop van Valkenisse is getting deeper over time mainly due to the dredging processes.

Part of the dredged sediment is dumped to the shoal between Schaar Van Walsoordene, and the visible elevation of the shoal height can be also explained by this partly. Since 1980s, the flood channel Schaar van Waarde had a small channel extending toward the shoal. With the growing length, this small channel finally took over the main channel and large volume of tidal discharge. This resulted in a huge sedimentation in the old channel. Apart from the major channel located to the north of shoal Van Ossenisse, there used to be a second connecting channel between channel Zuidergat and Overloop van Hansweert in 1960s. With more tidal discharge into the main channel, this second channel experienced sedimentation.

The middle of the estuary displayed in figure 2.4 (between x-coordinates 45 and 55 km) shows a very dynamic morphological change. In 1960s and 1970s, the major channel connected Middelgat with Gat van Ossenisse existed. However, the bend cut-off became dominant and generated a small connecting channel (Van den Berg et al., 1996) between Middelgat and Everingen. Until 2013, the direction of channel Middelgat still has the tendency towards north, although it is limited by embankment. The shoal volume on Rug van Baarland increased due to the migration of Middelgat and dumping events. The location of Gat van Ossenisse is stable during this whole period, probably because of the enhancement from dredging activities. The channel system of Everingen and Pas van Terneuzen is very stable (Van den Berg et al., 1996). During period 1965-1990, the volumetric changes between them is no more than 6% (Van den Berg et al., 1996). Shoal Middelplaten shows dynamic evolution. Small connecting channels are generated at the outlet of the ebb channel Pas van Terneuzen.

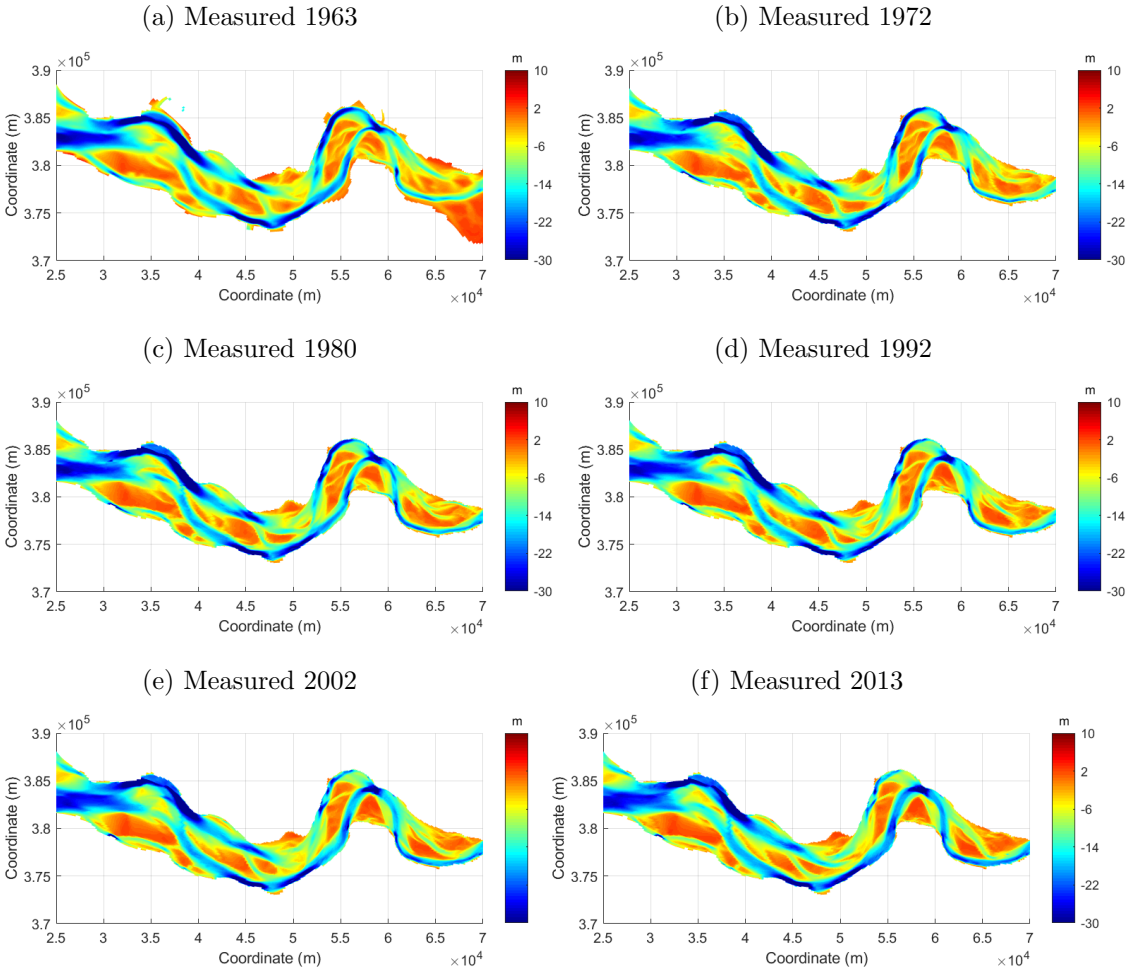

Figure 2.4: Bathymetry from year 1963-2013

2.5 Sediment

With respect to the elevation relative to the vertical tide, the various morphological features in the Western Scheldt can be distinguished into three parts: sub tidal areas, intertidal areas and salt marshes. The sediment composition in the Western Scheldt is mainly sand with less than 10 % mud in the channels and on the shoals. Alongside the estuarine margins, at the intertidal areas and salt marshes, the percentage of mud is much larger. Figure 2.5 (Kuijper et al., 2004) gives an illustration of medium grain size (d_{50}) distribution in our study area. It can been seen that coarse sediment is mainly distributed in the channels, whereas fine sediment is found on shoals. d_{50} in shoal Van Ossenisse varies from $120\mu m$ to $250\mu m$.

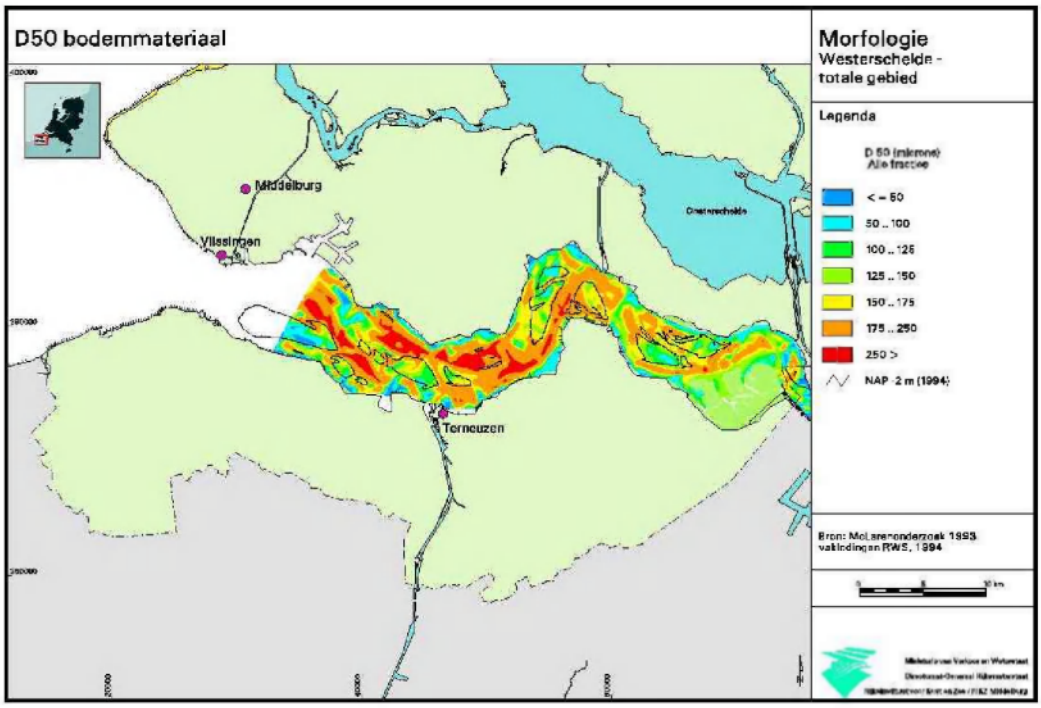

Figure 2.5: Medium grain size distribution (Kuijper et al., 2004)

The subsoil layer in Western Scheldt consists of both erosive and non-erosive layers. Layers consisting of Pleistocene layers, peat layers and highly consolidated clay are considered as non-erodible layer in this study. To model the morphological change, the thickness of erosive layer should be very clear. The level of non-erodible layer plus erodible sediment thickness is actual measured bed level. Following work by Van de Male (2004) and Dam (2013), non-erodible layer and sediment thickness is displayed in figure 2.6.

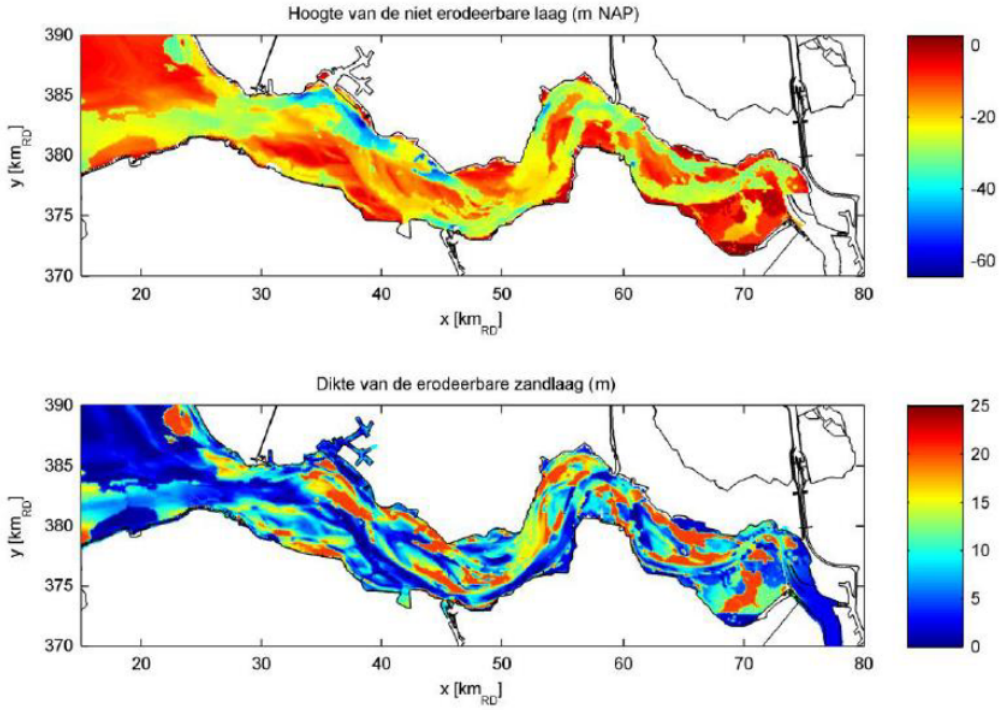

Figure 2.6: Height of the non-erodible layer wrt MSL (upper panel) and thickness of the erodible sand layer (Eindrapport, 2013)

2.6 Wind conditions

This model considers the local wind-wave impacts in shoal Van Ossenisse. The local and prevailing wind conditions determine the main wave climate. The main part of Western Scheldt is located in northern hemisphere at latitude of 51° and longitude around 3°. Due to the uneven atmosphere pressure distribution and Coriolis force, Western Scheldt is mainly subject to westerly winds with some seasonal variation (Van Rijn, 2012).

Chapter 3

Model

A process-based model Delft3D is applied here. It is an integrated flow and transport model system developed by Deltares. Many modules can be obtained from it to investigate different aspects of water system. In this research, Delft3D-Flow module including morphodynamic change coupled with Delft3D-Wave module is applied to calculate current-wave interaction. More information is referred to Delft3D Manual.

3.1 Model description

3.1.1 Hydrodynamic model

Delft3D-Flow solves the Navier Stokes equations for incompressible fluid, under the shallow water and the Boussinesq assumptions. In this research, we focus on 2D depth-averaged hydrodynamic equations, derived by integration over the total depth. The continuity equation is given by:

$$\frac{\partial \zeta}{\partial t} + \frac{\partial h\bar{u}}{\partial x} + \frac{\partial h\bar{v}}{\partial y} = Q \tag{3.1}$$

Where, U and V is the depth averaged velocities, Q is the source term or sink term.

The momentum equations in x- and y-direction are given by:

$$\frac{\partial \bar{u}}{\partial t} + \bar{u}\frac{\partial \bar{u}}{\partial x} + \bar{v}\frac{\partial \bar{u}}{\partial y} + g\frac{\partial \zeta}{\partial x} - fv = -c_f \frac{\bar{u}\sqrt{\bar{u}^2 + \bar{v}^2}}{h} + \nu_e(\frac{\partial^2 \bar{u}}{\partial x^2} + \frac{\partial^2 \bar{u}}{\partial y^2}) + M_x \tag{3.2}$$

$$\frac{\partial \bar{v}}{\partial t} + \bar{v}\frac{\partial \bar{v}}{\partial x} + \bar{u}\frac{\partial \bar{v}}{\partial y} + g\frac{\partial \zeta}{\partial y} + fu = -c_f \frac{\bar{v}\sqrt{\bar{u}^2 + \bar{v}^2}}{h} + \nu_e(\frac{\partial^2 \bar{v}}{\partial x^2} + \frac{\partial^2 \bar{v}}{\partial y^2}) + M_y \tag{3.3}$$

$$\tag{3.4}$$

in which
ζ water level with respect to datum, m;
h water depth, m;
$\bar{u}$ depth averaged velocity in x direction, m/s;
$\bar{v}$ depth averaged velocity in y direction, m/s;
g gravitational acceleration, m^2/s;
c_f friction coefficient;
ν_e eddy viscosity, m^2/s;
f Coriolis force, depending on the geographic latitude and the angular speed of rotation of the earth;
M_x and M_y contributions due to external sources or sink of momentum (discharge of water and wave stresses in this research).

In 2D depth-averaged model, since the vertical profile of horizontal velocity is not solved, the eddy viscosity is also not solved by turbulence closure model like in 3D model. In our model, the horizontal eddy viscosity coefficient is defined by the user-defined background horizontal viscosity in the input file. It represents 2D turbulence and dispersion coefficient.

3.1.2 Sediment transport and morphodynamic model

The sediment transport formula in this model is Van Rijn (1993). This formula distinguishes suspended load transport and bed load transport according to a reference height and can be used in the situation with waves. Bed load transport vector is determined by three parts: near-bed current, waves in the direction of wave propagation, and wave asymmetry effects on the suspended sediment transport. Bed slope effect is also used to correct bed load transport.

Suspended load transport

The transport of suspended sediment is solved by 2D advection-diffusion equation for the suspended sediment concentration, which is formulated as:

$$\frac{\partial hc}{\partial t} + \Delta \cdot (h\mathbf{u}c) = \Delta \cdot (h\kappa \Delta c) + hs \tag{3.5}$$

in which
κ diffusion coefficients,m^2/s;
c mass concentration of sediment, kg/m^3;
$uandv$ velocity components, m/s;
$\epsilon_{s,x}\epsilon_{s,y}$ eddy diffusivity of sediment, m^2/s;
w_s sediment settling velocity, m/s.

The flow velocity and eddy diffusivity are based on solutions of the hydrodynamic equations. Similarly, for 2D simulations, the horizontal eddy diffusivity include dispersion by the vertical variation of the horizontal flow solved by Horizontal Large Eddy Simulations (HLES approach), and user-defined horizontal background diffusion coefficient. In our research, only the latter is applied.

Since the user-defined sediment diameter D_50 multiplie the factor for suspended sediment(FACDSS) is $200mm \times 1 = 200mm$, the settling velocity of non-cohesive sediment is computed using the following formulation:

$$w_{s,0} = \frac{10\nu}{D_s}(\sqrt{1 + \frac{0.01(s-1)gD_s^3}{\nu^2}} - 1) \tag{3.6}$$

in which
s relative density ρ_s/ρ_w of sediment fraction;
D_s representative diameter of sediment factor, $D_s = D_50 \times FACDSS$;
ν kinematic viscosity coefficient of water, m^2/s;
$w_{s,0}$ the 'basic' sediment fraction specific settling velocity.

Rouse profile between the reference level a and the center of kmx-layer (reference layer) is provided to represent the sediment concentration distribution:

$$c_{kmx} = c_a(\frac{a(h - z_{kmx})}{z_{kmx}(h-a)})^A \tag{3.7}$$

in which
c_{kmx} concentration of sediment in the center of the kmx layer, calculated from advection-diffusion equation, kg/m^3;
c_a reference concentration of sediment, kg/m^3;
a Van Rijn's reference layer, and Van Rijn (1993) is used in this model, m;
h water depth, m;
z elevation of the center of the kmx layer, m;
A Rouse number.

In this model, reference concentration c_a is computed by Van Rijn (1993) approach. It is highly

related to bed-shear stress induced by currents and waves. The expression is given by:

$$c_a = 0.015\rho_s \frac{D_{50(T_a)^{1.5}}}{a(X_*^{0.3})} \tag{3.8}$$

in which
T_a non-dimensional bed-shear stress;
D_* non-dimensional particle diameter;
a elevation of reference level.

With the known reference concentration (from Van Rijn 1993) and the concentration in the center of the kms layer, the concentration and the concentration gradient at the bottom of the kmx layer are calculated:

$$c_{kml}(bot) = c_a(\frac{a(h - z_{kmx(bot)})}{z_k mx(bot)(h-a)})^A \tag{3.9}$$

$$\frac{\partial c_{kmx(bot)}}{\partial z} = Ac_a(\frac{a(h - z_{kmx(bot)})}{z_{kmx(bot)(h-a)}})^{A-1} \times (\frac{-ah}{z_{kmx(bot)^2}(h-a)}) \tag{3.10}$$

By knowing the concentration gradient at the bottom of the kmx layer in equation 3.10 the upward diffusion of sediment through the bottom of the kmx layer is given:

$$E = \epsilon_s \frac{\partial c}{\partial z} \tag{3.11}$$

By using bottom kmx layer as reference level of erosion or deposition flux to the flow, the erosive flux due to upward diffusion can be distinguished to source term and sink term:

$$Source_{erosion} = \frac{\alpha_2 \epsilon_s c_a}{\Delta z} \tag{3.12}$$

$$Sink_{erosion} = \frac{\alpha_2 \epsilon_s c_{kmx}}{\Delta z} \tag{3.13}$$

where α_2 is correction factor for sediment concentration.

In contrast to upward diffusion equation 3.11, the settling of sediment through the bottom of the kmx layer is given:

$$D = w_s c_{kmx(bot)} \tag{3.14}$$

where c_kmx is obtained from equation 3.9.

Therefore, the deposition sink term is:

$$Sink_{deposition} = \alpha_1 c_{kmx} w_s \tag{3.15}$$

Combined with erosion source and sink term in equation 3.12 and 3.13, the total source term and sink term is given by:

$$Source = \alpha_s c_a (\frac{\epsilon_s}{\Delta z}) \tag{3.16}$$

$$Sink = [\alpha_2 (\frac{\epsilon_s}{\Delta z}) + \alpha_1 w_s] c_{kmx} \tag{3.17}$$

with α_a and α_2 correction factors from equation 3.9 and equation 3.10.

Bedload transport

Bedload transport is important for sand sediment transport. Distinguished with mechanisms of suspended load transport, bedload transport is driven by shear stress inserting on the grain. In this research, wave is included, so the bedload transport is caused by currents and wave. In addition, suspended load due to waves is treated as bedload transport in Van Rijn (1993) formula. In conclusion, this model consists of three transport components that are treated as bedload:

- bedload due to currents, $S_b c$
- bedload due to waves, $S_b w$
- suspended load due to waves, $S_s w$

The bedload transport rate magnitude is computed as:

$$|S_b| = 0.006 \rho_s w_s D_{50} M^{0.5} M_e^{0.7} \tag{3.18}$$

$$M = \frac{v_{eff}^2}{(s-1) g D_{50}} \tag{3.19}$$

$$M_e = \frac{(v_{eff} - v_{cr})^2}{(s-1) g D_{50}} \tag{3.20}$$

$$v_{eff} = \sqrt{v_R^2 + U_{on}^2} \tag{3.21}$$

in which
S_b bedload transport rate, $kgm^{-1}s^{-1}$;
M sediment mobility number due to waves and currents;
M_e excess sediment mobility number;
v_{cr} critical depth averaged velocity for initialtion of motion (based on a parameterisation of the Shield curve), m/s;
v_R magnitude of an equivalent depth-averaged velocity computed from the velocity in the bottom computational layer, assuming a logarithmic velocity profile, m/s;
U_{on} near-bed orbital velocity in onshore direction based on the significant wave height, m/s.

As equations display, the non-linear combination of current and wave velocity determine the bedload transport rate magnitude.

The direction of bed load transport due to current ($S_{b,c}$) acts in the direction of the near-bed current, and which due to waves ($S_{b,w}$) acts in the direction of wave propagation. By knowing the total bedload transport due to current and wave and the angle between them, the two components are determined as follows:

$$S_{b,c} = \frac{S_b}{\sqrt{1 + r^2 + s|r|cos\phi}} \tag{3.22}$$

$$|S_{b,w}| = r|S_{b,c}| \tag{3.23}$$

$$r = \frac{(|U_{on}| - v_{cr})^3}{|v_R| - v_{cr}^3} \tag{3.24}$$

Suspended sediment transport due to wave asymmetry effects is also treated as bedload transport in this model. Its transport direction is equal to the wave propagation direction. It is calculated using an approximation method proposed by Van Rijn (2001):

$$S_{s,w} = f_{SUSW}\gamma U_A L_T \tag{3.25}$$

$$U_A = \frac{U_{on}^4 - U_{off}^4}{U_{on}^3 + U_{off}^3} \tag{3.26}$$

$$L_T = 0.007\rho_s D_{50} M_e \tag{3.27}$$

in which
$S_{s,w}$ wave-related suspended transport rate, $kgm^{-1}s^{-1}$;
f_SUSW user-defined tuning parameter;
γ phase lag coefficient.

$S_{b,c}$, $S_{b,w}$ and $S_{s,w}$ are imposed separately. By knowing their magnitude (equations 3.22, 3.23 and 3.25) and directions, the total bedload transport in this model can be computed.

Adjustment of bedload transport

Sediment bedload transport is not only determined by current and wave shear stress, but also influenced by bed slope gradient. In this model, two bedload transport directions caused by bed slope gradient are applied to adjust the bedload transport: the slope in the direction of unadjusted transport and the direction perpendicular to that.

The sediment transport rate results from longitudinal bed slope is given by:

$$\overrightarrow{S_b'} = \alpha_s \overrightarrow{S} \tag{3.28}$$

where

$$\alpha_s = 1 + \alpha_{bs}\left(\frac{tan(\phi)}{cos(tan^{-1}(\frac{\partial z}{\partial s}))(tan(\phi) + \frac{\partial z}{\partial s})} - 1\right) \tag{3.29}$$

in which
$\overrightarrow{S}$ unadjusted sediment transport vector, $m^3m^{-1}s^{-1}$;
$\overrightarrow{S^{-1}}$ adjusted sediment transport vector, $m^3m^{-1}s^{-1}$;
α user-defined coefficient;
ϕ internal angle of friction of bed material;
$\frac{\partial z_b}{\partial s}$ bed slope in longitudinal direction.

The sediment transport rate perpendicular to the unadjusted sediment transport direction is given by:

$$S_n = |\overrightarrow{S'}|\alpha_{bn}\frac{u_{cr}}{|\overrightarrow{u}|}\frac{\partial z_b}{\partial n} \tag{3.30}$$

in which
S_n additional bedload transport vector. The direction is normal to the unadjusted sediment transport direction, in the down slope direction, m^3m^{-1};
α_{bn} user-defined coefficient;
u_{cr} critical depth-averaged velocity, m/s; $\overrightarrow{u}$ near-bed fluid velocity vector, m/s; $\frac{\partial z_b}{\partial n}$ bed slope in the direction normal to the unadjusted sediment transport vector.

The resulting adjusted sediment transport vector is calculated by:

$$\overrightarrow{S_r} = \overrightarrow{S'} + \overrightarrow{S_n} \tag{3.31}$$

Morphological updating

The bed level elevation is updated at each hydraulic computational time step. The next time step hydraulic computation depends on the outcome of the newest bed level. In other words, hydraulic conditions are influenced by the updated morphological conditions and vice versa.

At each time step, the mass of bed material is changed due to the sediment sink and source and spatial gradients in sediment transport rates. According to the density of bed material, the bed level variation is translated by the change of mass.

To accelerating morphological change, morphological time scale factor is set by user. This technique multiplies the bed level change each time step with a factor to enhance bed level development. It is generally allowed as long as bed level changes in a timestep do not exceed 5% of the water depth.

3.1.3 Wave model

The Delft3D-Wave model is based on the SWAN model developed by Delft University of Technology. SWAN model describe waves with the two-dimensional wave action density spectrum, which is energy density divided by the relative frequency. The balance equation of wave action density spectrum reads:

$$\frac{\partial}{\partial t}N + \frac{\partial}{\partial x}c_x N + \frac{\partial}{\partial y}c_y N + \frac{\partial}{\partial \sigma}c_\sigma N + \frac{\partial}{\partial \theta}c_\theta N = \frac{S}{\sigma} \tag{3.32}$$

The term in right-hand side is the source term associated with wave processes: Generation by wind; dissipation by whitecapping, bottom friction and depth-induced breaking; non-linear wave-wave interaction.

In this model, Delft3D-Flow module and Delft3D-Wave module is online coupled. Flow has an impact on wave in terms of set-up, while waves has the effect on flow in terms via bed shear stress and wave-induced current. Wave module reads the results of Flow module from the previous time step in terms of water level, bathymetry and wind field. The results of Flow module is the input data of Wave module, but by the spatial interpolation from flow computational grids to wave computational grids. After calculation, Wave module provide results to Flow module also by spatial interpolation between computational grids.

3.1.4 Wave-current interaction

In shallow water area, waves play a very important role because of the following processes:

- The vertical mixing processes are enhanced due to turbulence generated near the surface by whitecapping and wave breaking, and near the bottom due to energy dissipation in the bottom layer.
- A net mass flux is generated which has some effect on the current profile, especially in cross-shore direction.
- In the surf zone long-shore currents and a cross-shore set-up is generated due to variations in the wave-induced momentum flux (radiation stress). In case of an irregular surf zone, bathymetry strong circulations may be generated (rip currents).
- The bed shear stress is enhanced; this affects the stirring up of sediments and increases the bed friction.

Stokes drift is applied in 2D model when it is used in Delft3D-MOR (take morphological process).

In my model, my wave module does not receive current from flow by turning on 'flow current unextended'.

3.2 Model Configurations

3.2.1 Basic Nevla model

It is based on NEVLA model developed by Deltares. It is well-calibrated for the hydrodynamic condition and is previously implemented in morphodynamic investigations.

NeVla model has been developed by Deltares to cover the entire Western Scheldt (from Gent to seaward side). Model from (Van der Wegen et al., 2017) applies the NeVla model in 2D with only sandy sediment but includes wind waves at estuary mouth and dredging operations. This modified model assesses the skill of Delft3D model in hindcasting morphological change between 1963 and 2011 for the whole Western Scheldt emphasizing on its mouth.

In our study, our main focus is shoal Van Ossenisse, so we did some adjustment for this modified model based on our requirements.

- Wind waves at estuary mouth is removed to save computational cost.
- Wind waves at shoal Van Ossenisse is applied.
- Grid size out of the domain with shoal Van Ossenisse is derefined and turned to not give significant difference.

- Modified model from (Van der Wegen et al., 2017) is separated into two time period parts, since the breakwater in Port Zeebrugge was reconstructed during the middle time. While our focus is shoal Van Ossenisse, so we didn't divide the simulation time. Instead, we use old breakwater throughout the whole simulation.

3.2.2 Computational grids

This model is a coupled flow and wave model. The flow model consists of five composition domains by using Parallel calculations. Multiple cores will be used automatically to reduce computational time. Within these five domains, four domains have relatively coarse grid with maximum grid size of 800m in most seaward side, and the domain with Van Ossenisse has maximum grid size of 160m in the outer bend and minimum size of 20m in the inner band. The average resolution over Van Ossenisse is around 40m. The total grid number is 583×1148. The seaward boundary is extended to 20 km from coastline and landward boundary ends up in Gent. The five flow domains are demonstrated in figure 3.1.

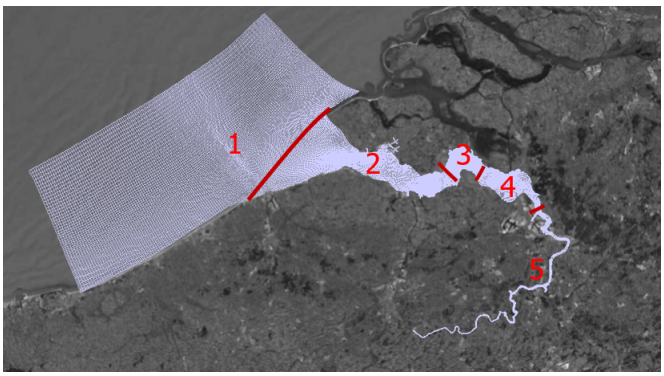

Figure 3.1: Flow computational grid

The wave computational grid (figure 3.2) covers the whole flow domain 3 and extends with the same grid resolution as domain 3. Therefore, a couple flow-wave calculation is executed in domain 3.

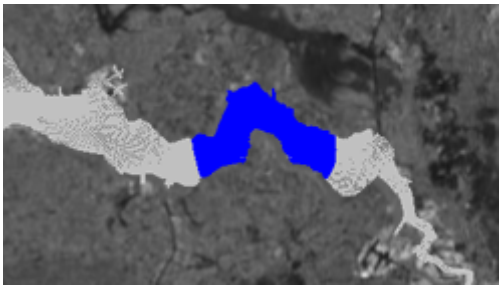

Figure 3.2: Wave computational grid

3.2.3 Boundary and initial conditions

Hydrodynamic forcing

The hydrodynamic boundary conditions consist of tide and river boundaries. 32 tidal constituents of 2011 conditions were applied into ZUNO model and the results are nested and bi-linear interpolated along the open boundaries of domain 1. The dominant tidal constituents are N2 (Larger lunar elliptic semidiurnal constituent), M2 (Principal lunar semidiurnal constituent), L2 (Smaller lunar elliptic semidiurnal constituent), S2 (Principal solar semidiurnal constituent). The sum of these sinusoidal curves with phase difference yields a spring-neap tide cycle. Spring tides occur twice each lunar month (new moon and full moon). The open boundaries in domain 1 are Riemann invariant in the northwest and currents in the southwest and northwest. River boundaries are constant discharge from two locations. One is 10 m^3/s from Niel, Belgium, and the other one is 5 m^3/s from Gent.

The hydrodynamic simulation time is six months. With morphological factor equal to 104, the morphodynamic simulation time is 50 years.

The boundary conditions in wave model stay in constant 0 m water level. Waves are only generated by wind. Wind speeds analyzed in previous chapter are applied.

Initial bed level and sediment availability

The initial bed level was derived from measured data of the year 1963. The erodible sediment thickness was derived by adopting the erodible sediment thickness of year 2011.

3.2.4 Dredging and dumping process

Figure 3.3 displays dredging and dumping area in this model. Dredging activities is mainly located in channel and dumping sites are on shoals. Dredging activities in this model are achieved by defining time-varying minimum water depth inside polygons. To reduce the complexity of results analysis, modification is carried out by removing dumping sites in shoal Rug van Baarland to outside of Western Scheldt. Proportion of dredged sediment is assigned into specific polygons of dumping sites. Detailed description is in Appendix A.

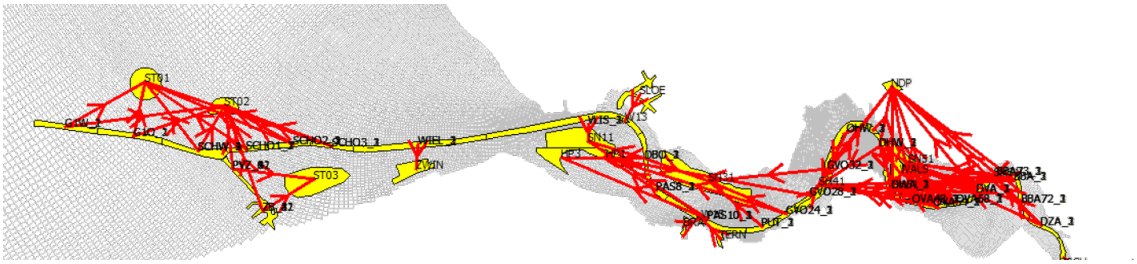

Figure 3.3: Dredging and dumping polygons in the model

3.2.5 Wind conditions

Wind data with 10 minutes interval detected from a wind station located in Port Terneuzen is chosen to simulate wind climate over shoal Van Ossenisse. It covers data of 18 years from 1999 to 2017 with a few years absent. A wind rose (figure 3.4) is obtained after processing wind data. It is clear that there are three dominant wind directions in this area from southwest, northeast and northwest, respectively. Based on this, wind condition is divided to three sections with different weight, the boarder is demonstrated in figure 3.4. Wind is most popular from southwest, accounting for 56.57%. Wind speed in different sections mainly lays between 3 m/s to 7 m/s. By estimating probability density function from Kernel density estimation, we choose wind speed and direction with highest probability in each section as dominant wind conditions. It is listed in table 3.1.

(a) Wind gauge station

(b) Wind Rose

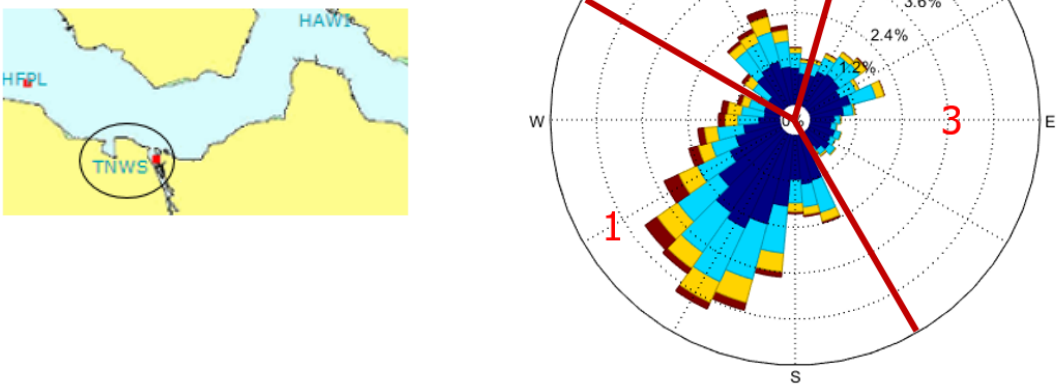

Figure 3.4: Wind rose of station TNWS

Wind conditions in these 5 scenarios is presented in table 3.1.

Table 3.1: Wind conditions with wind speed, wind direction (with reference to north) and weight

Wind condition	Wind range	Wind speed	Wind direction	Weight
Condition 1	150° - 300°	4.59m/s	207°	56.57%
Condition 2	15° - 150°	3.68m/s	70°	25.90%
Condition 3	300° - 15°	4.60m/s	340°	17.53%

3.2.6 Other model settings

Table 3.2: Other model parameters

Parameter	value
Dimensions	2D
Timestep	15s
Hydraulic forcing	nested from ZUNO model; all astronomic constituents
Wave communication interval	1 hour
Sediment transport formulation	Van Rijn (Delft3D default)
Sand diameter	120 μm
Transverse bed slope factor	40
Streamwise bed slope factor	1
Roughness	Spatial-varying manning
Hydraulic runtime	73 days
Morphological factor	104
Morphological runtime	50 years (1963-2013)

3.2.7 Sea level rise

RCP stands for 'Reprensentative Concentration Pathway'. It is used to predict climate change by seeing human's lifestyle behave in the future. In our study, initial boundary conditions are water level time series of year 2011. Ending boundary conditions are predicted water level under sea level rise after 100 years. RCP45 and RCP85 are modelled to predict global sea level rise. With 50^{th} percentile, they results in 96cm and 167cm global sea level rise. These numbers are used to derive the boundary water level in our model by using Delft3D Flexible Mesh Global Tide and Surge Model (GTSM). These results in respective 110cm and 195cm sea level rise in NeVla model boundary. With the initial boundary water level and ending boundary water level (after 100 years), we could get boundary condition over time by interpolation. Under each sea level rise, we assume a linear increase and an exponential (sinusoidal) increase (figure 3.5).

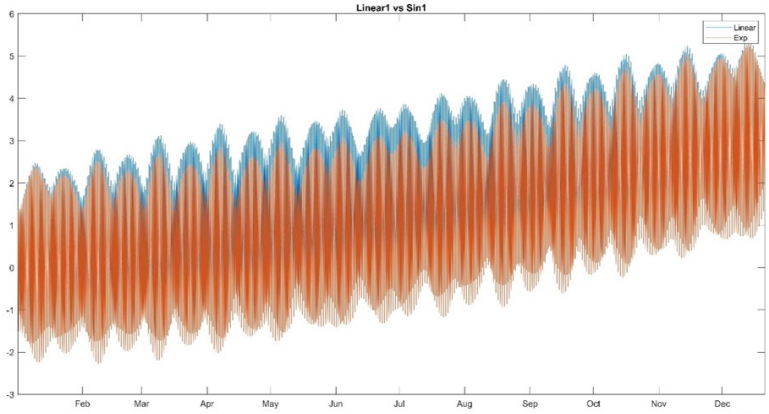

Figure 3.5: Sea level rise signal (source: Sea level rise scenarios Westernscheldt estuary, B. R. Röbke, M. v. d. Wegen H. Elmilady)

3.2.8 Scenario Description

Wind wave impact

Starting from a real bathymetry of year 1963, we performed 50-year simulations. Wind climate analyzed in section 3.2.5 shows three dominant wind conditions. We hence prescribe three wind conditions to investigate small local wind-waves impact on morphological change of estuary (mainly in the area where shoal Van Ossenisse is located). In total, 8 scenarios are carried out (see table 3.3). Scenario 1, 2 and 3 include flow and wind impact with wind coming from single different directions over the whole flow computational domain. Corresponding to scenario 1, 2 and 3, scenario 4, 5 and 6 include flow and wind over the whole domain but also add wind-generated waves impact only in domain 3 along with different wind directions. Scenario 7 includes flow, wind under three wind conditions at the same time. Scenario 8 includes flow, wind and waves impact under three wind conditions at the same time, to mimic reality. Scenario 8 aims to be compared with observations and show model performance.

Table 3.3: Scenarios with and without waves

Scenario	Wind speed + wind direction
Scenario 1 (no wave)	5m/s + 70°
Scenario 2 (no wave)	5m/s + 207°
Scenario 3 (no wave)	5m/s + 340°
Scenario 4 (wave)	5m/s + 70°
Scenario 5 (wave)	5m/s + 207°
Scenario 6 (wave)	5m/s + 340°
Scenario 7 (no wave)	3.68m/s + 70°, 4.59m/s + 207°, 4.60/s + 340°
Scenario 8 (wave)	3.68m/s + 70°, 4.59m/s + 207°, 4.60/s + 340°

Sea level rise (version 1)

Starting from a real bathymetry of year 1963, we performed a 100-year run sea level rise. We aim to investigate wave impact in different sea level rise scenario. At each sea level, the rise is prescribed as an increase in the mean sea-level based on linear and sinusoidal function. At each case, simulations with no wave and corresponding wave are executed. Among these scenarios, we only consider single wind condition from direction 207°. Model settings remain the same as the previous one called 'Wind wave impact', apart from the sea level rise boundary conditions and the accidentally increased 0.5m M2 tidal forcing. Boundary conditions in this case is water level boundary at three sections at seaward side. The modifications compared to 'wind wave impact' scenarios are listed below. All scenarios are concluded as in table 3.4.

- 100 years morphological simulation time
- Increased 0.5m M2 tidal forcing
- Different type of boundary conditions (water level boundary)

Table 3.4: Sea level rise scenarios

Scenario	sea level rise
Scenario 1 (no wave)	0cm
Scenario 2 (no wave)	96cm linear
Scenario 3 (no wave)	96cm sinusoidal
Scenario 4 (no wave)	167cm linear
Scenario 5 (no wave)	167cm sinusoidal
Scenario 6 (wave)	0cm
Scenario 7 (wave)	96cm linear
Scenario 8 (wave)	96cm sinusoidal
Scenario 9 (wave)	167cm linear
Scenario 10 (wave)	167cm sinusoidal

Sea level rise (version 2)

In 'Sea level rise version 1', M2 tidal forcing is accidentally increased by 0.5m. Approaching the end of this thesis, new runs with corrected tidal forcing are finished. Since this preliminary work is also for the further research, an increased sediment grain size, new dumping activities are also implemented. Modifications compared to 'wind wave impact' scenarios are listed below. All scenarios are concluded as in table 3.5.

- 100 years morphological simulation time
- Including dumping site at shoal Rug van Baarland
- Different type of boundary conditions (water level boundary)
- D_{50}=200μm

Table 3.5: Sea level rise scenarios

Scenario	sea level rise
Scenario 1 (no wave)	0cm
Scenario 2 (no wave)	96cm sinusoidal
Scenario 3 (no wave)	167cm linear
Scenario 4 (no wave)	167cm sinusoidal
Scenario 5 (wave)	0cm
Scenario 6 (wave)	96cm sinusoidal
Scenario 7 (wave)	167cm linear
Scenario 8 (wave)	167cm sinusoidal

Sensitivity Analysis

Sensitivity analysis is carried out by investigating the impact of some parameters and to see if our conclusion is still maintained with the change of time, sediment diameter, and wind speed. A single wind condition (direction 207°) is used. Scenario 1 and 2 are basic run without and with waves. Scenario 3 and 4 show shoal evolution after a longer term (100 years). Since shoal Van Ossenisse is in a high-variation wind climate. A large proportion of wind speed is higher than 5m/s (figure 3.4). Scenario 1, 2, 5,6 show morphological change when increasing wind speed in a reasonable range. Impact of coarser sediment is presented in scenario 1, 2, 7 and 8.

Table 3.6: Scenarios for sentivity analysis

Scenario	Wind speed + direction	Simulation time	D_{50}
Scenario 1 (no wave)	5m/s + 207°	50 years	120μm
Scenario 2 (wave)	5m/s + 207°	50 years	120μm
Scenario 3 (no wave)	5m/s + 207°	100 years	120μm
Scenario 4 (wave)	5m/s + 207°	100 years	120μm
Scenario 5 (wave)	6m/s + 207°	50 years	120μm
Scenario 6 (wave)	7m/s + 207°	50 years	120μm
Scenario 7 (no wave)	5m/s + 207°	50 years	200μm
Scenario 8 (wave)	5m/s + 207°	50 years	200μm

Chapter 4

Results

4.1 Erosion and Sedimentation Patterns

This section aims to provide a brief comparison between the modeled and observed evolution in the Western Scheldt Estuary by visually examining the bathymetry after 50 years (figure 4.1) along with the cumulative sedimentation/erosion patterns between 1963 and 2013 (figure 4.2). The model skill varies over the modeled domain. There are significant differences but also resemblances. The western part near the mouth of the estuary (between x-coordinates 25 and 40 km) is very dynamic in reality (Van den Berg et al., 1996), which appears difficult for model to reproduce. One of the reasons is that the current model setup does not apply waves originating from the sea. The access from channel Honte to Pas van Terneuzen is recognized. The pronounced sedimentation on shoal Hoogeplaten is overestimated probably due to dumping activities. The sediment and erosion pattern in the landward portion (between x-coordinates 50 and 70 km) are represented quite well by the model. Observation and model both show that channel Middelgat experiences sedimentation, and channel Gat van Ossenisse is eroded. The flood channel Schaar van Valkenisse had a small channel extending toward the shoal Plaat van Walsoordene, which is not observed in the model.

The Shoal Van Ossenisse keeps quite stable as in reality, although the shape differs comparing the observed and modeled evolution. Dredging events probably play an important role to regulate it. The Channel Gat van Ossenisse tends to develop a second extending channel next to the north of the shoal and flatten its alongshore line. Sedimentation takes place on top of the shoal. Measured data shows the secondary channel next to south of the Van Ossenisse get accretion and is filled by sediment, but in the model, it keeps serving as an ebb channel. Delft3D model may underestimate gravity-driven sediment transport from side-slopes, so model results show deeper channel than observations (Baar et al., 2019). Other explanations for the limited model

performance are related to schematized model settings, for example, a single sediment fraction and a single, uniform roughness value. We recognize that the model skill is not perfect in many locations and that there are differences between observations and model results. However, the aim of the current work is not to reproduce observed developments but rather to explore the impact of wind waves on morphodynamic development. To that purpose we consider the model performance is acceptable.

(a) Measured 2013

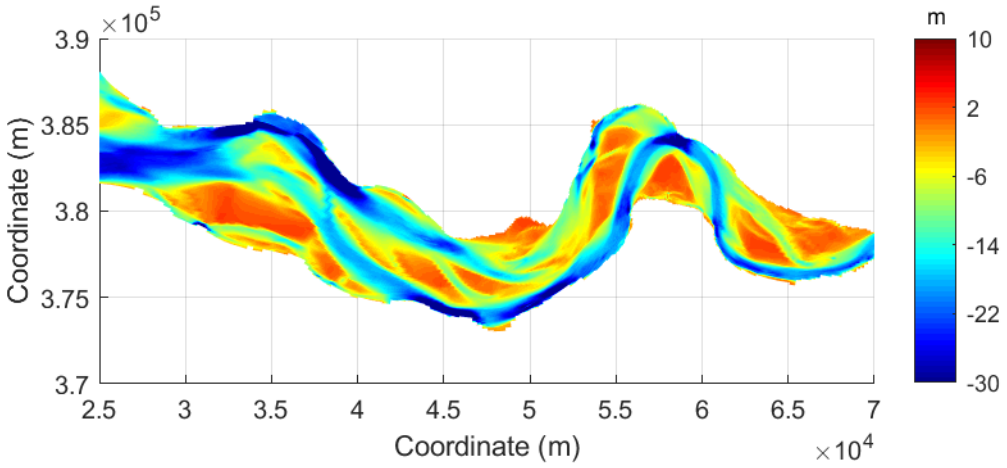

(b) Model 2013

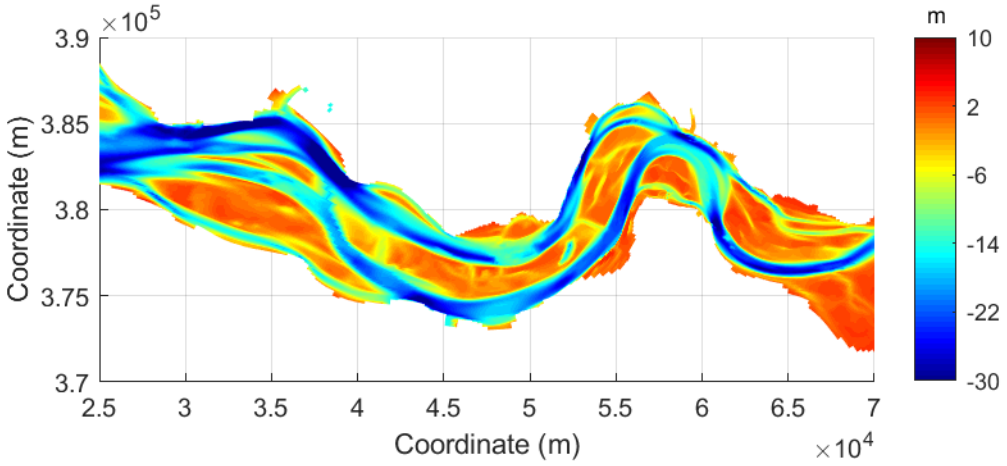

Figure 4.1: (a) Measured and (b) modelled bathymetries with waves from three directions at year 2013

(a) Measured 2013-1963

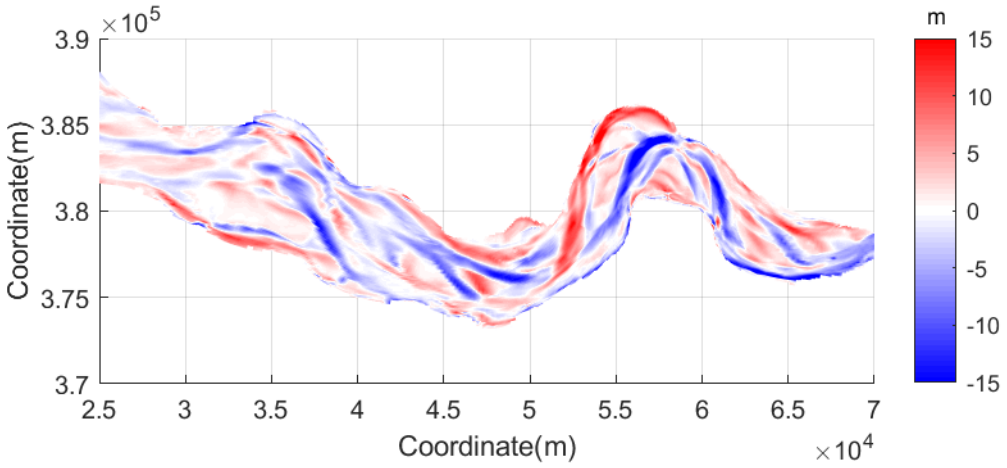

(b) Model 2013-1963

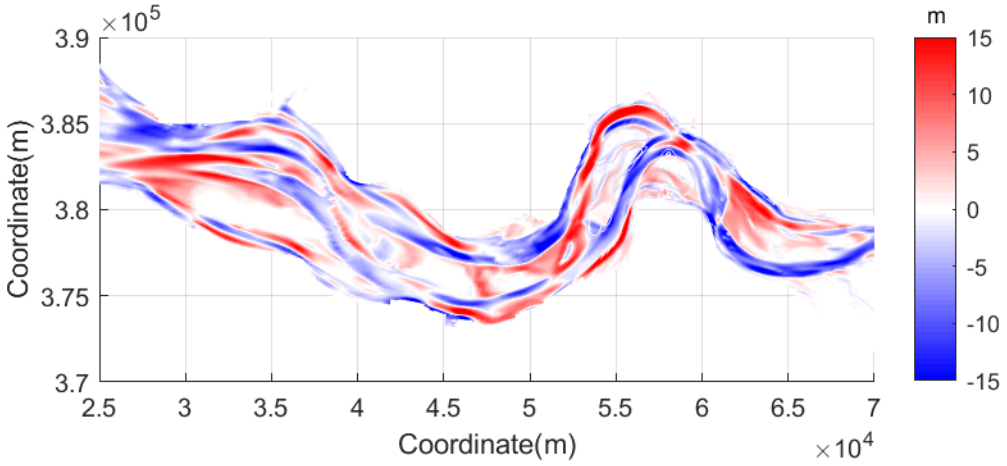

Figure 4.2: Cumulative erosion and sedimentation patterns between 1963 and 2013 of (a) measurements and (b) model results with waves from three directions

4.2 Wind Waves and Shoal Evolution

Previous section assesses the model's ability to reproduce morphological change over whole Western Scheldt, which gives reasonable boundary of hydraulic conditions and sediment supply for domain 3. In the following sections, we zoom on domain 3 and investigate the impact of small wind-waves on its morphological evolution with the focus upon shoal Van Ossenisse and adjacent channels (Figure 4.3). Figure 4.3 divides shoal Van Ossenisse and channel into subsection with abbreviations, which are used in following context.

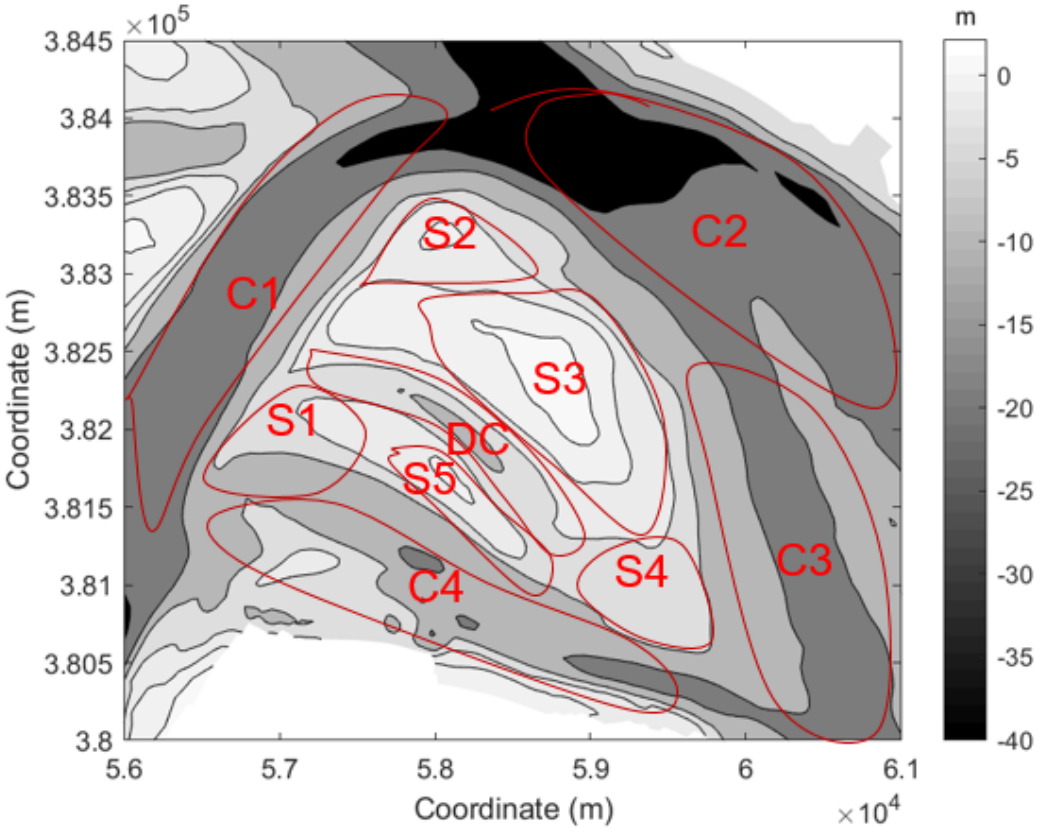

Figure 4.3: Schematic diagram of shoal Van Ossenisse with subsections and abbreviations

Figure 4.4 shows bathymetry difference over 50 years for different wave directions by subtracting bathymetry of their corresponding no wave case. At first sight, wave scenarios do not show significant change of the channel-shoal system. Shoal patterns remain similar with no wave scenarios. However, noticeable differences start to occur with time. First look at bathymetry difference with dominant wind direction 207° (first column of figure 4.4). After 10 years, waves starts to eroding the high sections of the shoal, and the upwind intertidal area (S1 and S5). More

sediment takes place on shoal edges below low water (western side of S1 and S2, and northern side of S2) and downwind side of the shoal. The observed more sediment can be due to more sedimentation or less erosion in wave case. Deeper section on top of the shoal also experience more sediment (eg. drainage channel (DC), gap between S2 and S3).

Keep looking at bathymetry difference with dominant wind direction 207°. Channels adjacent to the shoal started to getting deeper, mainly in the places where shoal edges receive more sediment (C1 and C2). This tendency continues over time. After 50 years, the observed erosion in the channel is spread out along channel axis and also found in the outer bend of channel C1.

Other wave scenarios from different directions show common trend with more/less sedimentation/erosion on edges and downwind side of the shoal (S1, S4, S5 and DC in direction 70°; S4, S5 and south of S1 in direction 340°), and more/less erosion/sedimentation in upwind intertidal area and in channels nearby (S2,S3 and C1 in direction 70°; west of S1, S2 and C4 in direction 340°). It is pronounced that the difference of bathymetry can be up to 3 meters after 50 years. Common observation is that shoal Van Ossenisse shows the trend to slightly migrate along wave direction. This tendencies are also found in shoal Molenplaat and Rug van Baarland.

(a) Direction 207° (10 years)

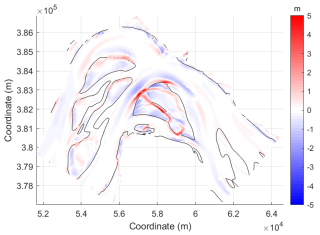

(f) Direction 70° (10 years)

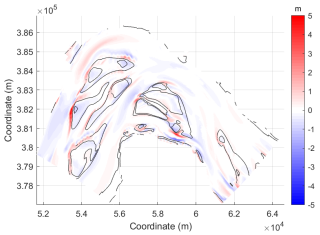

(k) Direction 340° (10 years)

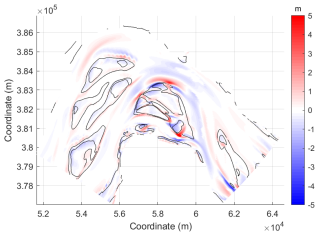

(b) Direction 207° (20 years)

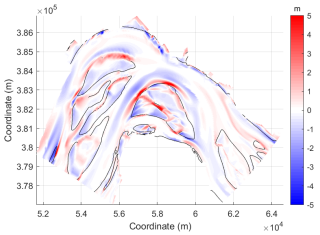

(g) Direction 70° (20 years)

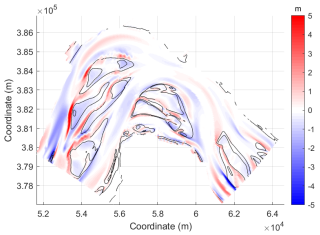

(l) Direction 340° (20 years)

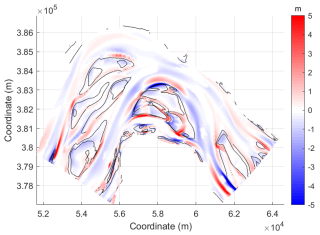

(c) Direction 207° (30 years)

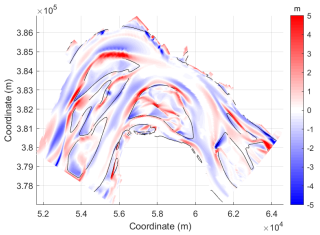

(h) Direction 70° (30 years)

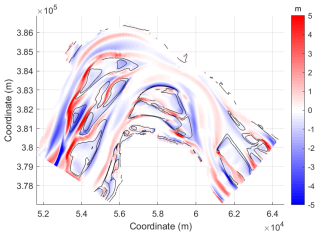

(m) Direction 340° (30 years)

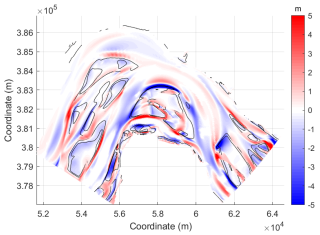

(d) Direction 207° (40 years)

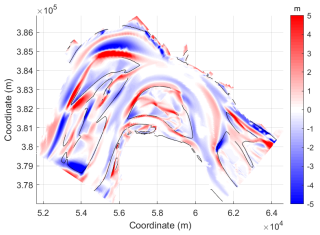

(i) Direction 70° (40 years)

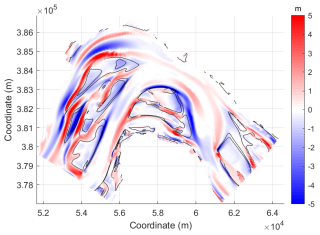

(n) Direction 340° (40 years)

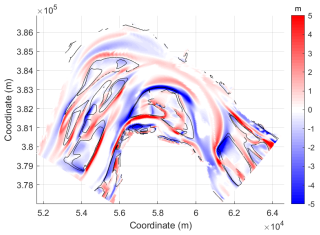

(e) Direction 207° (50 years) (j) Direction 70° (50 years) (o) Direction 340° (50 years)

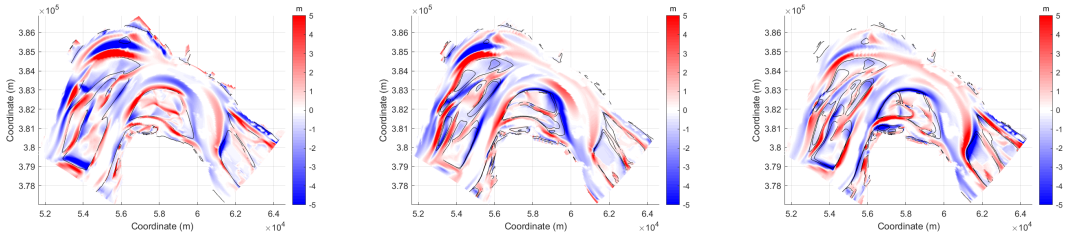

Figure 4.4: Bathymetry difference (wave - no wave) along time (10 to 50 years) from different wind directions. (a) to (e): direction 207°; (f) to (j): direction 70°; (k) to (o): direction 340°. Red color indicates more/less sedimentation/erosion in wave case; blue color represents less/more sedimentation/erosion in wave case. Contour is bed level=-2.3m

Intertidal area is defined as area that is covered at high tide and exposed at low tide. It is very sensitive to tidal and wave actions. Since this model experiences spring and neap tide with varying tidal range, we take the average of tidal range (high water at $2.2m$ and low water at $-1.8m$) to do calculations. Definitions are listed below:

- Intertidal area: area between bed level $2.2m$ and $-1.8m$ projected onto horizontal plane
- Intertidal volume: sediment volume between bed level $2.2m$ and $-1.8m$ on intertidal area
- Channel area: channel area at bed level $-1.8m$
- Channel volume: water volume the channel can accommodate below bed level $-1.8m$

Calculations are executed in whole domain 3 including shoal Van Ossenisse, shoal Molenplaat and Rug van Baarland and part of shoal Plaat van Walsoordene. Figure 4.5 demonstrates comparison between model and measurements. Model agrees with measurements in the increase of intertidal area and intertidal volume at the first 15 years but considerably overestimate them afterwards. Channel area decreases at the first 10 years and experiences slight fluctuation afterwards. Model captures the decline of channel area but underestimates it by showing continuous decrease over time. Model reflects the growth of channel volume, albeit with a slight underestimate.

Comparison between wave case and no wave case provides the influence of the wind-waves. Models with waves enlarge intertidal area gradually from beginning and reach approximately 12% larger area after 50 years. Larger intertidal area can arise from reduced elevation above high water level and widened shoal occupying channel. The latter is proved by less channel area in figure 4.5c. Despite of larger intertidal area, intertidal volume decreasingly deviates in the first 30 years. During that period, there is not too much high elevation area above $2.2m$ on

shoals (see hypsometry curve evolution figure 4.5a, b and c), so less intertidal volume implies more intertidal area erosion in wave cases. Self-behavior of estuary results in accretion on shoals over time. Waves, therefore, erode more sediment in high elevation and expand intertidal area and volume, as found in figure 4.5b from year 1995.

The wave case leads to narrower channel. The marked reduction of channel area in year 1982 is caused by dumping into channel Gat van Ossenisse. Channel experiences sedimentation in models at the beginning, before reaching a turning point in 1970s. From year 1978, large amount of dredging and dumping activites take place, which leads to large oscillation in channel volume between 1978-2000, after which, the channel evolves to a deep state which is not affected much by dredging settings in the model. Larger channel volume appears in wave cases. Comprehended with narrower channel area one may derive deeper channel in wave cases. Figures of intertidal area, channel area and volume see the deviation of quantity between wave cases and no wave case from the beginning. This divergence slightly remains in intertidal area and volume, while it is relatively constant in channel area and channel volume merely after 20 years except scenario of direction 340°.

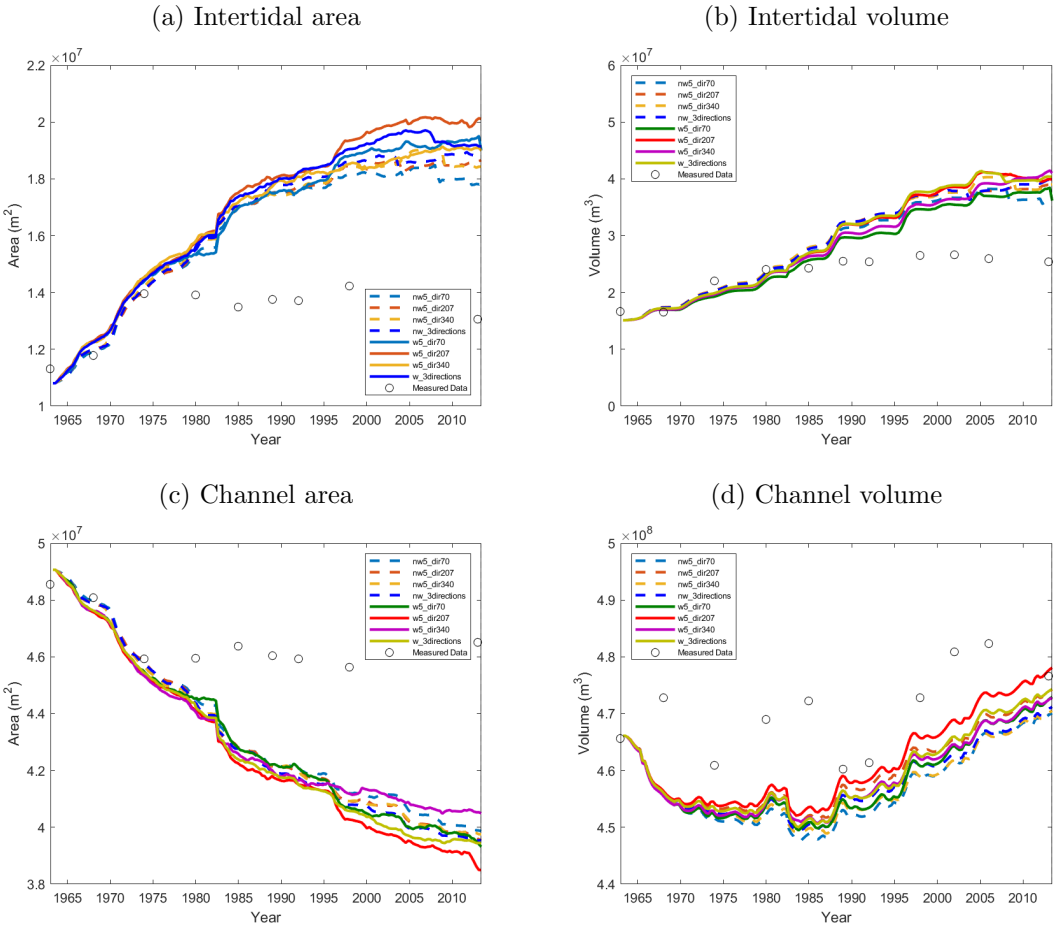

Figure 4.5: Development over 50 years of (a) intertidal area; (b) intertidal volume; (c) channel area; (d) channel volume. Dash line indicates no wave case, solid line with same color indicates wave case in the same wind condition

The hypsometry curve reveals the information that how much percentage of the area is situated below a certain bed level. It is a useful tool to get sight into the morphological state of the estuary. We compute hypsometry curve over the whole domain 3 and investigate how the morphology is impacted by waves. The measured data (black solid-dot line in figure 4.5a to e) shows that shoal accretes over time and the intertidal area gains elevation. Total channel area stay constant after first 10 years (around 76%). Profile of subtidal area develops from convex-up to concave-up. Model reflects the height of shoal accretion by showing the growth of the highest elevation with measured data (compare figure 4.5a to e), but it overestimates the overall elevation in intertidal area (elevation $2.2m$ to $-1.8m$). An overestimate of intertidal volume is also reflected by looking at figure 4.5b. In subtidal area (around $-2m$ to $-10m$), model does not predict its trend to become concave-up. Even more, it has a clear tend to become convex-up. The junction point

between model and measurement is at water level around $-9m$, below which, area percentage only has slight oscillation over time (maybe show the figures of both evolution). A horizontal section at water level $-15m$ is caused by dredging event. In the deeper part of channel (between $-15m$ to $-35m$), channel tends to become deeper and wider in the model, while its tendency is hard to be clarified in reality.

Generally, the evolution in domain 3 between wave cases and no wave cases is very similar, their area percentage difference below a certain bed level is no more than 5%. We subtract hypsometry curves of wave cases by their corresponding no wave cases, in order to make the differences more visible (4.5f to j). Initially, changes happen above bed level around $-5m$ up to top of the shoal. Within this region, low water level is a demarcation. More area is below bed level above low water and less area is below bed level below low water. In other words, the top of the shoal is lowered so as to have more intertidal area and shoal is widened under low water level, simultaneously. Since morphological change has not been significant among three scenarios by that time, they show a very similar quantity at beginning (figure 4.5f). Overtime, differences gradually extend towards the deeper sections. In figure 4.5 g, a turning point is clearly demonstrated around elevation $-10m$, below which, less area is below a certain bed level. In other words, channel is getting steeper and wider below this turning point. This type of profile develops and extends to the channel bottom after 50 years (figure 4.5j). In addition, elevation below which the area percentage is zero is less in wave cases. This means channel is deeper in wave cases. Hydraulic-morphological interactions take place all the time, so the difference between wave cases and no wave cases fluctuates over time. Despite of this, four clear features in wave cases are still obtained: top of the shoal is lowered with more intertidal area; shoal is wider in subtidal area; channel is wider in deeper bathymetry (below around $-10m$); channel is deeper. This behavior is presented in a schematized cross-section profile (figure 4.6). Different scenarios may show different quantity after a long term morphological change. However, features in wave cases still maintained although the demarcation points may shift.

(a) 10 years

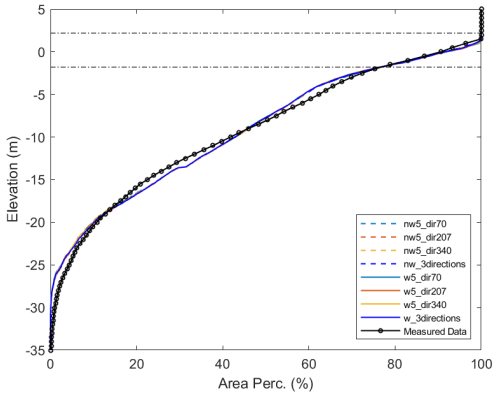

(f)

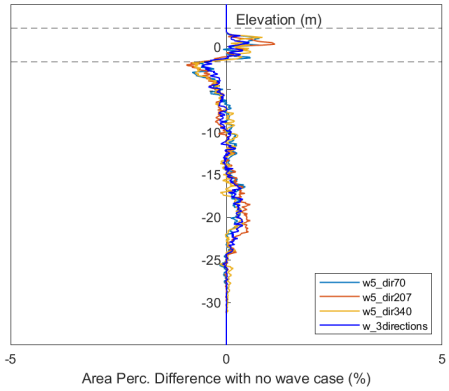

(b) 20 years

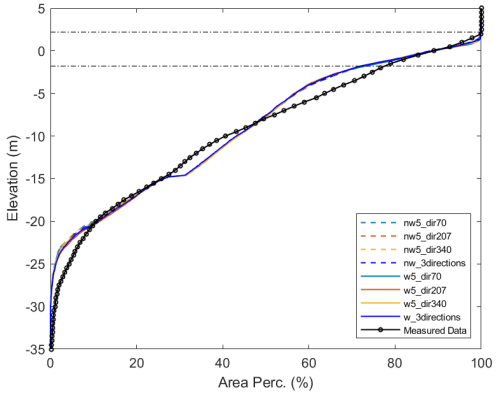

(g)

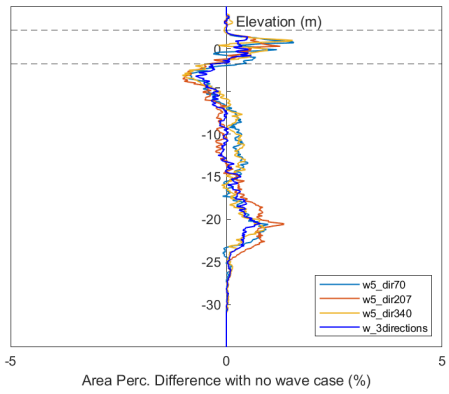

(c) 30 years

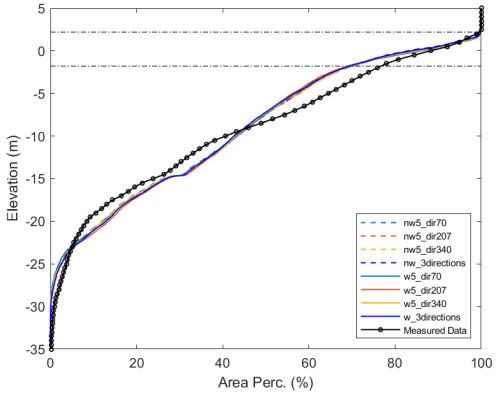

(h)

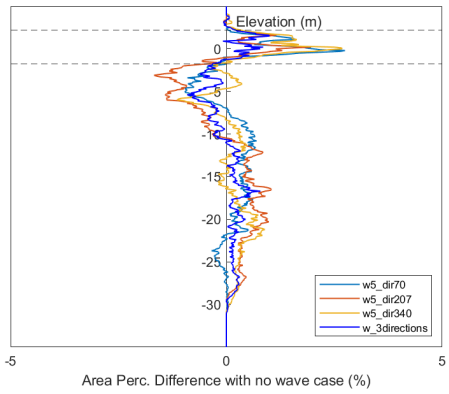

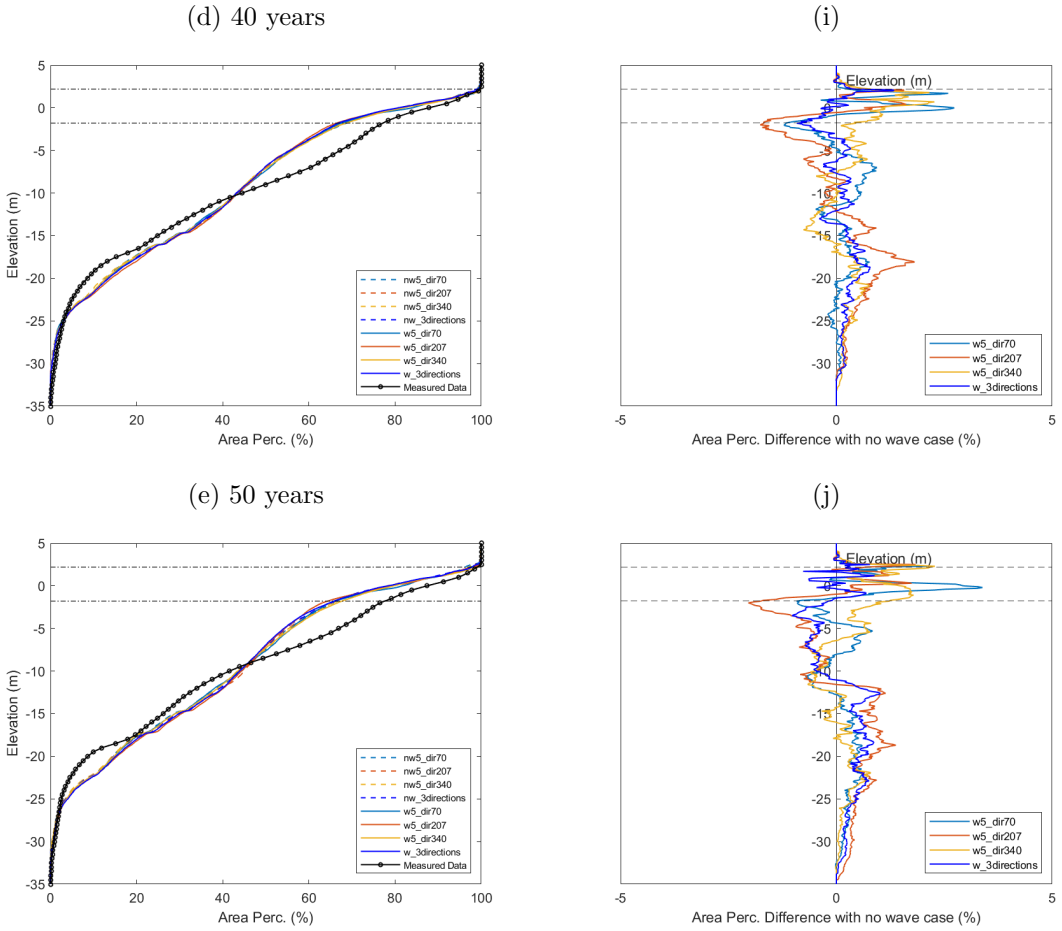

Figure 4.5: Hypsometry curve along time (10 to 50 years). (a) to (e): Hypsometry curve for all scenarios: dash line indicates no wave case, solid line with same color indicates wave case in the same wind condition; (f) to (j): Area percentage difference between wave case and its corresponding no wave case. positive values mean lower elevation in case of waves

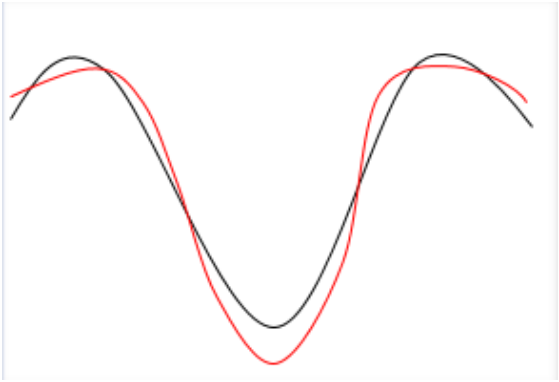

Figure 4.6: Schematic diagram of wave impact on cross-section channel-shoal profile: black line is no wave case; red line is wave case

4.3 Wind Waves Impact on Sediment Transport

Based on model results, a hypothesis of wind-wave impact on estuarine shoal evolution is proposed: waves erode intertidal area of the shoal by exerting enhanced high bed shear stress, which raises suspended sediment concentration. On the top section of the shoal, high SSC combined with wave asymmetry and wind-driven flow enhance sediment transport rate along wave direction, causing more sediment appearing in the lee side of the shoal. In addition, the increase in suspended sediment transports to the shoal edges around low water level by tidal currents. As a result, the shoal is widened and channel area is decreased. This leads to convergence of velocity in the channel, which induces the deep part of channel to widen and deepen. This hypothesis will be substantiated and discussed in the next section.

In this section, we investigate the underlying controlling mechanisms behind the modelled behaviors. We fixed the initial bathymetry (turn off hydraulic-morphological interaction) and rerun scenario 1-6 for 6 hydraulic days, which is during the middle of spring and neap tide signal. Then, we zoom in on domain 3 to study the difference of sediment transport under the impact of waves.

Taking dominant wind from direction 207° as an example. The characteristics of this wind direction is that it is aligned with residual currents (northeast due to centrifugal) on the shoal. Figure 4.7 displays shoal Van Ossenisse, and instantaneous suspended sediment concentration (SSC) every 1.5 hours over one tidal cycle with normalized instantaneous sediment transport vector on the top of it. Since Western Scheldt experiences spring-neap tide, the demonstrated tidal cycle is in the middle of spring and neap.

Plots start from water level decreasing to 0m, when ebb current takes place with maximum ebb

velocity. Wave-induced bed shear stress exerts in the area right below contour 0m in the upwind area and induce a bit more SSC in wave case. Between t=1.5 to 3 hrs (figure 4.7b and c), water level continues to drop and low water slack occurs. During this time, the flow velocity is low. Area experiencing wave-induced bed shear stress is limited due to low water level. Some part of upper part of subtidal area starts to feel wave motion. However, its magnitude is too small to generate more SSC in wave case. Sediment transport vector mainly towards southwest at this time, but wave cases shows some vectors alter to wave direction in upwind side of the shoal (S1).

At t=4.5 hrs, water level is in rising period and equal to -1m. Flood currents take over. Sediment transport on the shoal changes from southwest direction to northeast. In wave case, higher SSC occurs around low water level (contour=-1.8m), where higher bed shear stress takes place. Waves break before they reaches the top of the shoal. Drainage channel is not wide enough for waves to develop again, so there is no wave-induced bed shear stress in S2 and S3. During the next 1.5 hours, water level keeps growing and flood current velocity reaches to its maximum. Compared to t=0 hrs, t=6 hrs shows larger SSC at the same water level. This is explained by horizontal flow asymmetry and non-linear wave-current interaction. This area experiences larger flood velocity than ebb velocity at water level=0m. In addition, in a result of non-linear wave-current interaction, larger flood velocity leads to much larger total bed shear stress and hence larger SSC. As water level continues to rise at t=7.5 hrs, more area starts to feel wave motion in upwind location. Still, high bed shear stress occurs around bed level contour 0m, before wave breaking. Combining with high flood velocity, it elevates SSC in the lower part of intertidal area (S1, S5 and north of drainage channel). At high water level (t=9 hrs), water depth is too high to maintain wave motion on the bed level. In addition to that, current velocity becomes very low during this high water slack. Therefore, only small amount of resuspension appears on the high elevation of the shoal.

During low water period, the influence of wave can be extended to subtidal domain. However, the amount of affected area is very limited. Furthermore, low velocity during low water slack makes it no difference between wave and no wave case in terms of SSC and sediment transport. During high water period, wave-induced bed shear stress has impact on large amount of area and induces high SSC in the intertidal area, especially in the upwind side. The induced suspended sediment is transported by ebb and flood currents. However, the sediment transport is not symmetric within a tidal cycle. It relies on horizontal tidal velocity. In the example of wind direction 207°, wave impact is mainly on the area with flood-dominant tidal current. Together with non-linear wave-current interaction, more SSC and hence larger suspended sediment transport occur during flood period. At high water slack, water depth is so high that bed level hardly feel wave motion. The low current velocity also retards sediment motion.

(a) t=0 hrs, water level=0m

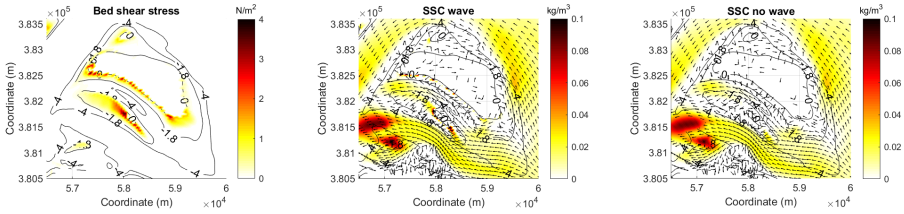

(b) t=1.5 hrs, water level=-1.2m

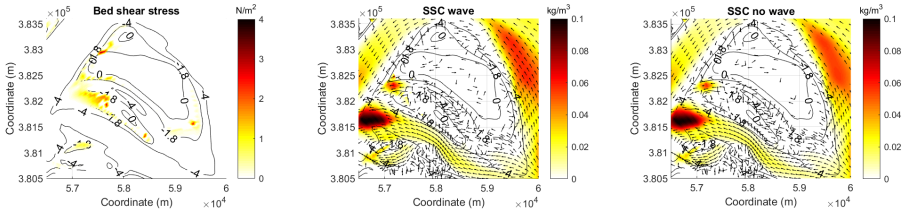

(c) t=3 hrs, water level=-2.1m

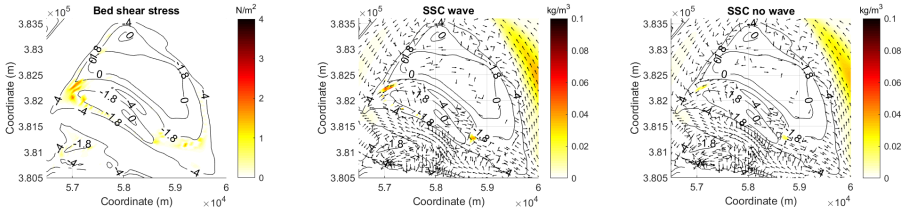

(d) t=4.5 hrs, water level=-1m

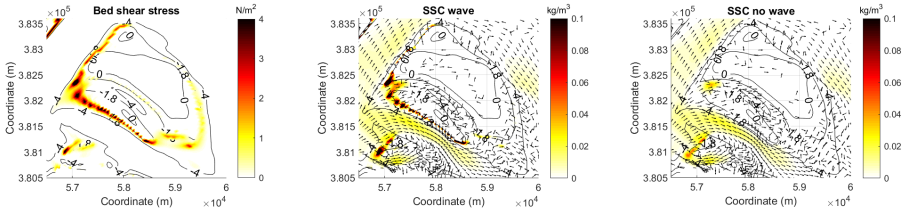

(e) t=6 hrs, water level=0m

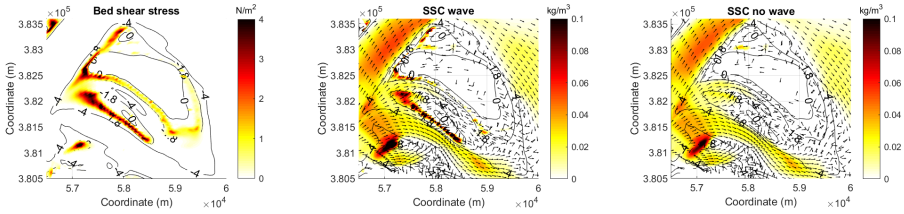

(f) t=7.5 hrs, water level=1m

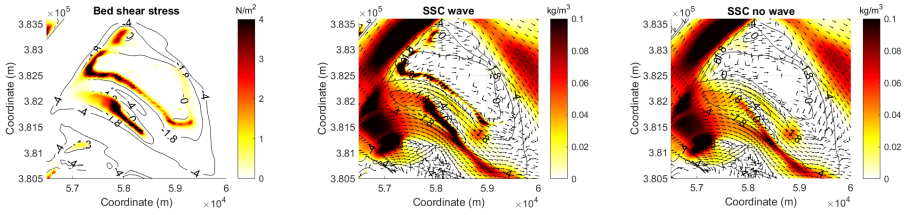

(g) t=9 hrs, water level=2.3m

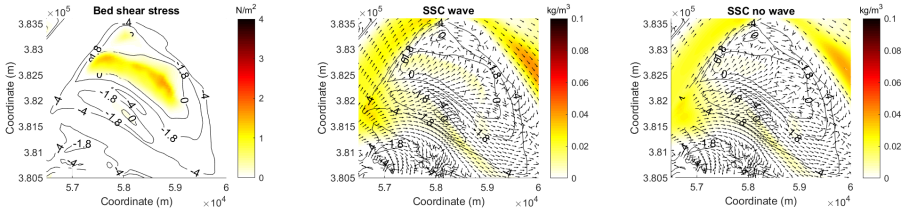

(h) t=10.5 hrs, water level=1m

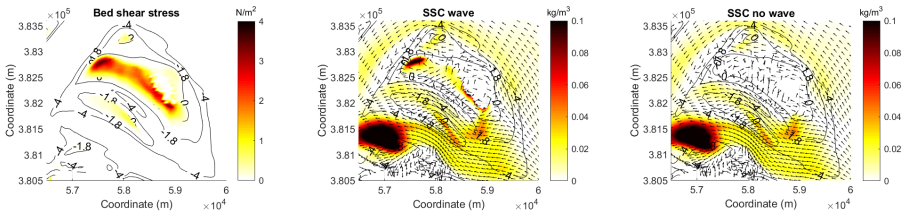

Figure 4.7: First column: instantaneous wave-induced bed shear stress and its magnitude (color map). Second column: in wave case, SSC and its magnitude (color map) with normalized suspended sediment transport arrow on the top. Third column: in no wave case, SSC and its magnitude (color map) with normalized suspended sediment transport arrow on the top.

After inspecting the intratidal variations, we inspect the wave-induced bed shear stress and residual sediment transport over this tidal cycle (figure 4.8, figure 4.9, 4.10, 4.11). Figure 4.8 displays spatial distribution of wave-induced bed shear stress over the whole domain 3. It calculates tidally-averaged wave-induced bed shear stress under inundation duration. Wave-induced bed shear stress is associated with significant wave height and water depth. At the upwind side of the shoal, wave has experienced a relatively long fetch to develop, so it has high significant wave height. As it propagates across the shoal, bottom friction and wave breaking results in its energy dissipation. However, if the drainage channel in shoal is wide enough, it provides wave a good environment to develop again. Figure 4.8a displays wave-induced bed shear stress from direction 207°. In shoal Van Ossenisse, the upwind side of the shoal experiences high wave-induced bed shear stress (S1 and S5). The magnitude is also very high in S3 with elevation above 0m. That is mainly because we calculate wave-induced bed shear stress under inundation duration. High elevation section experiences short inundation duration but feels active wave motion when it is under water. Similarly, figure 4.8b and c shows larger wave-induced shear stress in upwind side of S2 and S3, and on the high elevation of S3. However, their magnitude is relatively lower compared with figure 4.8a. This is because fetch length is shorter for wave direction 70° and 340°, resulting a lower significant wave height and hence lower wave-induced bed shear stress.

(a) Direction 207 (b) Direction 70 (c) Direction 340

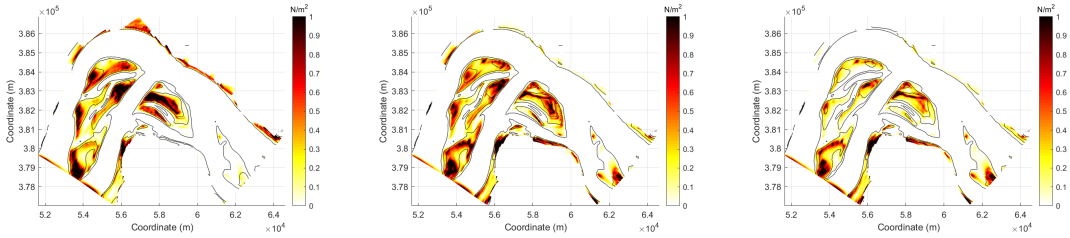

Figure 4.8: Tidally averaged wave-induced bed shear stress at the intertidal area

To understand underlying sediment transport mechanisms, residual flow pattern and residual sediment transport pattern in the same tidal cycle are analyzed. (a) in figure 4.9, 4.10 and 4.11 is residual flow pattern. (b), (c) and (d) show the bathymetry and dimensionless residual sediment pattern, which are calculated by averaged residual sediment transport over its RMS value per cell over one tidal cycle.

Residual flow pattern shows that waves do not make a big difference in flow currents both in terms of its magnitude and direction. Some insignificant change is due to stokes drift in the direction of wave propagation and mainly happens in lower intertidal area with high significant wave height. The western side of the shoal (S1 and S2) experiences flood dominant by the centrifugal force along the bend and eastern side of the shoal (S3 and S4) is ebb-dominant with high ebb flow coming from channel Zuidergat. Both western and eastern side of the shoal show high flow asymmetry. C4 next to the south of the shoal mainly accommodate ebb flood separated from channel Zuidergat. Flow diverges when encountering high elevation (S1 and S4) and also distorts caused by high flow gradient or high bed level slope. Horizontal flow asymmetry also appears in the high elevation of the shoal (S3), but its magnitude is much less compared to that in the channel. In low elevation region, flow pattern is mainly determined by tidal current. However, wind-driven flow is of high relevance in high elevation region. This is comparable in S3 of figure 4.9a, 4.10a and 4.11a. Flow tends to be directed by wind in high elevation of the shoal.

Suspended sediment transport incorporates with advection and diffusion processes. In figure 4.9b, residual suspended sediment transport vector reveals similar direction pattern as residual flow, with northeastern direction in western side and northwestern direction in eastern side of the shoal Van Ossenisse. On the one hand, by inducing higher SSC in water column, the presence of waves enhances sediment transport rate over the whole shoal. The non-linear wave-current also increases residual sediment transport rate along residual flow direction. On the other hand, flow direction is altered by wind in high elevation of the shoal, suspended sediment is transport from upwind side to downwind side. This is obvious in S2 and S3 when comparing figure 4.9b, 4.10b and 4.11b. That is why more sediment is found in downwind side of the shoal (figure 4.4). Simultaneously, diffusion process takes place where there is suspended sediment concentration

gradient. In S1 from figure 4.9b, sediment transport is more diverged towards its western and southern part. Waves erode S1 and elevates SSC. Advection and diffusion process enhance it disperse to place with low bed shear. This phenomenon can also be found in S2 of figure 4.10b (wind direction 70°).

Bed load transport is mainly determined by bed shear stress induced by flow and waves, and bed slope effect. In Delft3D, suspended sediment transport caused by wave asymmetry is also included into bed load transport equation. In the intertidal area (figure 4.9c, 4.10c and 4.11c), bed load transport without waves show similar patterns in different single wind direction with only noticeable difference in elevation higher than contour 1m. However, the presence of waves strongly alter its direction along wave propagation over the whole intertidal area. This is caused by relatively high magnitude of suspended sediment transport by wave asymmetry. Since magnitude of bed load sediment transport is much small, total sediment transport pattern (figure 4.9d, 4.10d and 4.11d) is followed by suspended sediment transport. Only in high elevation on the shoal and high bathymetry slope, eg. bank of DC and C4, bed load transport in these area has showed its importance.

Overall, on shoal area, by stirring higher sediment concentration in the water column, the presence of waves lead to more sediment transport along its direction and also enhance sediment dispersion from high SSC to low SSC.

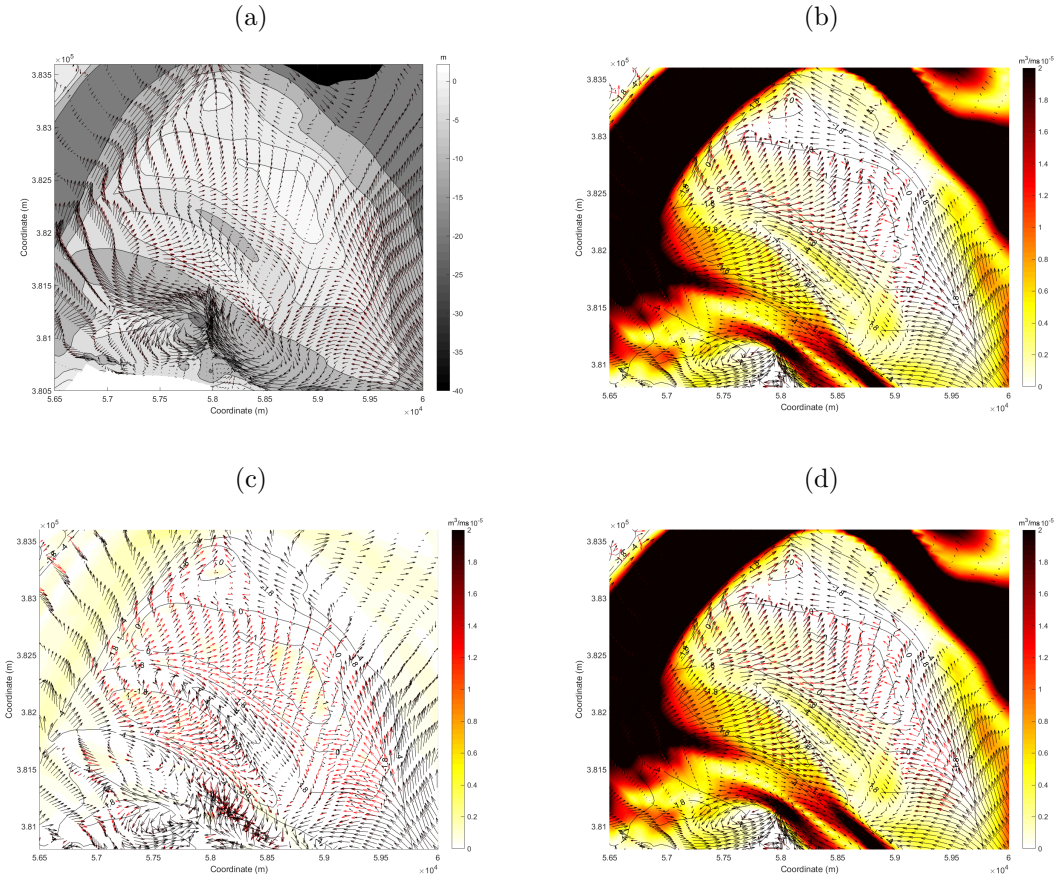

Figure 4.9: From wind direction 207°. Comparison of (a) Residual flow pattern; (b) Normalized suspended sediment transport pattern; (c) Normalized bedload sediment transport pattern; (d) Normalized total sediment transport pattern. Color maps of (b) (c) (d) are the sediment transport magnitude in wave case. Black and red arrows indicate transport direction of wave and no wave case, respectively

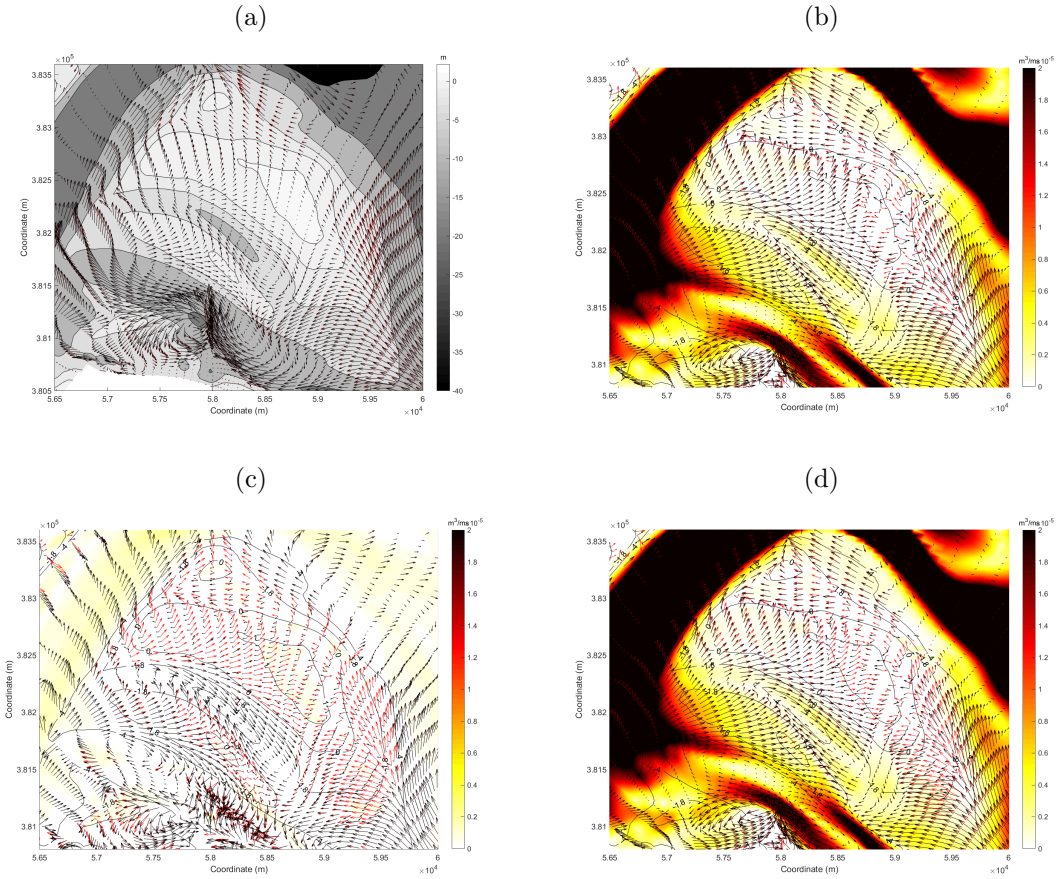

Figure 4.10: From wind direction 70°. Comparison of (a) Residual flow pattern; (b) Normalized suspended sediment transport pattern; (c) Normalized bedload sediment transport pattern; (d) Normalized total sediment transport pattern. Color maps of (b) (c) (d) are the sediment transport magnitude in wave case. Black and red arrows indicate transport direction of wave and no wave case, respectively

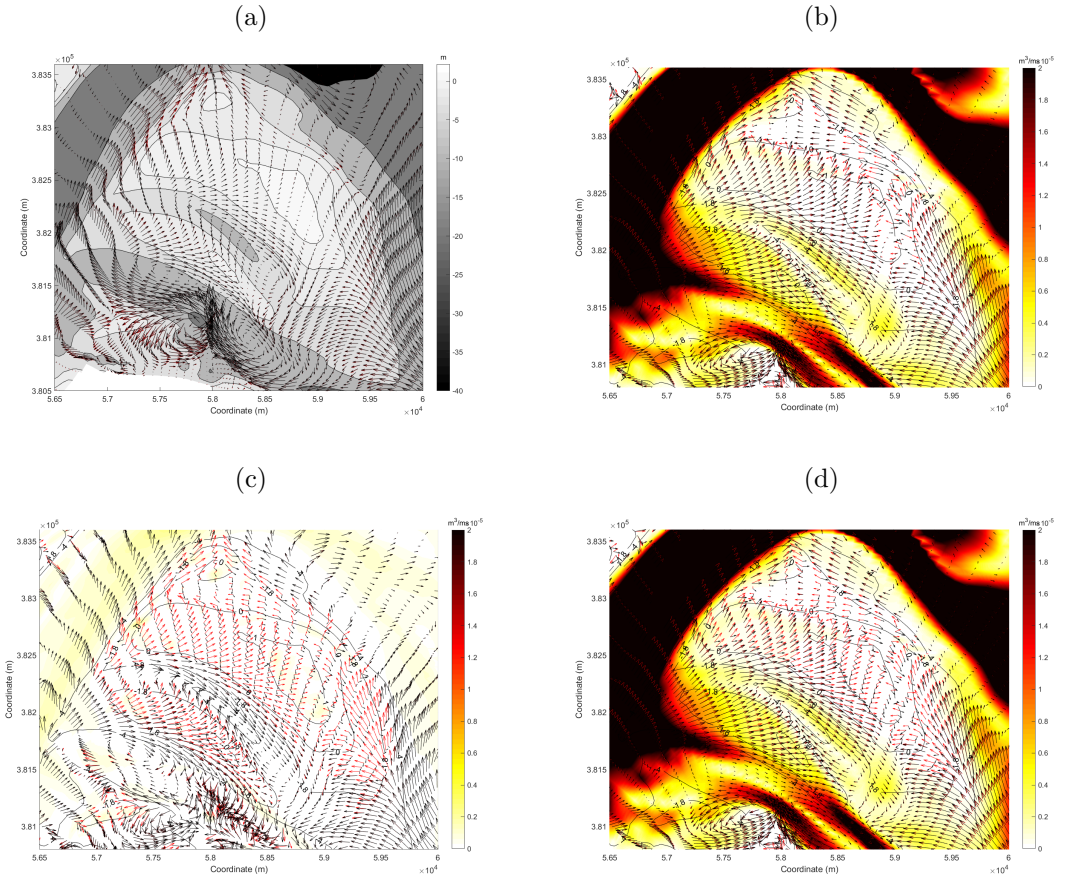

Figure 4.11: From wind direction 340°. Comparison of (a) Residual flow pattern; (b) Normalized suspended sediment transport pattern; (c) Normalized bedload sediment transport pattern; (d) Normalized total sediment transport pattern. Color maps of (b) (c) (d) are the sediment transport magnitude in wave case. Black and red arrows indicate transport direction of wave and no wave case, respectively

Hypsometry curve (figure 4.5) implies that discrimination of morphology between wave and no wave case initially takes place in the intertidal area. More sediment on the edge of the shoal is related to resuspension due to waves. Residual sediment transport pattern suggests that sediment can disperse from intertidal area of the shoal to its edge. Nevertheless, why channel volume increases (figure 4.5d) and why channel is deepened (figure 4.6) in wave case remains unclear. One hypothesis is the redistribution of velocity and this is explained in the following part.

Figure 4.12 shows the subtraction of mean velocity magnitude over one tidal cycle between wave case and no wave case after 5 years morphological change. Red color represents larger mean

velocity magnitude by including wave. 4 scenarios with wave all reveal larger velocity in channel, especially near the place with wider shoal. This can explain the hypsometry curve (figure 4.5) in which wave tends to deepen the channel. The deepening of the channel is not directed influenced by wave forcing, but caused by hydrodynamic and morphodynamic interaction. Sediment is stirred up by wave and transported to the edge of the shoal, causing wider shoal area compared to no wave case. To ensure continuity conservation, channel velocity increases with response to narrowing channel area (also proved by figure 4.5c), resulting in more suspended sediment and deeper channel. Figure 4.5 reveals that the amount of sediment removed from high elevation is not enough to compensate the wider shoal area (at bed level between around -1m and -11m), which means sediment supply from channel has huge contribution to the growth of intertidal and subtidal domain. Less total sediment volume deviates from the beginning for around 25 years, after which, the deviation stays constant at $6 \times 10^6 m^3$. This value is more or less the same in different wind direction. Since the intertidal volume does not see clear difference (figure 4.5)b, the reduced sediment volume mainly due to channel erosion. Total sediment evolution (figure 4.13) implies that, at first, wave induces sediment exchange between domain 3 and its outer part. It leads to less sediment stored in the domain. However, the influence of waves become more and more smaller after a certain state when estuary adapts to waves. Sediment exchange rate between estuary sections then become the same as no wave case.

(a) Direction 70°

(b) Wave from direction 207°

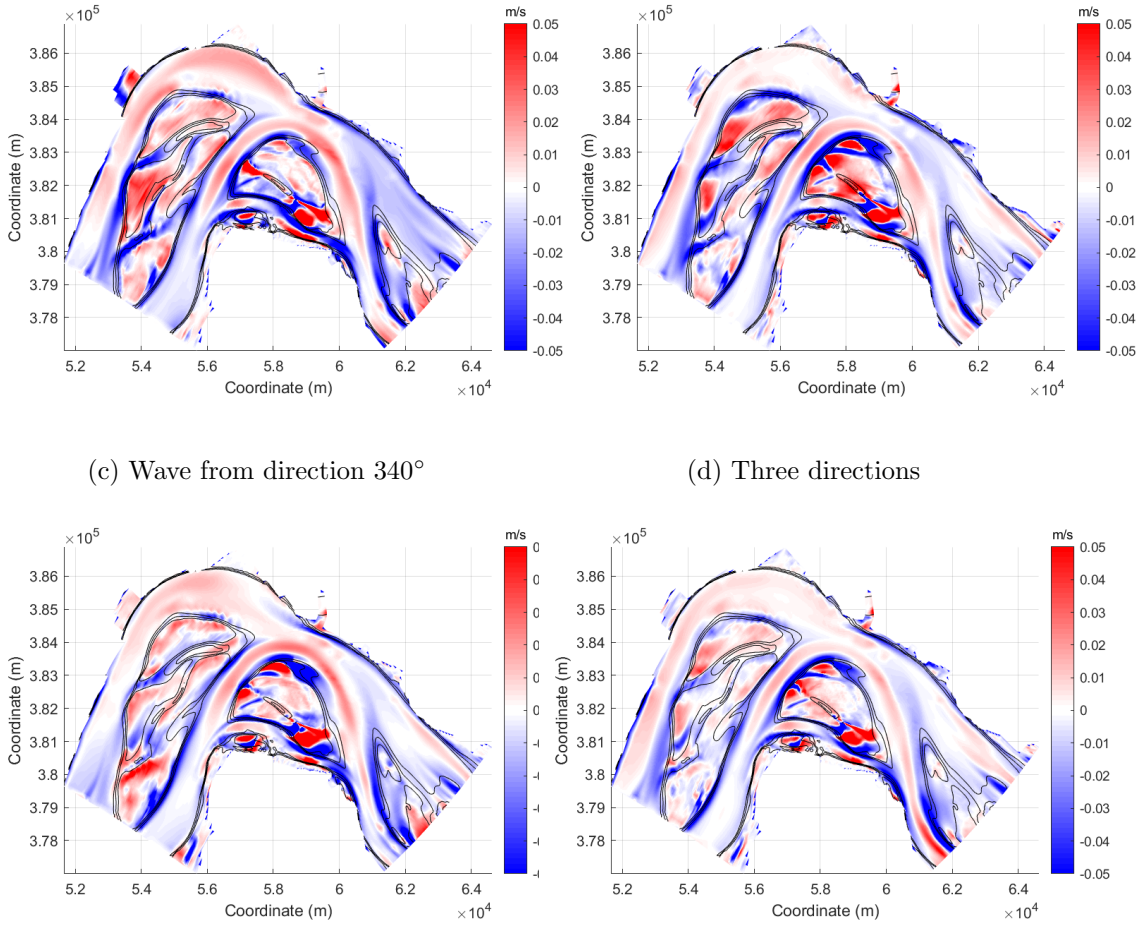

(c) Wave from direction 340°

(d) Three directions

Figure 4.12: Subtraction (wave - no wave) of mean velocity magnitude over one tidal cycle after 5 years morphological change. Red color indicates larger magnitude in wave case

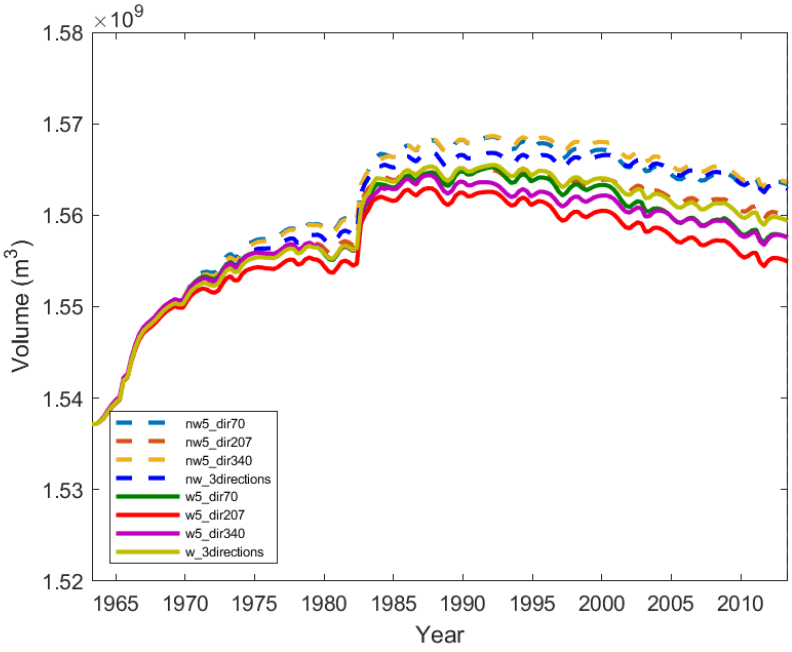

Figure 4.13: Total sediment volume over 50 years. Dash line indicates no wave case, solid line with same color indicates wave case in the same wind condition

4.4 Impact of Waves with Sea level rise (version 1)

It is noted that the boundary condition from GTSM derived tidal range 0.5m larger than in reality accidentally. This may cause significant morphological difference than we observed in section 4.2.

With no sea level rise, after 100 years, shoal areas in the estuary is expanding (figure 4.14). This is especially obvious in shoal Hoogeplaten, Middelplaten and Plaat van Walsoordene. In addition, the height of the shoal grows massively. Compared with no sea level rise, sea level rise leads to higher elevation on large proportion of the shoal, eg. shoal Hoogeplaten, Rug van Baarland and Plaat van Walsoordene, but lower elevation on a small percentage of the shoal, eg. shoal Middelplaten (figure 4.14). Most channels are observed deeper depth, eg. channel Everingen, Middelgat, Gat van Ossenisse, Schaar van Valkenisse and Zuidergat. Shoal Van Ossenisse is also expanding along with self-behavior of estuary after 100 years. Shoal accretion happens with sea level rise. However, shoal edges are highly eroded, which is most serious in SLR 167cm. The shoal has a tendency to migrate landward but regulated by erodible layer imposed in models. Channel next to west of the shoal sees erosion, while channel next to its eastern side shows sedimentation.

Comparing figure 4.14b and h, it can be seen, even wave is only imposed in small scale area (between x-coordinates 53 and 62 km), its impact on morphological change is extending to estuary mouth. Shoal Hoogeplaten expands massively to its north. Due to sea level rise, in the middle part (between x-coordinates 40 and 50 km), channel Honte is eroded in wave case instead of being deposited in no wave case. Zooming in on shoal Van Ossenisse, significant discrimination due to waves is observed.

It should be mentioned that an incorrect boundary conditions with accidental 0.5m larger tidal range cause different morphological behaviors. Nevertheless, some logical observations are still obtained. A large amount of erosion takes place in the upwind side of the shoal, resulting in massive sedimentation in the downwind side of the shoal. Deepening of the channel (C2) happens near the wider area of the shoal (S3). Larger tidal forcing is used in this scenario. This leads to more area under erosion and with higher erosion depth in the shoal. A distinction with section 4.2 is more sediment in channel Overloop van Hansweert (C1). Probably, due to the lower elevation of intertidal area, velocity in C1 is widely distributed and decrease, resulting in more sediment. With sea level rise, shoal Van Ossenisse migrates landward (from contour line in figure 4.15). Bathymetry difference pattern is remained. High sea level rise sees larger proportion of erosion area in shoal Van Ossenisse.

(a) Initial bathymetry (no wave)

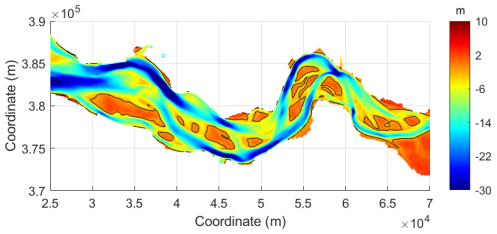

(g) Initial bathymetry (wave)

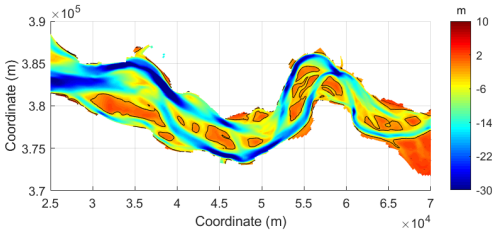

(b) After 100 years SLR 0cm (no wave)

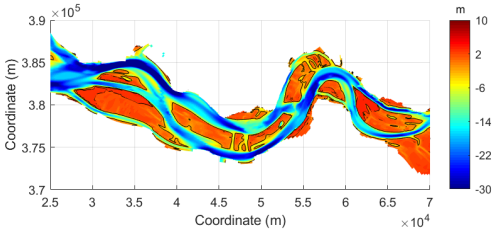

(h) After 100 years SLR 0cm (wave)

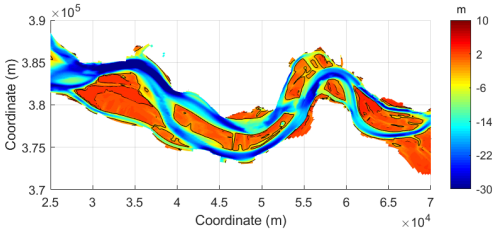

(c) SLR 96cm linear - SLR 0cm (no wave)

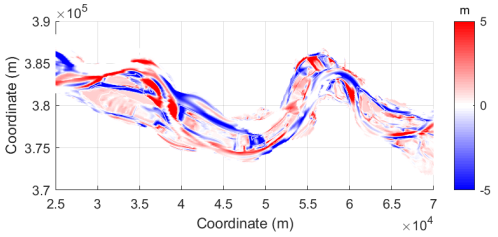

(i) SLR 96cm linear - SLR 0cm (wave)

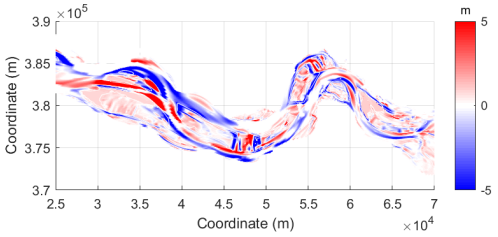

(d) SLR 96cm sin - SLR 0cm (no wave)

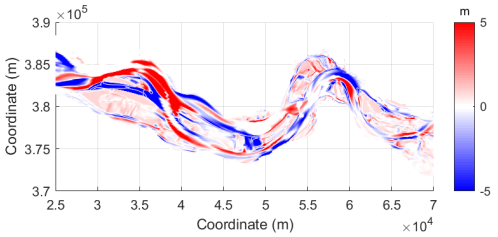

(j) SLR 96cm sin - SLR 0cm (wave)

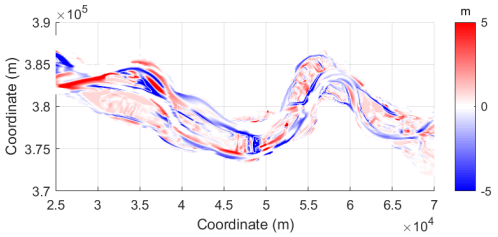

(e) SLR 167cm linear - SLR 0cm (no wave)

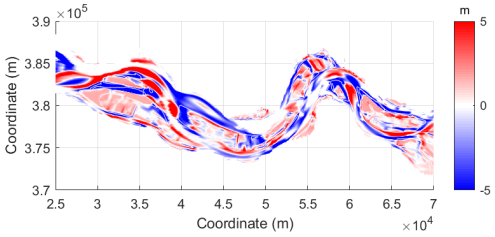

(k) SLR 167cm linear - SLR 0cm (wave)

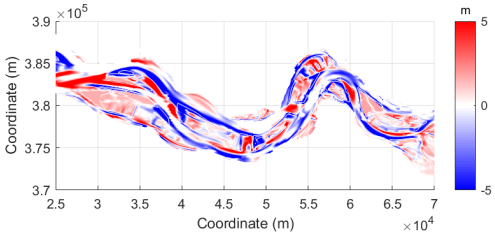

(f) SLR 167cm sin - SLR 0cm (no wave)

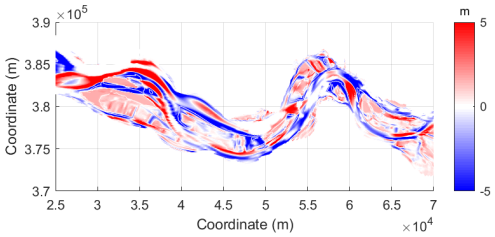

(l) SLR 167cm sin - SLR 0cm (wave)

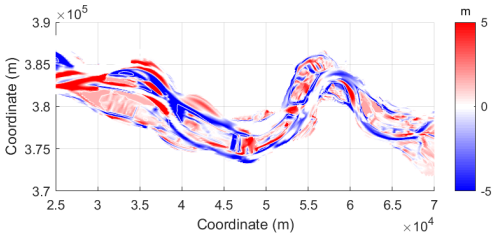

Figure 4.14: First column: sea level rise impact in no wave case. (c) to (f): after 100 years, bathymetry subtraction between SLR and No SLR in no wave case. Second column: sea level rise impact in wave case. (i) to (l): after 100 years, bathymetry subtraction between SLR and No SLR in wave case. Red color indicates more sediment due to sea level rise

(a) Initial bathymetry (year 1963)

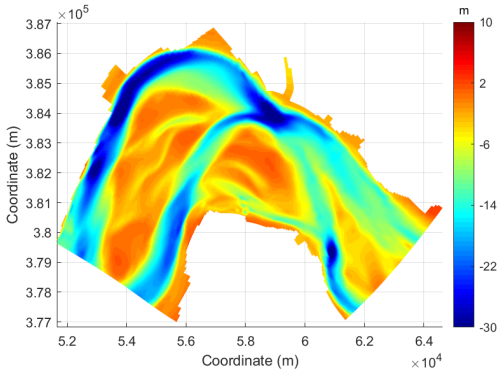

(b) SLR 0cm

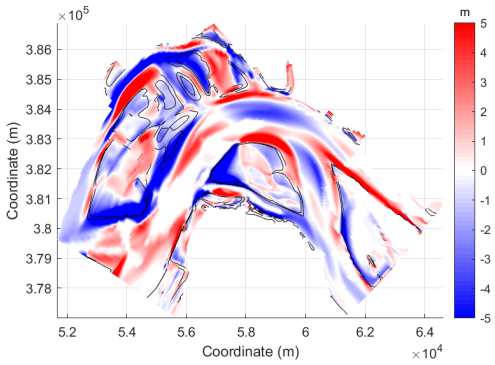

(c) SLR 96cm linear

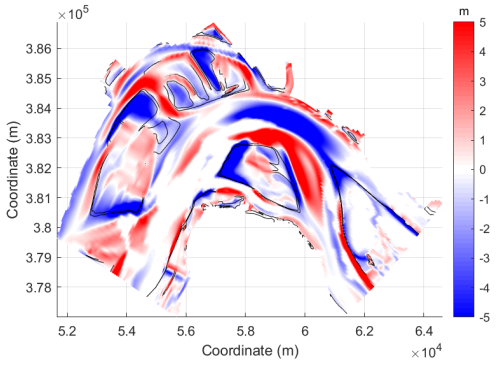

(d) SLR 96cm sin

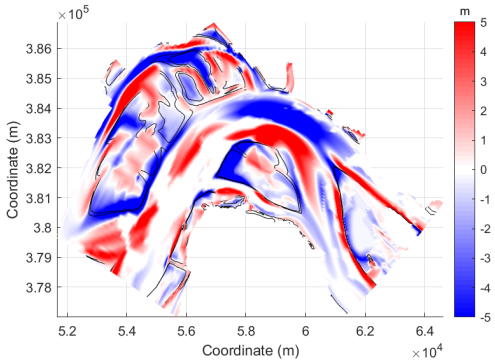

(e) SLR 167cm linear

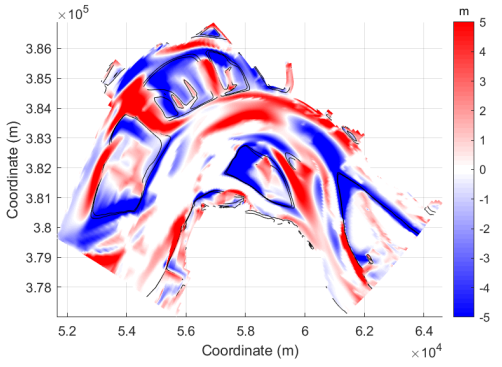

(f) SLR 167cm sin

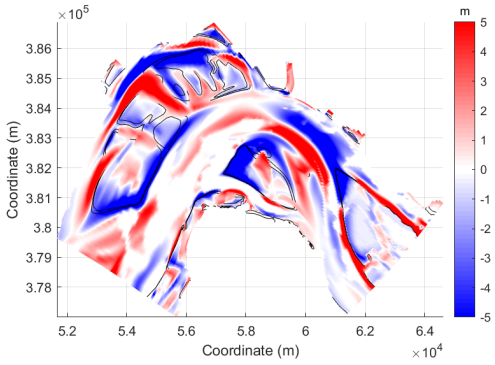

Figure 4.15: Bathymetry difference between wave and no wave case after 100 years in different SLR scenarios. Positive value indicates more sediment due to waves

Doing calculation in domain 3, figure 4.16 displays its initial hypsometry curve and that after 100 years. To better interpret it, figures on the right calculate percentage difference with SLR 0cm. Under sea level rise, after 100 years, the intertidal area is elevated and presents convex-up profile. More channel area appears in the deep part of the channel. Elevation below which the area percentage is 100% roughly equals to sea level rise, and remains equivalent regardless of wave. That is because sediment brought from currents forms a high bar on the shoal, where waves break before achieving. However, the presence of waves slow down this formation process, so the area with highest elevation is less in wave cases. Above reference level 0m, sea level rise leads to steeper slope. Logically, the increase of sediment is supplied from channel. This partly explains the wider channel area in sea level rise. The presence of waves lower the height of intertidal area in all sea level rise cases.

Area between averaged high water level $2.2m$ and low water level -1.8 represents intertidal area in no sea level rise. For comparison purpose, this water level is also used to do calculation for different sea level rise. So, it should be noticed that 'intertidal area' here does not precisely presents intertidal area. Definitions are listed below:

- Intertidal area: area between bed level $2.2m$ and $-1.8m$ projected onto horizontal plane
- Channel area: channel area at bed level $-1.8m$
- Channel volume: water volume the channel can accommodate below bed level $-1.8m$
- Total sediment volume: sediment volume above bed level $-35m$

Total sediment volume suggests that domain 3 imports sediment from outside within the first 40 years, and seems to adapt the larger tidal range at seaward boundary. After that time, it shifts to export sediment. Sea level rise induces less total sediment stored in this domain, with SLR 167cm-linear having the highest drop. In each sea level rise, linear signal presents more pronounced change than sinusoidal signal. Sediment loss due to sea level rise could be both in the intertidal area (figure 4.17a) and channel (figure 4.17c). As seen from hypsometry curve (figure 4.16), steeper slope appears in intertidal area with sea level rise. This is corresponding to less intertidal area in figure 4.17a. Hence, with larger channel area (figure 4.17b).

Different from section 4.2, we observe some opposite trends due to waves by imposing larger tidal range. The intertidal area is enlarged by waves from beginning, but reduced after a certain period. Correspondingly, waves decrease channel area before increasing it again. This conflicts with what we discussed in section 4.1. The reason behind will not be investigated at this stage.

Generally, waves play the same role in each sea level rise. It increases intertidal area/volume (during a certain period) and channel volume, and reduces total sediment volume. The dominant mechanisms are assumed to be the one as we discussed in section 4.1. The deviation in intertidal area between wave and no wave is accelerated by sea level rise. In figure 4.17a, visible deviation

first appears in SLR 167cm-linear. SLR 167cm-linear also sees a large amount of reduction in total sediment volume due to waves faster than others. Despite of this, the quantity difference between no wave and wave in these four indexes does not show linear change with sea level rise. As a whole, combined with sea level rise and wave impact, the channel volume is larger and less sediment is remained in the estuary.

(a) No wave case

(b) Difference with No SLR

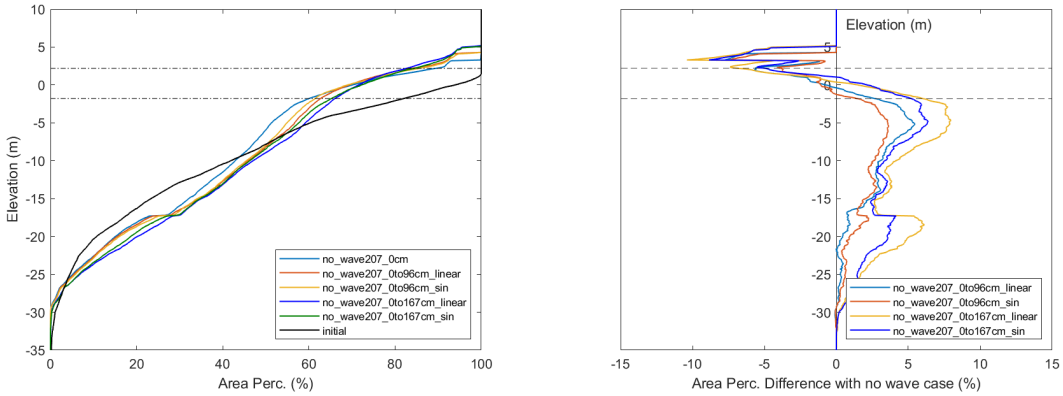

(c) Wave case

(d) Difference with No SLR

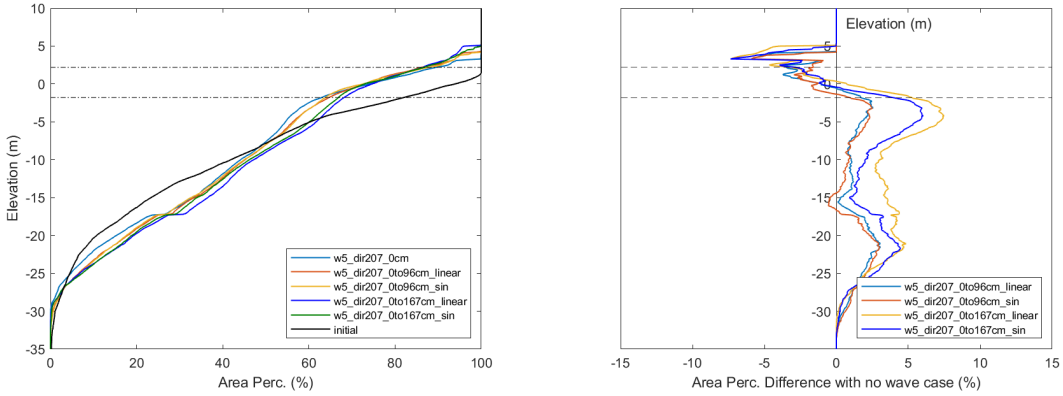

(e) All scenarios

(f) Difference between wave and no wave

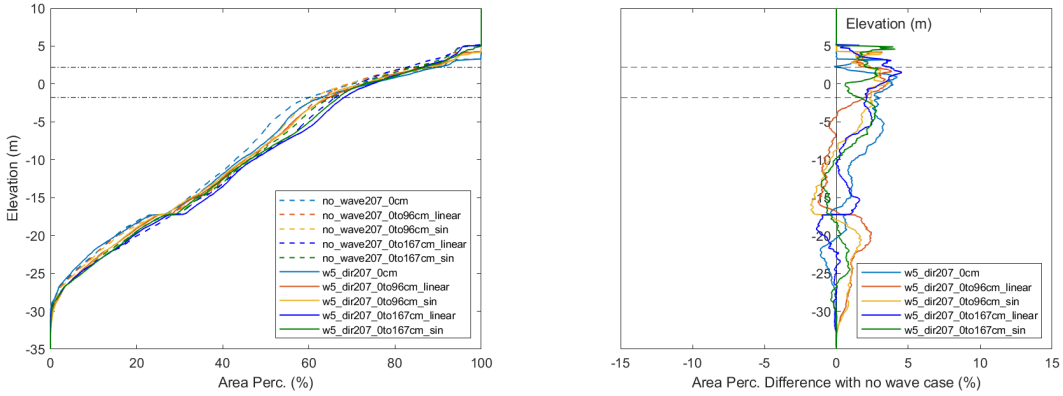

Figure 4.16: Hypsometry curve after 100 years. (b) is in no wave case, hypsometry curve difference between SLR and no SLR. Positive values mean lower elevation in case of SLR. (d) is in wave case, hypsometry curve difference between SLR and no SLR. Positive values mean lower elevation in case of SLR. (f) is at each SLR, hypsometry curve difference between wave and no wave. Positive values mean lower elevation in case of wave.

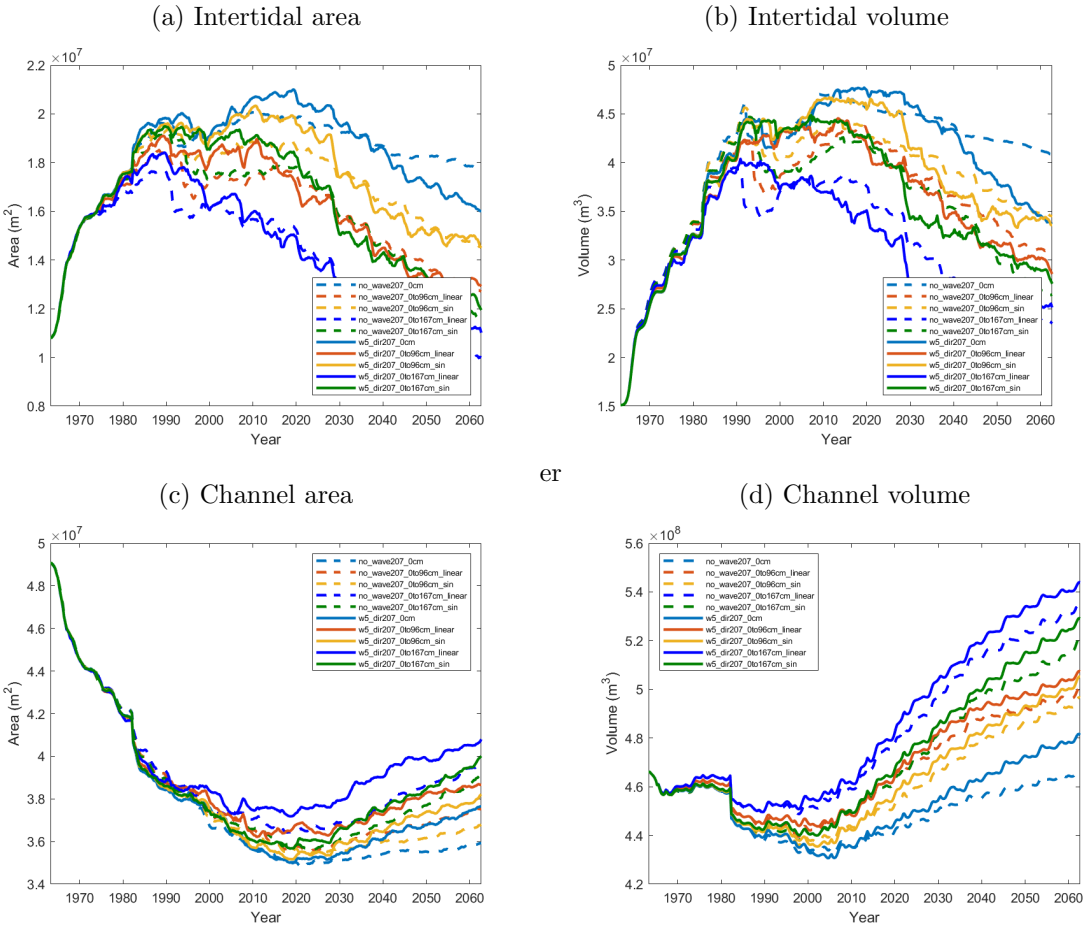

er

Figure 4.17: (a) Intertidal area; (b) Intertidal volume (c) Channel area; (d) Channel volume over 100 years

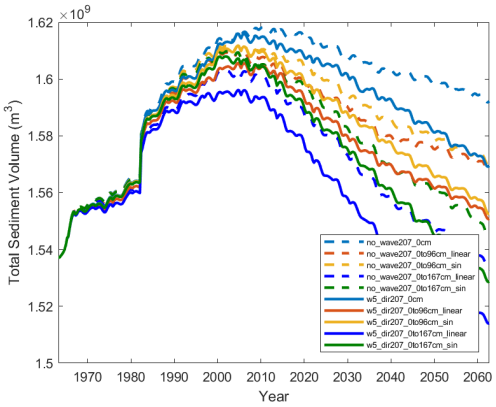

Figure 4.18: Total sediment volume over 100 years

4.5 Impact of Waves with Sea level rise (version 2)

As a reminder, among these scenarios, compared to section 4.2 sediment grain size is increased to $D_{50} = 200\mu m$. Dumping site at shoal Rug van Baarland is added.

Overview, with no sea level rise, shoal area expends over the entire Western Scheldt after 100 years (figure 4.19b and h). Channel Middelgat is shallower. Channel Overloop van Hansweert and Zuidergat around shoal Van Ossenisse experiences deepening. Both wave and no wave case show same signs with sea level rise. Most intertidal areas are elevated and lost of the shoal edges is observed. Some of the channels are observed to become deeper (eg. channel Vaarwater langs Hoofdplaat, south of Zuidergat), while some are not (eg. north of channel Overloop van Hansweert and Zuidergat) and even show sedimentation. Channel Pas van Terneuzen presents limited change under sea level rise, even with higher mean sea level rise (167cm).

Under no sea level rise, generally, waves lead to erosion in the intertidal area and sedimentation in shoal creeks (figure 4.20 b). In shoal van Ossenisse, more sediment happens in the lee side of the shoal. Different from section 4.2, western of the shoal (S1 and S2) shows less sediment in the shoal edge but more sediment in its adjacent channel (C1). Reasons of the observed difference could come from larger grain size and different boundary conditions. However, the potential reason is not isolated, so conclusion is not able to be made. Under the sea level rise 96cm-sinusoidal and 167cm-linear, the observations maintain. However, SLR 167cm-sinusoidal presents a clear sign of more sediment in the shoal edge and less sediment in the channel.

(a) Initial bathymetry (no wave)

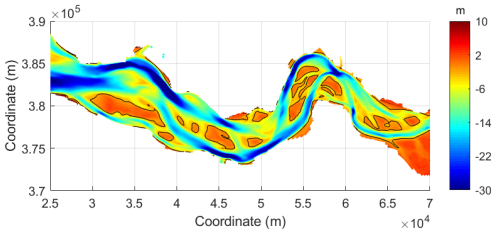

(g) Initial bathymetry (wave)

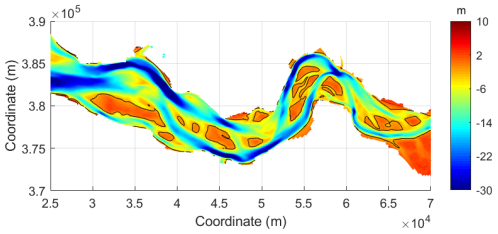

(b) After 100 years SLR 0cm (no wave)

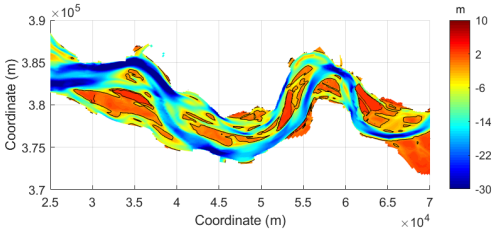

(h) After 100 years SLR 0cm (wave)

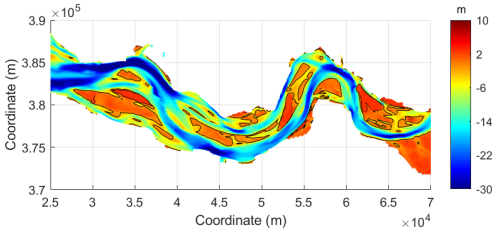

(d) SLR 96cm sin - SLR 0cm (no wave)

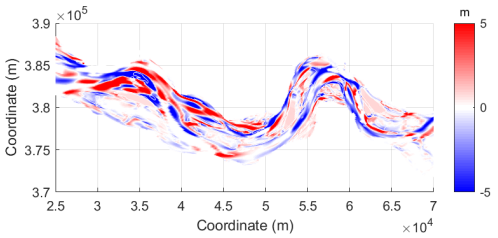

(j) SLR 96cm sin - SLR 0cm (wave)

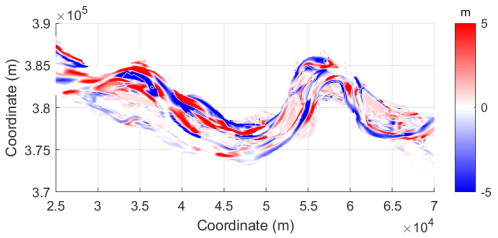

(e) SLR 167cm linear - SLR 0cm (no wave)

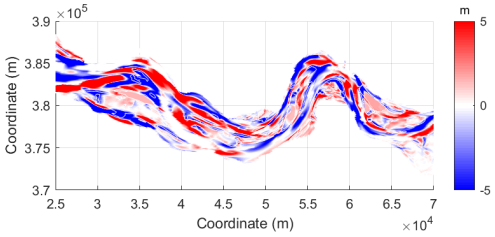

(k) SLR 167cm linear - SLR 0cm (wave)

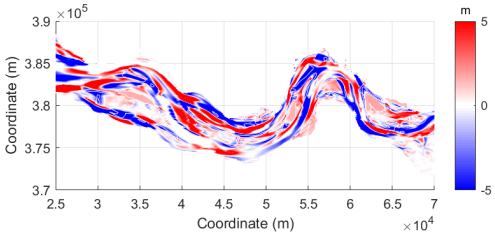

(f) SLR 167cm sin - SLR 0cm (no wave)

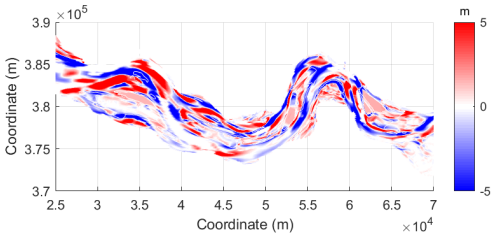

(l) SLR 167cm sin - SLR 0cm (wave)

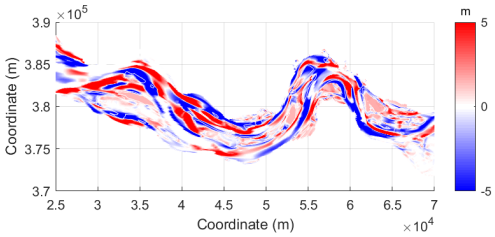

Figure 4.19: First column: sea level rise impact in no wave case. (c) to (f): after 100 years, bathymetry subtraction between SLR and No SLR in no wave case. Second column: sea level rise impact in wave case. (i) to (l): after 100 years, bathymetry subtraction between SLR and No SLR in wave case. Red color indicates more sediment due to sea level rise

(a) Initial bathymetry (year 1963)

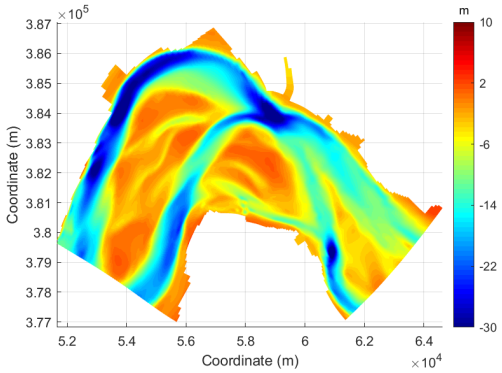

(b) SLR 0cm

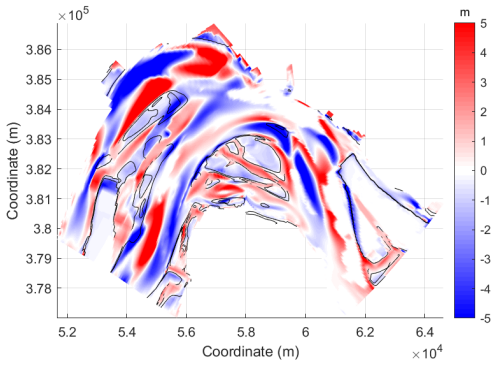

(c) SLR 96cm sin

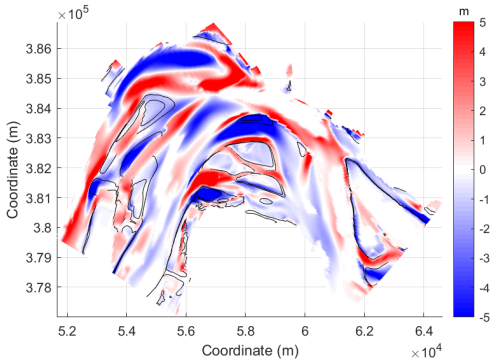

(d) SLR 167cm linear

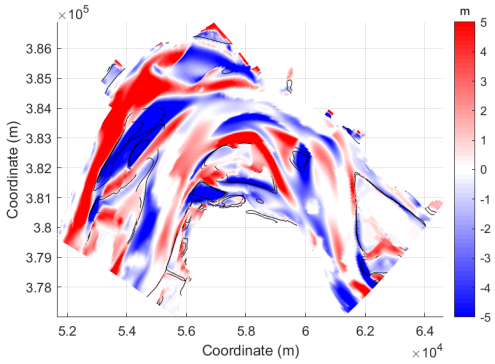

(e) SLR 167cm sin

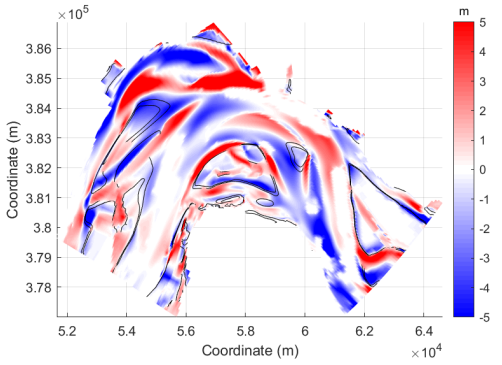

Figure 4.20: Bathymetry difference between wave and no wave case after 100 years in different SLR scenarios. Positive value indicates more sediment due to waves

Figure 4.21a and c show hypsometry curves under sea level rise in no wave and wave case, respectively and figure 4.21b and d are their difference with no sea level rise, respectively. Both in wave and no wave case, intertidal area is elevated with the growth of mean sea level. Channel has wider area from low water level to the channel bottom with deeper level. The influence of wind-waves is presented in figure 4.21e and f. Same observation as section 4.2 is showed in intertidal area lowered by wave. Due to the rising mean sea level, the elevation of lowered intertidal area also rises. Wave enlarges shoal area between elevation around 0.5m to -10m in no SLR, 1m to -2.5m in SLR96cm, 2.2m to -1.5m. In other word, the tendency of wave leading to lowered intertidal area and wider shoal is the same, but the elevation where these happen increases with sea level rise. However, the impact of wave on the deep part of the channel shows vague signs. No SLR shows wave causes wider channel area under elevation -10m, but SLR 96cm-sinusoidal and SLR 167cm-linear change this phenomenon by showing narrower channel width.

The fixed elevation range between 2.2m and -1.8m is still used to calculate intertidal area. The decreased value of intertidal area (figure 4.22) implies the lose of shoal edges due to sea level rise. Correspondingly, sea level rise leads to less intertidal volume and larger channel area at water level -1.8m. Channel volume increases by 6% with SLR 96cm and 10.8% compared to no SLR. The increased channel volume also reflects the reduced total sediment volume. Domain 3 imports sediment in the first 40 years, after which it shifts to export sediment. Sea level rise does not change the trend of estuarine morphodynamic evolution. Under sea level rise, wave maintains its function to enlarge intertidal area and volume. As a result, the channel area is reduced, which is comparable with section 4.2. Under no SLR, wave leads to less channel volume and hence more total restored sediment volume, which is different trend with section 4.2. This is mainly due to the shallower channel bottom observed in hypsometry curve figure 4.21e and f. This different phenomenon can be due to either the increased grain size or different type of boundary conditions or both. This implies that wave impact is very sensitive to grain size or type of boundary conditions or both, which is recommended to be further investigated by isolating variable. However, despite of this, the impact of waves does not change the signal with the sea level rise. In no SLR and each different SLR, wave shows the same function to increase intertidal area and volume, decrease channel area and volume and increase total sediment volume. In addition, estuary remain its own morphological despite of the presence of waves.

(a) No wave case

(b) Difference with No SLR

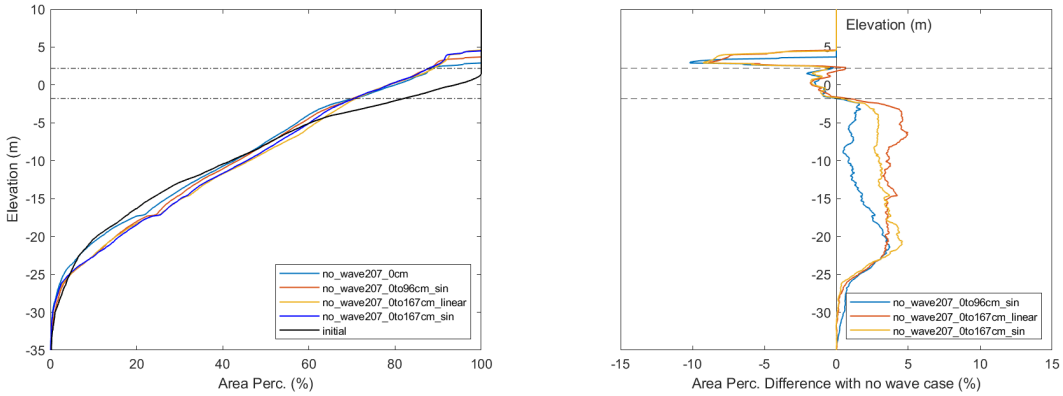

(c) Wave case

(d) Difference with No SLR

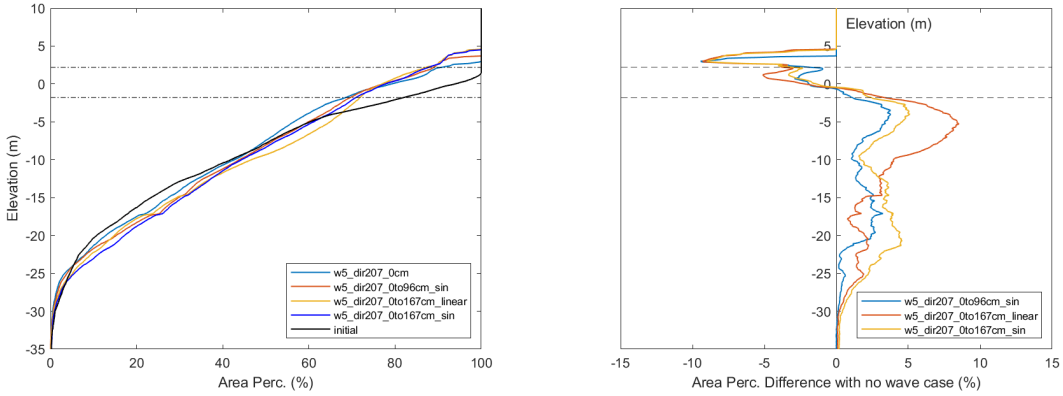

(e) All scenarios

(f) Difference between wave and no wave

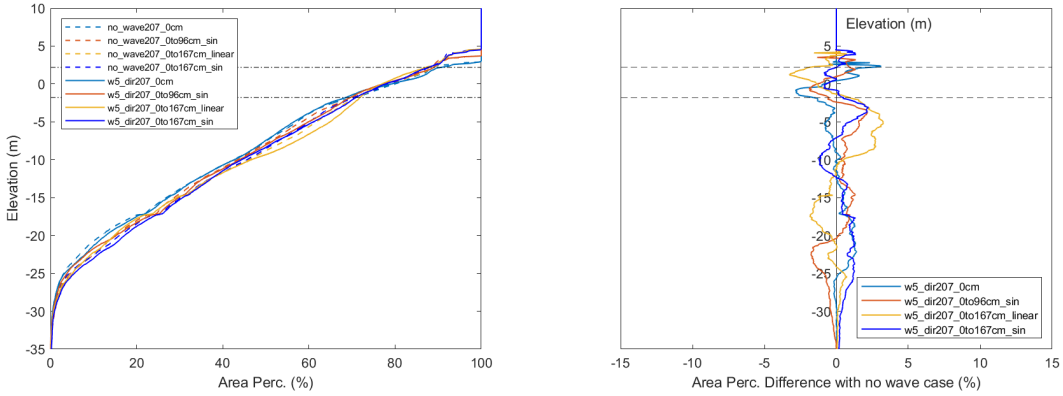

Figure 4.21: Hypsometry curve after 100 years. (b) is in no wave case, hypsometry curve difference between SLR and no SLR. Positive values mean lower elevation in case of SLR. (d) is in wave case, hypsometry curve difference between SLR and no SLR. Positive values mean lower elevation in case of SLR. (f) is at each SLR, hypsometry curve difference between wave and no wave. Positive values mean lower elevation in case of wave.

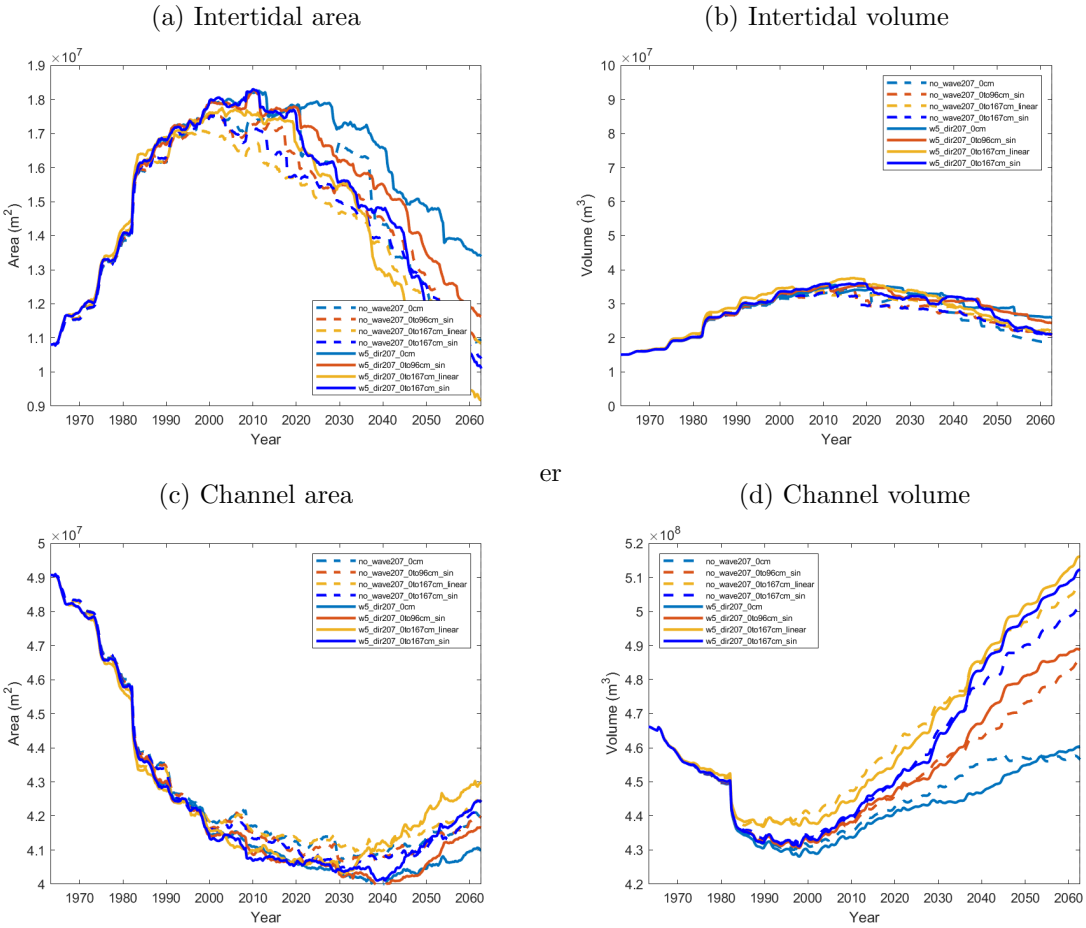

Figure 4.22: (a) Intertidal area; (b) Intertidal volume (c) Channel area; (d) Channel volume over 100 years

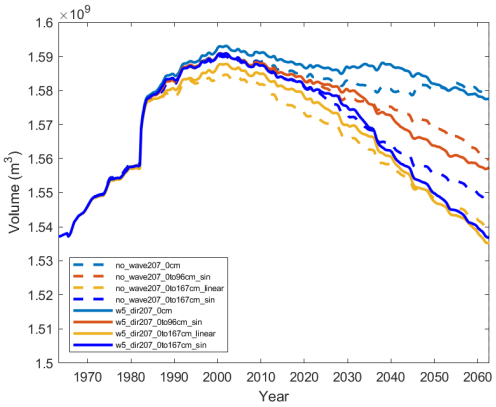

Figure 4.23: Total sediment volume over 100 years

Chapter 5

Discussions

5.1 Sensitivity Analysis

Sensitivity analysis is carried out by investigating the impact of some parameters and to see if our conclusion is still maintained with the change of time, sediment diameter, and wind speed.

From figure of development of intertidal area, channel area and channel volume (figure 5.2a c and d), it is seen that in a longer period after 50 years, the tendency of morphological change by waves is still maintained with larger intertidal area and larger channel volume. In addition, the quantity differences in these indexes keeps constant after 50 years. The difference between wave and no wave in terms of channel volume remains around $6 \times 10^6 m^3$ for 70 years until year 2063. This value is identical with the decreased total sediment volume in the domain after 50 years (figure 4.13). Wave shows difference value in these indexes but does not fundamentally change the trend of the estuarine morphodynamic evolution. This probably means wave induces morphological difference in the estuary, for example, enlarge the channel volume, but once the estuary adjust itself to wave case, it keeps the same behavior.

The increase of wind speed enhances the tendency of morphological change difference by waves. Shoal develops wider and shows a more convex-up profile with larger wind speed (figure 5.1). Scenario with wind speed $7m/s$ results in a double higher intertidal area than wind speed $5m/s$ compared with no wave case. However, the larger sedimentation in subtidal area compensates the larger erosion in channel bottom, which leads to a close channel volume value in different wind speed. Differences of intertidal area and channel area with no wave case keep deviating after 50 years, but which of channel volume keeps constant from an early stage.

Coarser sand with $D_{50} = 250\mu m$ is tested in simulation of no wave and wave case. From the view of hypsometry curve, it is closer to the measurement data. The profile below -20m nicely fits.

Its intertidal area has a steeper slope and with larger area in high elevation on top of the shoal. One explanation is that the coarser sediment shows more difficulty to be moved by wave and currents. Compared to its corresponding no wave case, shoal width also becomes wider (between elevation -5m to -12m). The elevation range with wider area is located lower than finer sediment scenario (between elevation 0m to -8m). The bed slope effect is assumed to play a role. Sediment eroded by waves disperses to shoal edges and gradually move to lower place driven by gravity. This agrees with the evolution of intertidal area (figure 5.2 a), in which, intertidal area is larger in wave case at the beginning and shows the opposite trend after 40 years. With response to shoal widening, bottom of the channel is adapted to have larger space.

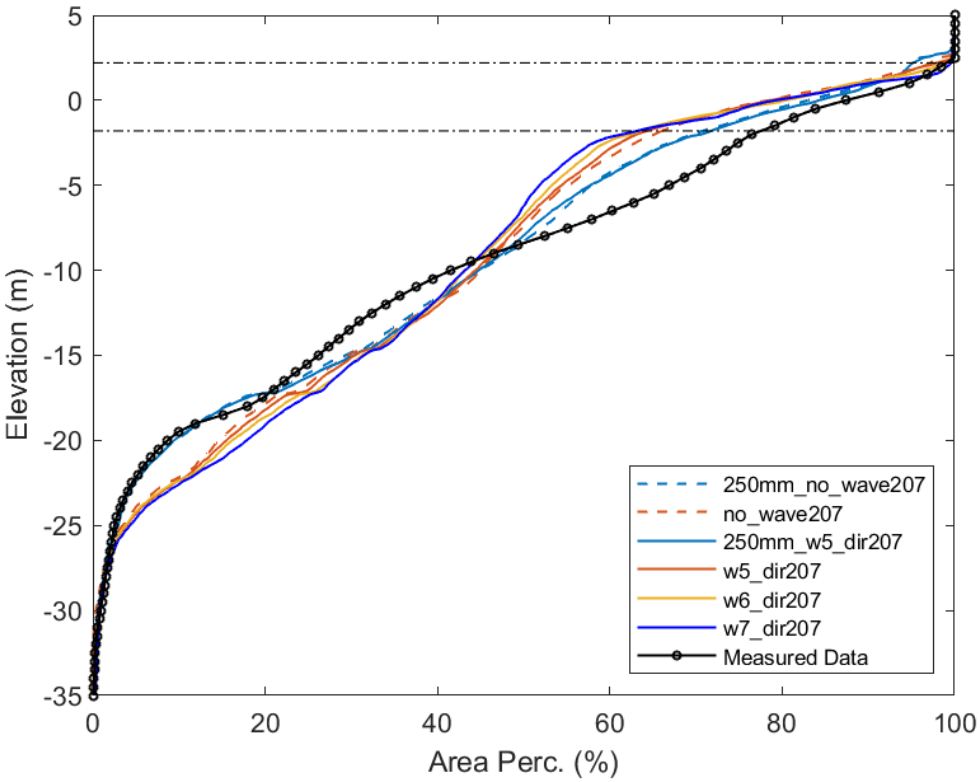

Figure 5.1: Hypsometry curve after 50 years

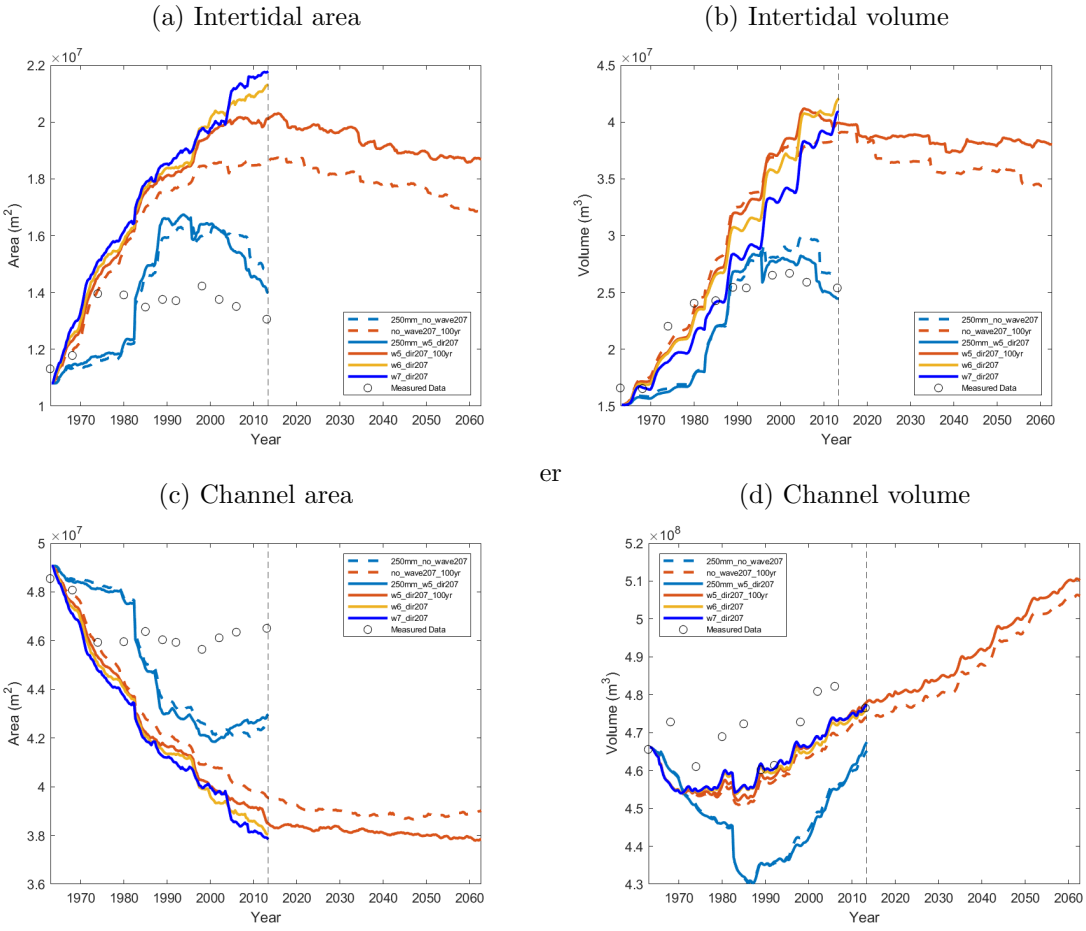

er

Figure 5.2: (a) Intertidal area; (b) Intertidal volume (c) Channel area; (d) Channel volume over 100 years

Chapter 6

Conclusions and Recommendation

Our current work starts from a real bathymetry and simulates 50 years morphological evolution of estuarine shoals in the case of waves and no waves. Comparison of their morphology and sediment transport are carried out.

From the global view, wave case and no wave case show similar evolution of channel-shoal patterns over the entire 50 years. However, wave case shows the tendency to slightly migrate along wave direction. Initially, with the presence of waves, more/less erosion/sedimentation is shown in the high elevation section of the shoal and also in the upwind side of intertidal area, while less/more erosion/sedimentation is observed at edge of the shoal and downwind side of the intertidal area. Waves lower intertidal elevation and cause larger intertidal area and hence less channel area. At the same time, deeper channel is found near the shoal edge with more sediment. This trend continues over time. Hypsometry curve suggests that the morphological difference between wave and no wave starts from intertidal area and gradually extends to the channel bottom. After 50 years, bathymetry difference in some part of shoal edge can be up to 3 meters. Shoal is widened in lower intertidal area and upper subtidal area (around between -1m and -10m). Larger channel volume is presented with the observation of deeper and wider channel below around -10m.

The underlying mechanism behind these morphological differences starts with resuspension induced by wave. Waves propagate onto the shoal and cause high bed shear stress in the high elevation section of the shoal and upwind side of intertidal area. Consequently, high suspended sediment concentration is induced in the water column. This increases sediment transport rate over the whole shoal. It is more obvious during high water level and also enhanced by non-linear wave-current interaction. During low water period, the influence of waves exists and can be extended to subtidal domain, but the amount of affected area is very limited. On the high elevation

of the shoal, wind-driven flow combined with high SSC increase sediment transport along wind direction, so more sediment is found in downwind side of intertidal area. On the other hand, by enlarged advection and diffusion process, suspended sediment also disperse to shoal edges with low bed shear stress. Bedload transport shows insignificance on the morphological difference. Wave asymmetry-induced suspended sediment transport plays a small role on sediment transport along wave direction, especially in deep intertidal area where high significant wave height exists.

In the wave case, deepening of the channel takes response to the narrower channel area. Increase of channel volume is identical to the reduction of total sediment volume. This implies that wave leads to sediment lost in the whole domain, which mainly happens in the channel, despite the fact that channel receives sediment from the shoal. However, on a longer timescale (100 years), the difference between wave and no wave remains not present. Instead, the difference keeps constant after a certain period in terms of intertidal area, intertidal volume, channel area and channel volume. With the presence of wave, the estuary adjusts itself by lowering shoal elevation, enlarging shoal width and exporting sediment from the channel, but its autonomous behavior is not influenced by waves.

However, the impacts of waves are sensitive to sediment grain size. When the grain size increases to $250\mu m$, intertidal area is still lowered by wave, but wider shoal edge is presented in lower elevation, and channel volume tends to become smaller. More sediment becomes to show inside the channel. This might be induced by larger gravity-driven force of larger sediment grain size. Less channel volume and shallower channel depth also happen in No SLR scenario among scenarios from sea level rise version 2. However, both grain size and type of boundary condition change, the reason of the smaller channel volume can not be confirmed.

Sea level rise scenarios are carried out by imposing gradually rising mean sea level at seaward boundary. Simulation time is over 100 years from 1963 to 2063. Both in wave and no wave case, sea level rise leads to elevation of shoal height and area lose in shoal edges, resulting in steeper slope in the intertidal area. Larger channel area and volume are presented with sea level rise. Hence, less total sediment is stored in the domain. Waves maintain its function under the sea level rise. It lowers and widens the shoal, resulting in the increase of intertidal area and volume. Waves impact on the inner channel show difference with the change of sensitive parameters (eg. sediment grain size, tidal range, type of boundary conditions). However, once a set of parameters are implemented in sea level rise scenarios, waves impact do not change with sea level rise. Still under sea level rise, waves do not lead to fundamental difference on estuarine long-term behaviors.

Sediment grain size and type of boundary conditions show the potential to influence wind-waves impact on the estuarine evolution. Further research can isolate the change of grain size and type of boundary conditions to do more investigations. In addition, scenarios with no dredging and non-erodible layer implementation can be carried out to study their impact. Model performance may be improved by enhanced bed slope formulations, sediment grading (multiple sediment

fractions), or space and time varying bed roughness formulations.

Appendix A

Dredging and dumping implementation

Dredging series is listed in second column of table A.1. The distributed dumping site and the corresponding percentage from a certain dredging polygon is listed in the fourth column.

Table A.1: Dredging and dumping activities

Polygon	Dredging period	Dredging depth [m]	Dumping site (%)
BBA	1982-1996; 1996-2008; 2008-2013	14.70; 16.00; 17.20	NDP(11); SH41(19); SH51(7); SH61(51); SN51(11); WALS(1)
DBO	1982-1996; 1996-2008; 2008-2013	14.70; 16.00; 17.20	HP1(24); HP3(26); SN11(47); SN31(3)
DHW	1965-1975; 1975-1978; 1978-2013	13.50; 14.00; 14.70	NDP(9); SH41(37); SH51(12); SN51(23); WALS(19)
DVA	1982-1996; 1996-2008; 2008-2013	14.70; 16.00; 17.20	NDP(3); SH41(56); SH51(1); SN51(17); WALS(23)
DWA	1982-1996; 1996-2008; 2008-2013	14.70; 16.00; 17.20	NDP(2); SH41(56); SH51(34); SN51(8)
GVO24	1982-1996; 1996-2008; 2008-2013	14.70; 16.00; 17.20	HP1(30); SN31(70)
GVO28	1982-1996; 1996-2008; 2008-2013	14.70; 16.00; 17.20	HP1(20); NDP(25); SH41(55)
GVO32	1982-1996; 1996-2008; 2008-2013	14.70; 16.00; 17.20	NDP(20); SH41(68); SN31(12)
BBA73	1982-1996; 1996-2008; 2008-2013	14.70; 16.00; 17.20	NDP(28); SH51(22); SH61(31); SN51(19)

OHW	1982-1996; 1996-2008; 2008-2013	14.70; 16.00; 17.20	SH41(100)
OVA48	1982-1996; 1996-2008; 2008-2013	14.70; 16.00; 17.20	NDP(29); SH41(64); SN51(7)
OVA54	1982-1996; 1996-2008; 2008-2013	14.70; 16.00; 17.20	NDP(11); SH41(63); SH51(23); SN51(3)
OVA58	1982-1996; 1996-2008; 2008-2013	14.60; 16.00; 17.20	SH41(62); SH51(3); SN51(17); WALS(18)
PAS10	1982-1996; 1996-2008; 2008-2013	14.70; 16.00; 17.20	HP3(68); SN11(32)
PAS8	1982-1996; 1996-2008; 2008-2013	17.15; 17.15; 17.15	HP1(100)
PUT	1982-1996; 1996-2008; 2008-2013	14.70; 16.00; 17.20	SN31(100)
DZA	1982-1996; 1996-2008; 2008-2013	14.70; 16.00; 17.20	NDP(19); SH61(48); SN51(33)
BBA72	1982-1996; 1996-2008; 2008-2013	14.70; 16.00; 17.20	SH61(5); SN51(95)
VLIS	1982-1996; 1996-2008; 2008-2013	17.02; 17.02; 17.02	SN11(100)
WIEL	1982-1996; 1996-2008; 2008-2013	16.98; 16.98; 16.98	ZWIN(100)
G1W	1996-2004; 2004-2013	18.40; 18.70	ST01(70); ST02(30)
G1O	1996-2004; 2004-2013	18.10; 18.70	ST01(70); ST02(30)

SCHW	1982-1986; 1986-1996; 1996-2004; 2004-2013	15.00; 16.80; 18.00; 18.70	ST01(70); ST02(30)
SCHO1	1986-1997; 1997-2004; 2004-2013	16.50; 17.80; 18.00	ST01(70); ST02(30)
SCHO2	1986-1997; 1997-2004; 2004-2013	16.30; 17.70; 17.90	ST01(70); ST02(30)
SCHO3	1986-1997; 1997-2004; 2004-2013	16.20; 17.70; 17.90	ST01(70); ST02(30)
ZB	1980-1981; 1981-1982; 1982-1996; 1996-2008; 2008-2013	15.00; 16.00; 16.98; 16.98; 16.98	ST02(10); ST03(90)
PVZ	1980-1981; 1981-1982; 1982-1986; 1986-1998; 1998-2004; 2004-2013	13.00; 14.00; 15.00; 16.30; 17.70; 18.30	ST02(10); ST03(90)
ZSCH	1980-1981; 1981-1982; 1982-1986; 1986-1998; 1998-2004; 2004-2013	13.00; 14.00; 15.00; 16.30; 17.70; 18.30	ST02(10); ST03(90)

Appendix B

Model results from Delft3D Flexible Mesh

As a starting point, we set up D-Flow FM model to do this research in favour of its unstructured grid and convenience of making high resolution in our study shoal area. The idea is to first test its ability of simulating long-term morphological change by using the exact same settings with Delft3D and compare their results. D-Flow FM model is used to be set up with the help of previous study from Van der Wegen and Roelvink (2012). The grids were constructed by Van der Wegen and Roelvink (2012) but inverted to unstructured grids (see Figure B.1). The grid cell size is about 100m by 200m in the central area. The seaward boundary is extended to 20 km from coastline and landward boundary is almost up to Gent. The north-western seaward boundary is water level forced by tide and south-western and north-western seaward boundaries are Neumann boundary conditions. The hydrodynamic simulation time is from 2003-10-31 to 2004-05-01. The morphodynamic simulation time is 200 years.

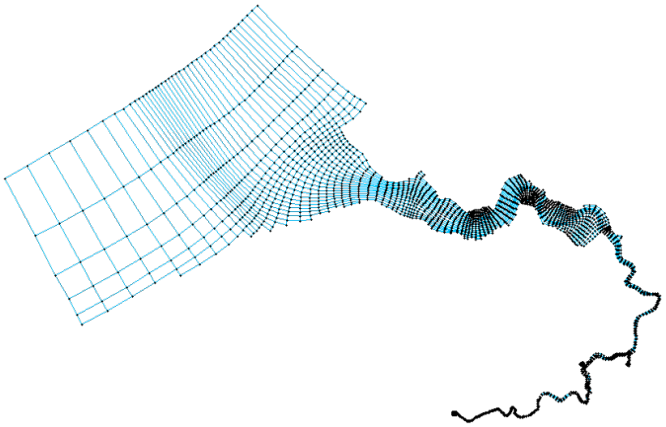

Figure B.1: D-Flow FM computational grid

The initial bed level was derived from bathymetry of year 1998. The value was averaged over the whole domain, which means the initial bed level is horizontal flat bed level and there is no sediment exchange between this domain and outer of the domain. According to the bed composition Kuijper et al. (2004), sand accounts the major part, so we assume that the morphological change is conducted by sandy sediment transport. Non-erodible layer is imposed over the whole domain. The basic parameters that were used is shown in table B.1.

Table B.1: Parameters of model

Parameters	Settings
Sediment transport formulation	Van Rijn (1993)
Dimensions	2D
Bed slope factor (α_{bn})	10
River discharge	15 m^3/s
Tidal components	M2, M4 and M6
Horizontal diffusivity (Dicouv)	10
Morphological factor	40
Time step	1m
Maximume time step	1m
Type of sediment	sand
D_{50}	$2\mu m$

Same parameter settings are implemented in D-Flow FM and Delft3D, respectively, and the morphology after 200 years are compared. A number of sensitivity analysis is carried out. Table B.2 presents an overview of the abbreviation used in the sensitivity analysis to refer to different

runs. Figure B.2 shows comparison in terms of different parameter sets.

Table B.2: Abbreviations applied for run specifications

Parameters	Abbreviation
Van Rijn transport 1993	VR1993
Van Rijn transport 2004	VR2004
Bed slope factor (α_{bn}) value X	abnX
Horizontal diffusivity value X	DiffX
Spiral flow turned on	spir1
Spiral flow turned off	spir0
Including non-erodible layer	nel
No non-erodible layer	el

(a) VR1993 abn50 Diff10 spir1 nel

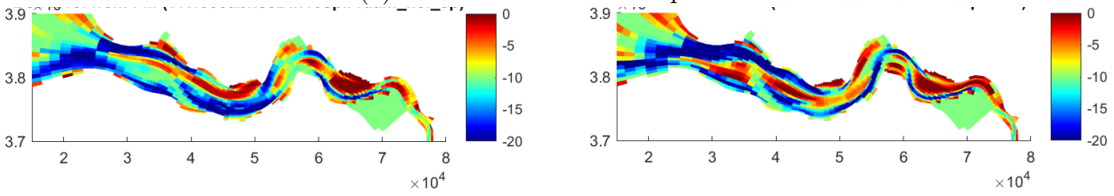

(b) VR2004 abn50 Diff10 spir1 nel

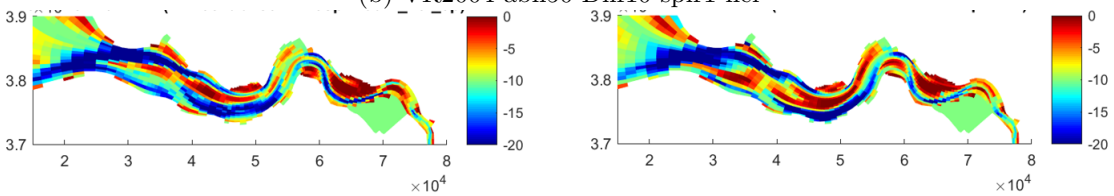

(c) VR1993 abn50 Diff30 spir1 nel

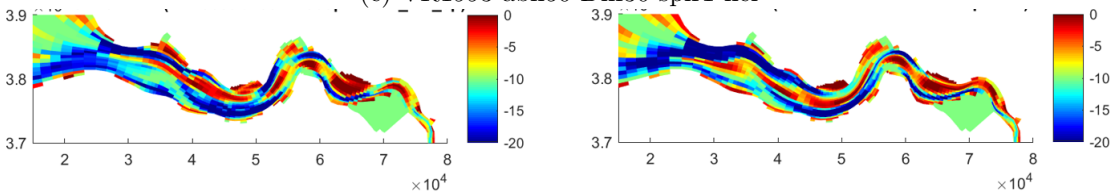

(d) VR2004 abn50 Diff30 spir1 nel

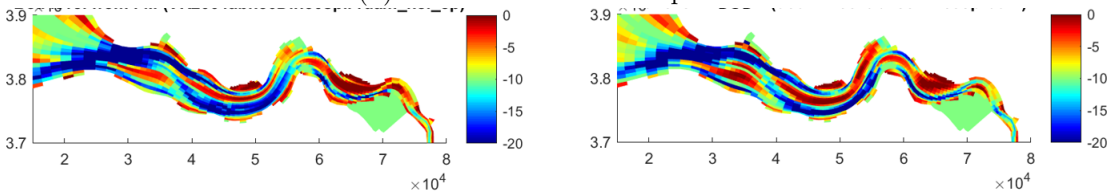

(e) VR2004 abn10 Diff10 spir1 nel

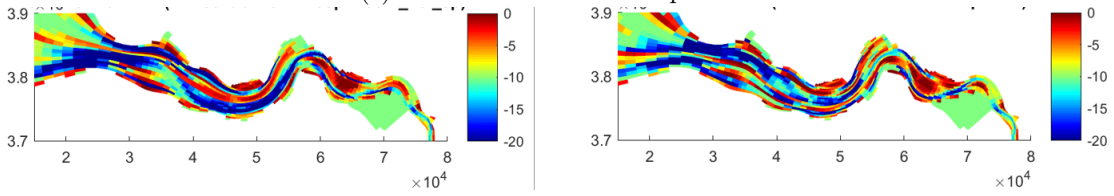

(f) VR2004 abn50 Diff10 spir0 nel

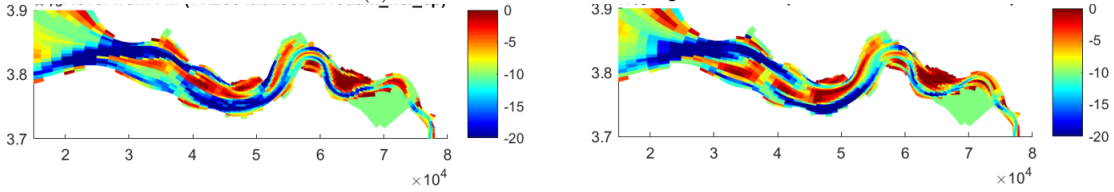

(g) VR2004 abn50 Diff10 spir1 el

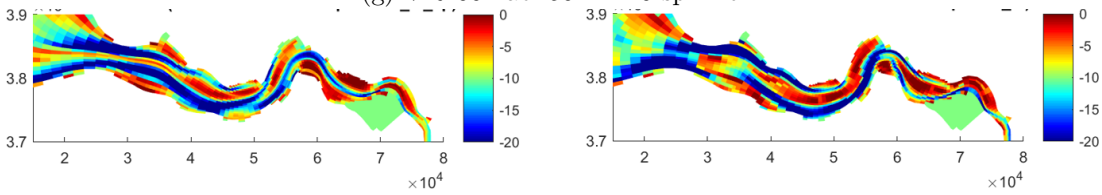

Figure B.2: Comparison of morphology after 200 years between D-Flow FM (left panels) and Delft3D (right panels)

Bibliography

Ahnert, F. (1960). Estuarine meanders in the Chesapeake Bay area. *Geographical review*, 50(3):390–401.

Allen, J. and Duffy, M. (1998). Medium-term sedimentation on high intertidal mudflats and salt marshes in the severn estuary, sw britain: the role of wind and tide. *Marine Geology*, 150(1-4):1–27.

Baar, A. W., Boechat Albernaz, M., Van Dijk, W. M., and Kleinhans, M. G. (2019). Critical dependence of morphodynamic models of fluvial and tidal systems on empirical downslope sediment transport. *Nature Communications*, 10(1).

Brand, A., Lacy, J. R., Hsu, K., Hoover, D., Gladding, S., and Stacey, M. T. (2010). Wind-enhanced resuspension in the shallow waters of south san francisco bay: Mechanisms and potential implications for cohesive sediment transport. *Journal of Geophysical Research: Oceans*, 115(C11).

Carter, R. W. G. (2013). *Coastal environments: an introduction to the physical, ecological, and cultural systems of coastlines*. Elsevier.

Dam, G. and Labeur, R. J. (2008). Long term process-based morphological model of the Western Scheldt Estuary Habitatmapping Zeeschelde / Sea Scheldt (inner Scheldt Estuary) View project Tsunami modelling View project.

Dam, G., Wegen, M., Labeur, R. J., and Roelvink, D. (2016). Modeling centuries of estuarine morphodynamics in the Western Scheldt estuary.

DHV (2004). Western Scheldt Estuary (the Netherlands). 31(0):1–14.

Dissanayake, D., Roelvink, J., and Van der Wegen, M. (2009). Modelled channel patterns in a schematized tidal inlet. *Coastal Engineering*, 56(11-12):1069–1083.

Dissanayake, D. M., Ranasinghe, R., and Roelvink, J. A. (2012). The morphological response of large tidal inlet/basin systems to relative sea level rise. *Climatic Change*, 113(2):253–276.

Eindrapport, C. (2013). Actualisatie van het finel2d model van de westerschelde.

Elmilady, H., Van der Wegen, M., Roelvink, D., and Jaffe, B. E. (2019). Intertidal Area Disappears Under Sea Level Rise: 250 Years of Morphodynamic Modeling in San Pablo Bay, California. *Journal of Geophysical Research: Earth Surface*, 124(1):38–59.

EPA, U. S. (1997). *Volunteer stream monitoring a methods manual.* DIANE Publishing.

Fagherazzi, S., Palermo, C., Rulli, M. C., Carniello, L., and Defina, A. (2007). Wind waves in shallow microtidal basins and the dynamic equilibrium of tidal flats. *Journal of Geophysical Research*, 112(F2):F02024.

Friedrichs, C. (2011). Tidal Flat Morphodynamics: A Synthesis. *Treatise on Estuarine and Coastal Science*, pages 137–170.

Friedrichs, C. and Aubrey, D. (1996). *Uniform bottom shear stress and equilibrium hypsometry of intertidal flats*, volume 50, pages 405–429.

Friedrichs, C. T. (1993). *Hydrodynamics and morphodynamics of shallow tidal channels and intertidal flats.* PhD thesis, Woods Hole Oceanographic Institution.

Hibma, A., de Vriend, H. J., and Stive, M. J. F. (2003). Numerical modelling of shoal pattern formation in well-mixed elongated estuaries. *Estuarine, Coastal and Shelf Science*, 57(5-6):981–991.

Hibma, A., Schuttelaars, H., and de Vriend, H. (2004). Initial formation and long-term evolution of channel–shoal patterns. *Continental Shelf Research*, 24(15):1637–1650.

Hu, Z., Wang, Z. B., Zitman, T. J., Stive, M. J. F., and Bouma, T. J. (2015). Predicting long-term and short-term tidal flat morphodynamics using a dynamic equilibrium theory. *Journal of Geophysical Research: Earth Surface*, 120(9):1803–1823.

Hunt, S., Bryan, K. R., and Mullarney, J. C. (2015). The influence of wind and waves on the existence of stable intertidal morphology in meso-tidal estuaries. *Geomorphology*, 228:158–174.

Janssen-Stelder, B. (2000). The effect of different hydrodynamic conditions on the morphodynamics of a tidal mudflat in the dutch wadden sea. *Continental shelf research*, 20(12-13):1461–1478.

Jarrett, J. T. (1976). Tidal prism-inlet area relationships. Technical report, ARMY ENGINEER WATERWAYS EXPERIMENT STATION VICKSBURG MISS.

Kemp, A. C., Horton, B. P., Donnelly, J. P., Mann, M. E., Vermeer, M., and Rahmstorf, S. (2011). Climate related sea-level variations over the past two millennia. *Proceedings of the National Academy of Sciences*, 108(27):11017–11022.

Kirby, R. (2000). Practical implications of tidal flat shape. *Continental Shelf Research*, 20(10-11):1061–1077.

Kuijper, C., Steijn, R. C., Roelvink, D., and der Kaaij, T. V. (2004). Morphological modelling of the Western Scheldt: validation of DELFT3D. Technical report, Delft.

Lesser, G., Roelvink, J., Van Kester, J., and Stelling, G. (2004). Development and validation of a three-dimensional morphological model. *Coastal Engineering*, 51(8-9):883–915.

Maan, D. C., Van Prooijen, B. C., Zhu, Q., and Wang, Z. B. (2018). Morphodynamic Feedback Loops Control Stable Fringing Flats. *Journal of Geophysical Research: Earth Surface*, 123(11):2993–3012.

MacVean, L. J. and Lacy, J. R. (2014). Interactions between waves, sediment, and turbulence on a shallow estuarine mudflat. *Journal of Geophysical Research: Oceans*, 119(3):1534–1553.

Meire, P., Ysebaert, T., Van Damme, S., Van den Bergh, E., Maris, T., and Struyf, E. (2005). The scheldt estuary: a description of a changing ecosystem. *Hydrobiologia*, 540(1-3):1–11.

O'Brien, M. P. (1969). Equilibrium flow areas of inlets on sandy coasts. *Journal of the Waterways and Harbors Division*, 95(1):43–52.

Osborn, K. (2017). Seasonal fish and invertebrate communities in three northern california estuaries.

Parris, A., Bromirski, P., Burkett, V., Cayan, D., Culver, M., Hall, J., Horton, R., Knuuti, K., Moss, R., Obeysekera, J., Sallenger, A., and Weiss, J. (2012). *Global Sea Level Rise Scenarios for the US National Climate Assessment. NOAA Tech Memo OAR CPO-1.*

Roberts, W., Le Hir, P., and Whitehouse, R. J. (2000). Investigation using simple mathematical models of the effect of tidal currents and waves on the profile shape of intertidal mudflats. *Continental Shelf Research*, 20(10-11):1079–1097.

Robinson, A. (1960). Ebb-flood channel systems in sandy bays and estuaries. *Geography*, 45(3):183–199.

Schramkowski, G. P., Schuttelaars, H. M., and de Swart, H. E. (2002). The effect of geometry and bottom friction on local bed forms in a tidal embayment. *Continental Shelf Research*, 22(11-13):1821–1833.

Schuttelaars, H. M. and de Swart, H. E. (1999). Initial formation of channels and shoals in a short tidal embayment. *Journal of Fluid Mechanics*, 386:15–42.

Sistermans, P. and Nieuwenhuis, O. (2004). Holland coast (the netherlands). *Eur. Case Study*, 31:1–17.

Sutherland, J., Peet, A. H., and Soulsby, R. L. (2004). Evaluating the performance of morphological models. *Coastal Engineering*, 51(8-9):917–939.

Tan, H. T., Chou, L., Yeo, D., and Ng, P. (2007). The natural heritage of singapore.

Toffolon, M. and Crosato, A. (2007). Developing Macroscale Indicators for Estuarine Morphology: The Case of the Scheldt Estuary. *Journal of Coastal Research*, 231:195–212.

Van den Berg, J. H., Jeuken, C. J., and Van der Spek, A. J. (1996). Hydraulic processes affecting the morphology and evolution of the westerschelde estuary. *Estuarine Shores: Evolution, Environments and Human Alterations. John Wiley, London*, pages 157–184.

Van der Spek, A. J. F. (1994). *Large-scale evolution of Holocene tidal basins in the Netherlands*. Universiteit Utrecht, Faculteit Aardwetenschappen.

Van der Wegen, M. (2013). Numerical modeling of the impact of sea level rise on tidal basin morphodynamics. *Journal of Geophysical Research: Earth Surface*, 118(2):447–460.

Van der Wegen, M., Jaffe, B., Foxgrover, A., and Roelvink, D. (2016). Mudflat Morphodynamics and the Impact of Sea Level Rise in South San Francisco Bay. *Estuaries and Coasts*, 40(1):37–49.

Van der Wegen, M., Jaffe, B. E., and Roelvink, D. (2011). Process-based, morphodynamic hindcast of decadal deposition patterns in San Pablo Bay, California, 1856-1887. *Journal of Geophysical Research: Earth Surface*, 116(2):1–22.

Van Der Wegen, M. and Roelvink, J. A. (2008). Long-term morphodynamic evolution of a tidal embayment using a two-dimensional, process-based model. *Journal of Geophysical Research: Oceans*, 113(3):1–23.

Van der Wegen, M. and Roelvink, J. A. (2012). Reproduction of estuarine bathymetry by means of a process-based model: Western Scheldt case study, the Netherlands. *Geomorphology*, 179:152–167.

Van der Wegen, M., Van der Werf, J. J., De Vet, P. L. M., and Röbke, B. R. (2017). Hindcasting Westerschelde mouth morphodynamics (1963-2011).

Van der Wegen, M., Wang, Z. B., Savenije, H. H., and Roelvink, J. A. (2008). Long-term morphodynamic evoluation and energy dissipation in a coastal plain, tidal embayment. *Journal of Geophysical Research: Earth Surface*, 113(3).

Van der Werf, J. J. and Briere, C. D. E. (2013). The influence of morphology on tidal dynamics and sand transport in the Scheldt estuary. Consortium Deltares, IMDC, Svašek, Arcadis, report G4. Technical report.

Van der Werf, J. J., Van Oyen, T., de Maerschalck, B., Nnafie, A., Van Rooijen, A., Taal, M., Tonnon, P. K., Verwaest, T., de Vet, L., Vroom, J., and Van der Wegen, M. (2015). Modeling the morphodynamics of the mouth of the Scheldt estuary.

Van Goor, M. A., Zitman, T. J., Wang, Z. B., and Stive, M. J. F. (2003). Impact of sea-level rise on the morphological equilibrium state of tidal inlets. *Marine Geology*, 202(3-4):211–227.

Van Leeuwen, S. M. and De Swart, H. E. (2004). Effect of advective and diffusive sediment transport on the formation of local and global bottom patterns in tidal embayments. In *Ocean Dynamics*, volume 54, pages 441–451.

Van Rijn, L. C. (2012). Influence of Wave Climate Schematisation on the Simulated Morphological Development of the Western Scheldt Entrance. (August):161.

Van Veen, J. (1950). Eb-en vloedschaar systemen in de Nederlandse getijwateren. *Tijdschrift van het Koninklijk Nederlandsch Aardrijkskundig Genootschap (Ser. 2)*, 67:303–350.

Wang, Z. B., Jeuken, M., Gerritsen, H., de Vriend, H., and Kornman, B. (2002). Morphology and asymmetry of the vertical tide in the Westerschelde estuary. *Continental Shelf Research*, 22(17):2599–2609.

Wang, Z. B., Louters, T., and de Vriend, H. J. (1995). Morphodynamic modelling for a tidal inlet in the Wadden Sea. *Marine Geology*, 126(1-4):289–300.

Wang, Z. B and Elias, EPL and Briere, C. (2007). Long-term interaction between the Dutch coast and the tidal basins. *Z4169*.